Institut für Erd- und Umweltwissenschaften
Mathematisch-Naturwissenschaftliche Fakultät
Universität Potsdam

Development of techniques for earthquake microzonation studies in different urban environment

Dissertation
zur Erlangung des akademischen Grades
"doctor rerum naturalium"
(Dr. rer. nat.)
in der Wissenschaftsdisziplin Geophysik

eingereicht an der
Mathematisch-Naturwissenschaftlichen Fakultät
der Universität Potsdam

von
Angelo Strollo

Potsdam, im September 2010

Ad Alfredo, Antonella e tutti gli
altri che ci hanno creduto...

Acknowledgements

First of all, thanks to Stefano Parolai and Dino Bindi for their continuous support and guidance that was well beyond a cooperation within the research activities. Their care has been fundamental in keeping me focused on this thesis. The second special thanks goes to my advisor Prof. Zschau that has been always a reference during my staying at the GFZ. I will always remember his kindness and his ability in finding the right words/solutions to any kind of scientific discussion.

I have to express my gratitude to all the colleagues of the section 2.1, in particular to: Claus and Regina Milkereit, Ralf Bauz, Susanne Köster, Erwin Günther, Birger Lühr, Heiko Woith. Each of them contributed in a different way to the work I carried out at the GFZ.

I would like to acknowledge also Prof. Mucciarelli that offered to me, some years ago, the possibility to know the "Potsdamer science".

Many thanks and for many reasons to the friends and colleagues: Matteo, Domenico, Marco, Andrea, Joel, Kevin, Babu, Paolo, Veronica, Luciana, Fabiana, Mahdi, Francisco. I will keep in my heart the very nice time spent together between Potsdam and Berlin. In particular, I will always remember the infinite patience of Kevin in supporting us with his precious English proof-reading.

My final thoughts are for my parents and sisters. They always supported in every situation my efforts although in some cases has been very difficult.

Last but not least, my infinite gratitude goes to Antonella. She shared with my stressful periods with great patience and I am sure she will enjoy the happiness for having written these lines. A particular thanks goes also to Alfredo that in his unique way contributed as well to this effort.

*...ecco la "dissertation" dopo una lunga pausa di riflessione
in giro per il Centro Asia!*

Abstract

The proliferation of megacities in many developing countries, and their location in areas where they are exposed to a high risk from large earthquakes, coupled with a lack of preparation, demonstrates the requirement for improved capabilities in hazard assessment, as well as the rapid adjustment and development of land-use planning. In particular, within the context of seismic hazard assessment, the evaluation of local site effects and their influence on the spatial distribution of ground shaking generated by an earthquake plays an important role. It follows that the carrying out of earthquake microzonation studies, which aim at identify areas within the urban environment that are expected to respond in a similar way to a seismic event, are essential to the reliable risk assessment of large urban areas. Considering the rate at which many large towns in developing countries that are prone to large earthquakes are growing, their seismic microzonation has become mandatory. Such activities are challenging and techniques suitable for identifying site effects within such contexts are needed.

In this dissertation, I develop techniques for investigating large-scale urban environments that aim at being non-invasive, cost-effective and quickly deployable. These peculiarities allow one to investigate large areas over a relative short time frame, with a spatial sampling resolution sufficient to provide reliable microzonation. Although there is a negative trade-off between the completeness of available information and extent of the investigated area, I attempt to mitigate this limitation by combining two, what I term layers, of information: in the first layer, the site effects at a few calibration points are well constrained by analyzing earthquake data or using other geophysical information (e.g., shear-wave velocity profiles); in the second layer, the site effects over a larger areal coverage are estimated by means of single-station noise measurements. The microzonation is performed in terms of problem-dependent quantities, by considering a proxy suitable to link information from the first layer to the second one. In order to define the microzonation approach proposed in this work, different methods for estimating site effects have been combined and tested in Potenza (Italy), where a considerable amount of data was available. In particular, the horizontal-to-vertical spectral ratio computed for seismic noise recorded at different sites has been used as a proxy to combine the two levels of information together and to create a microzonation map in terms of spectral intensity ratio (SIR).

In the next step, I applied this two-layer approach to Istanbul (Turkey) and Bishkek (Kyrgyzstan). A similar hybrid approach, i.e., combining earthquake and noise data, has been used for the microzonation of these two different urban environments. For both cities, after

having calibrated the fundamental frequencies of resonance estimated from seismic noise with those obtained by analysing earthquakes (first layer), a fundamental frequency map has been computed using the noise measurements carried out within the town (second layer). By applying this new approach, maps of the fundamental frequency of resonance for Istanbul and Bishkek have been published for the first time. In parallel, a microzonation map in terms of SIR has been incorporated into a risk scenario for the Potenza test site by means of a dedicated regression between spectral intensity (SI) and macroseismic intensity (EMS). The scenario study confirms the importance of site effects within the risk chain. In fact, their introduction into the scenario led to an increase of about 50% in estimates of the number of buildings that would be partially or totally collapsed.

Last, but not least, considering that the approach developed and applied in this work is based on measurements of seismic noise, their reliability has been assessed. A theoretical model describing the self-noise curves of different instruments usually adopted in microzonation studies (e.g., those used in Potenza, Istanbul and Bishkek) have been considered and compared with empirical data recorded in Cologne (Germany) and Gubbio (Italy). The results show that, depending on the geological and environmental conditions, the instrumental noise could severely bias the results obtained by recording and analysing ambient noise. Therefore, in this work I also provide some guidelines for measuring seismic noise.

Zusammenfassung

Aufgrund des enormen Wachstums neuer Megastädte und deren Vordringen in gefährdete Gebiete auf der einen Seite sowie der mangelnden Erdbebenvorsorge in vielen Entwicklungsländern auf der anderen Seite sind verbesserte Verfahren für die Beurteilung der Gefährdung sowie eine rasche Umsetzung bei der Raumplanung erforderlich. Im Rahmen der seismischen Gefährdungsabschätzung spielt insbesondere die Beurteilung lokaler Standorteffekte und deren Einfluss auf die durch ein Erdbeben verursachte räumliche Verteilung der Bodenerschütterung eine wichtige Rolle. Es ist daher unabdingbar, mittels seismischer Mikrozonierungsstudien diejenigen Bereiche innerhalb dicht besiedelter Gebiete zu ermitteln, in denen ein ähnliches Verhalten im Falle seismischer Anregung erwartet wird, um daraus eine zuverlässige Basis bei der Risikoabschätzung großer städtischer Gebiete zu erhalten. Aufgrund des schnellen Wachstums vieler Großstädte in Entwicklungsländern ist eine seismische Mikrozonierung zwingend erforderlich, stellt aber auch eine große Herausforderung dar; insbesondere müssen Verfahren verfügbar sein, mit deren Hilfe rasch eine Abschätzung der Standorteffekte durchgeführt werden kann. In der vorliegenden Arbeit entwickle ich daher Verfahren für die Untersuchung in Großstädten, die darauf abzielen, nicht-invasiv, kostengünstig und schnell durchführbar zu sein. Damit lassen sich innerhalb eines relativ kurzen Zeitraums große Gebiete untersuchen, falls der räumlichen Abstand zwischen den Messpunkten klein genug ist, um eine zuverlässige Mikrozonierung zu gewährleisten. Obwohl es eine gegenläufige Tendenz zwischen der Vollständigkeit aller Informationen und der Größe des untersuchten Gebiets gibt, versuche ich, diese Einschränkung durch Verknüpfung zweier Informationsebenen zu umgehen: In der ersten Ebene werden die Standorteffekte für einige Kalibrierungspunkte durch die Analyse von Erdbeben oder mittels anderer geophysikalischer Datensätze (z.B. Scherwellengeschwindigkeitsprofile) bestmöglich abgeschätzt, in der zweiten Ebene werden die Standorteffekte durch Einzelstationsmessungen des seismischen Rauschens für ein größeres Gebiet bestimmt. Die Mikrozonierung erfolgt hierbei mittels spezifischer, fallabhängiger Parameter unter Berücksichtigung eines geeigneten Anknüpfungspunktes zwischen den beiden Informationensebenen. Um diesen Ansatz der Mikrozonierung, der in dieser Arbeit verfolgt wurde, zu präzisieren, wurden in Potenza (Italien), wo eine beträchtliche Menge an Daten verfügbar war, verschiedene Verfahren untersucht. Insbesondere kann das Spektralverhältnis zwischen den horizontalen und vertikalen Seismometerkomponenten, welche für das seismische Rauschen an mehreren Orten aufgenommen wurde, als eine erste Näherung für die relative Verstärkung der

Bodenbewegung verwendet werden, um darauf aufbauend die beiden Informationsebenen zu verknüpfen und eine Mikrozonierung hinsichtlich des Verhältnisses der spektralen Intensität durchzuführen. Anschließend führte ich diesen Zwei-Ebenen-Ansatz auch für Istanbul (Türkei) und Bischkek (Kirgisistan) durch. Für die Mikrozonierung dieser beiden Städte habe ich denselben Hybridansatz, der Daten von Erdbeben und von seismischem Rauschen verbindet, verwendet. Für beide Städte wurde nach Gegenüberstellung der Resonanzfrequenz des Untergrunds, die zum einen mit Hilfe des seismischen Rauschens, zum anderen durch Analyse von Erdbebendaten bestimmt worden ist (erste Ebene), eine Karte der Resonanzfrequenz unter Verwendung weiterer Messungen des seismischen Rauschens innerhalb des Stadtgebiets erstellt (zweite Ebene). Durch die Anwendung dieses neuen Ansatzes sind vor kurzem zum ersten Mal auch Karten für die Resonanzfrequenz des Untergrunds für Istanbul und Bischkek veröffentlicht worden. Parallel dazu wurde für das Testgebiet in Potenza eine auf dem spektralen Intensitätsverhältnis (SIR) basierende Mikrozonierungskarte in ein Risikoszenario mittels der Regression zwischen SIR und makroseismischer Intensität (EMS) integriert. Diese Szenariostudie bestätigt die Bedeutung von Standorteffekten innerhalb der Risikokette; insbesondere führt deren Einbeziehung in das Szenario zu einem Anstieg von etwa 50% bei der Zahl der Gebäude, für die ein teilweiser oder gar vollständiger Zusammenbruch erwartet werden kann. Abschließend wurde der im Rahmen dieser Arbeit entwickelte und angewandte Ansatz auf seine Zuverlässigkeit geprüft. Ein theoretisches Modell, das zur Beschreibung des Eigenrauschens verschiedener Instrumente, die in der Regel in Mikrozonierungsstudien (z. B. in Potenza, Istanbul und Bischkek) zum Einsatz kommen, wurde untersucht, und die Ergebnisse wurden mit Daten verglichen, die vorher bereits in Köln (Deutschland) und Gubbio (Italien) aufgenommen worden waren. Die Ergebnisse zeigen, dass abhängig von den geologischen und umgebenden Bedingungen das Eigenrauschen der Geräte die Ergebnisse bei der Analyse des seismischen Rauschens stark verzerren kann. Deshalb liefere ich in dieser Arbeit auch einige Leitlinien für die Durchführung von Messungen des seismischen Rauschens.

Contents

List of tables

List of figures

List of abbreviations

CASCADE   Central Asian Cross-border Natural Disaster Prevention

DAS   Digital Acquisition System

EC8   Euro Code 8

EHV   Earthquake Horizontal to Vertical Spectral Ratio

EMS   European Macroseismic Scale

ESAC   Extended Spatial Autocorrelation technique

f_0 Fundamental frequency of vibration

F-K   Frequency-wavenumber

GEM   Global Earthquake Model

GIT   Generalised Inversion Technique

GrMPEs   Ground Motion Prediction Equations

H/V   Horizontal to Vertical spectral ratio

MLM   Maximum likelihood method

NEHRP   National Earthquake Hazard Reduction Program

NHNM   New High Noise Model (*Peterson,* 1993)

NHV   Noise Horizontal to Vertical Spectral Ratio

NLNM   New Low Noise Model (*Peterson*, 1993)

PDF   Probability Density Function

PSD   Power Spectral Density

PVS   Pseudo-velocity spectrum

RMS   Root Mean Square

RSM   Reference Site Method

S/N   Signal-to-Noise ratio

SI   Spectral Intensity

SIR   Spectral Intensity Ratio

SPES   Short Period Electromagnetic Sensor

SSR   Standard Spectral Ratio

I herewith declare that I have produced this paper without the prohibited assistance of third parties and without making use of aids other than those specified; notions taken over directly or indirectly from other sources have been identified as such. This paper has not previously been presented in identical or similar form to any other German or foreign examination board.

Potsdam, 09.09.2010

Angelo Strollo

Chapter

1

General introduction

1.1 Foreword

In many developing countries prone to large earthquakes, megacities are often growing rapidly without following the building requirements suggested by suitable seismic building codes. Therefore, under the perspective of a global seismic risk assessment as required by recent initiatives such as the Global Earthquake Model, this rapid increase in vulnerability requires the development of highly dynamic tools to estimate and communicate the associated seismic risk in an effective way.

Both Engineers and Seismologist are improving their tools to quickly react to this need. On the one hand, larger vulnerability and exposure data sets are becoming available by applying various techniques to investigate large areas (e.g., analysis of satellite images). On the other hand, the availability of new high quality seismological data provides considerable assistance to efforts in improving seismic hazard assessment at regional scales for many regions of the world. When seismic risk is evaluated at urban spatial scale, the assessment of local site amplification effects becomes a fundamental step for any reliable hazard oriented study (Figure 1.1). Therefore, earthquake microzonation studies, which aim at identifying macro-areas that are expected to respond in a similar way to a seismic event, become mandatory. Such activities are challenging when applied to large urban areas, and techniques suitable to evaluate the site effects within such contexts are required.
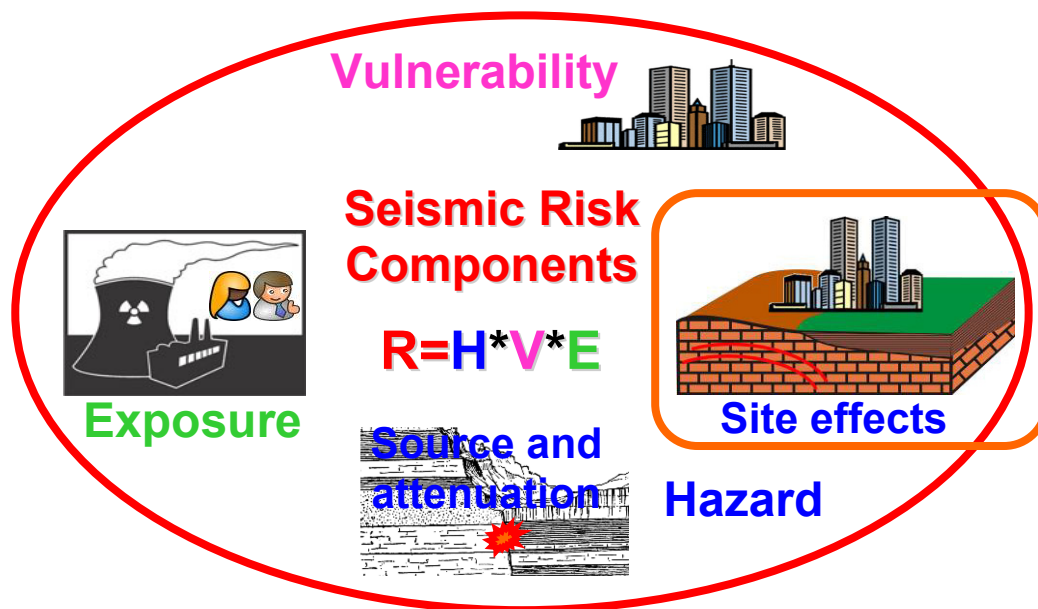
Fig. 1.1 Definition of the seismic risk R in terms of hazard (H), vulnerability of buildings (V) and exposure (E) of the considered site, for example in terms of population density or presence of critical facilities. The seismic hazard is defined by the combination of source, propagation and site effects.

Earthquake microzonation studies are generally considered over three different levels: 1) the first level is based on *"qualitative"* information inferred from geological maps by

simply discriminating between soft soil and hard rock; 2) the second level considers *"quantitative"* descriptions of the sites, such as site responses obtained from earthquake recordings, spectral intensities, fundamental frequencies of vibration, etc; 3) the third level merges the information from level 2 with that coming from invasive techniques, such as borehole data and geotechnical parameters obtained *in situ*.

While microzonation studies at the first level are generally available, only a few cities prone to large earthquakes have a second or third microzonation level adequately embedded in the city's urban planning schemes. In order to reduce this gap, the development of earthquake microzonation techniques suitable for providing at least a second level of microzonation with a relatively small effort in terms of time and resources is a crucial, although challenging, action.

Therefore, the main effort of the present thesis was directed towards the development of methodologies suitable for investigating site effects over large-scale urban environments, with the aim of them being non-invasive, cost-effective and quickly deployable. Different approaches, using seismic noise measurements as a central thread, are discussed and the results obtained by applying the proposed methodology to different towns are presented.

1.2 Overview

Site effects can be estimated by means of numerical simulations and experimental methods. The former range from simple 1D numerical calculations to methods that consider complex phenomena and model geometry. In general, the experimental methods are subdivided into two categories: reference site and non-reference site techniques (see, e.g., *Bard*, 1995).

Borcherdt (1970) was the first to propose the reference site method (RSM), which consists of comparing records at nearby sites, using one of them as the reference site. It is assumed that records from the reference site (in general a station installed on outcropping hard rock) contain the same source and propagation effects as records from the other sites. Therefore, differences observed between the sites are explained as being due to local site effects. This method is generally applicable only to data from dense, local arrays.

Andrews (1986) extended this method to large networks. He proposed the separation of the contributions of the path, the source, and the site by means of an inversion scheme termed the generalized inversion technique (GIT). Since in general the site amplification at a reference (hard rock) site is set to unity, this approach provides results analogous to those obtained by the RSM method. The major drawback of these methods is that a suitable reference site may not always be available (*Steidl et al.*, 1996). Therefore, non-reference site

techniques such as the horizontal-to-vertical (H/V) spectral ratio method are widely used. *Nogoshi and Igarashi* (1970) first introduced this technique, but *Nakamura* (1989) developed it further as a means of estimating the site response to S-wave propagation. Originally, it was proposed for interpreting ambient seismic noise measurements (NHV). *Lermo and Chavez-Garcia* (1993) applied the H/V technique to the S-waves of earthquake recordings (EHV) and developed a theoretical background for the technique using numerical modelling of SV waves.

The comparison of site responses obtained by the reference and non-reference site techniques (e.g. *Field and Jacob,* 1995; *Bonilla et al.,* 1997; *Riepl et al.,* 1998; *Triantafyllidis et al.,* 1999; *Parolai et al.,* 2000; 2001a; 2004) has shown that RSM and EHV usually provide site responses with similar shapes when the S-wave part of the seismogram is used in the analysis, while the fundamental resonance frequency of a site is consistently estimated by both methods. However, they can provide different levels of amplification, in particular at frequencies higher than the fundamental one. *Parolai and Richwalski* (2004) showed, by means of numerical simulations, that differences between the RSM and the EHV results are caused by the effect of waves converted at the bedrock depth that are included in the analysed windows.

NHV was shown to provide (by, amongst many others, *Haghshenas et al.,* 2008) a good estimate of the fundamental resonance frequency of the S-waves, but it underestimates the level of amplification with respect to GIT and RSM. Also, by using the P-wave part of the seismograms, the RSM and EHV methods have been found to provide consistent results only in some cases.

Recently, the engineering community has focused its attention on the spectral intensity (*Housner,* 1952) parameter as a tool for describing the severity of ground shaking, due to its stability (i.e., *Ueong,* 2009) in accounting for both the amplitude and frequency content of ground shaking. *Masi et al.* (2010) proposed spectral intensity as the suitable parameter to represent the severity of an earthquake, since it can be linked to macroseismic intensities via empirical relationships, and therefore can be easily adopted for calculating hazard and risk scenarios. When a reference site is available, the spectral intensity ratio (SIR) with respect to a reference site can also be calculated and used as a description of the local site amplification (*Pergalani et al* 1999, *Marcellini and Pagani* 2004, *Pergalani et al.* 2009). Importantly, it was found (*Marcellini and Pagani* 2004) that the range in the amplification found by SIR is comparable with the range of soil correction coefficients prescribed by several seismic codes. In particular, with respect to standard engineering practice in Italy, the design soil coefficient "S" given by *Rey et al.* (2002), (EC8) is directly comparable with SIR.

In this study I will show that a microzonation approach based on the combination of earthquake data and seismic noise can be used to carry out quantitative microzonation of urban areas. The method is first calibrated in Potenza (Southern Italy) and then applied, with the necessary modifications, to two large urban areas, namely Istanbul (Turkey) and Bishkek (Kyrgyzstan). Particular attention will be paid to the optimal combination of instruments and set up for seismic noise analysis.

1.3 Methods

As commented above, the empirical methods can be classified into two categories: reference site and non-reference site techniques (*Bard,* 1995). While the former need the existence of a station installed on a hard rock outcrop (the reference site), the latter assumes that one of the components of the ground motion (generally the vertical one) provides the input ground motion at the bedrock. As also stated above, methods based on spectral intensity can also be used as a reference site method.

Reference site techniques

Reference site techniques can be used by taking the direct spectral ratio of the same component of ground motion recorded at two nearby stations (Standard Spectral Ratio SSR) (Figure 1.2) or by deriving the site response via an inversion procedure (generalized inversion technique GIT).
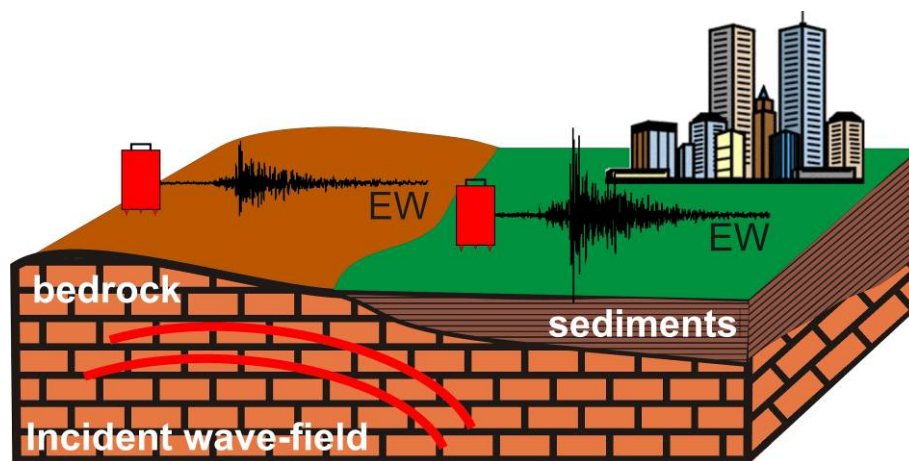
Fig. 1.2 Schematic description of the Reference Site Method. The reference site is taken to be that located on the bedrock.

Generalized inversion technique

The natural logarithm of the spectral amplitude $U_{ij}(f,r)$, observed at a recording site *j* for an event *i*, can be represented by:

$$\ln U_{ij}\left(f,r\right)=\ln S_i\left(f\right)+\ln Z_j+\ln A_{ij}\left(f,r\right) \qquad (1)$$

where $S_i(f)$ is the source function, $Z_j(f)$ is the site response, $A_{ij}(f,r)$ is a function accounting for attenuation, f is the frequency and r is the hypocentral distance.

For all events and stations, equation (1) describes a linear system of the form ***Ax=b***, which can be solved by using suitable inversion algorithms. The inversion can even be performed in two steps according to the procedure of *Castro et al.* (1990). In the first step, the inversion is carried out to separate the source and attenuation effects without introducing any parametric model to describe the attenuation term $A_{ij}(f,r)$. The trade-off between attenuation and source is resolved by requiring that attenuation assumes an *a priori* chosen value at a given distance, irrespective of frequency. In the second step, the inversion is carried out for the source and site functions, using the observed data that have been corrected for the attenuation results. The undetermined degree of freedom of the second inversion is resolved by constraining the logarithm of the site amplification of the reference station to 0, irrespective of frequency

Standard Spectral Ratio method

The Standard Spectral Ratio technique (SSR) consists of comparing records at nearby sites, using one as the reference site. It is assumed that records from the reference site (in general a station installed on outcropping hard bedrock) contain the same source and propagation effects as records from the other sites. This leads to

$$\frac{U_{ij}(f,r)}{U_{ik}(f,r)} = \frac{S_i(f)Z_jA_{ij}(f,r)}{S_i(f)Z_kA_{ik}(f,r)} \tag{2}$$

where k indicates the reference station and i and j are again the event and a recording site, respectively. If the stations are nearby and the reference station is not affected by site effects, then $Z_k=1$ and $A_{ij}(f,r) \approx A_{ik}(f,r)$. Therefore, the spectral ratio directly provides the site response. The major drawback of these methods is that rock stations may also still have their own site response.

Non reference site techniques

Non reference site techniques try to avoid the requirement of having a hard rock reference station, either by making the assumption that the vertical component of the ground motion is not affected by amplification and that it is similar to the horizontal component at the bedrock (when earthquake recordings are used), or by using seismic noise recordings which are generally dominated by surface waves (Figure 1.3). While the assumption in the first cannot be true for frequencies higher than the fundamental one (*Parolai and Richwalski,* 2004), the second suffers from the lack of correlation between the estimated amplification

level and that measured by earthquake data analysis. Nonetheless, both methods can satisfactorily estimate the fundamental resonance frequency of a site.
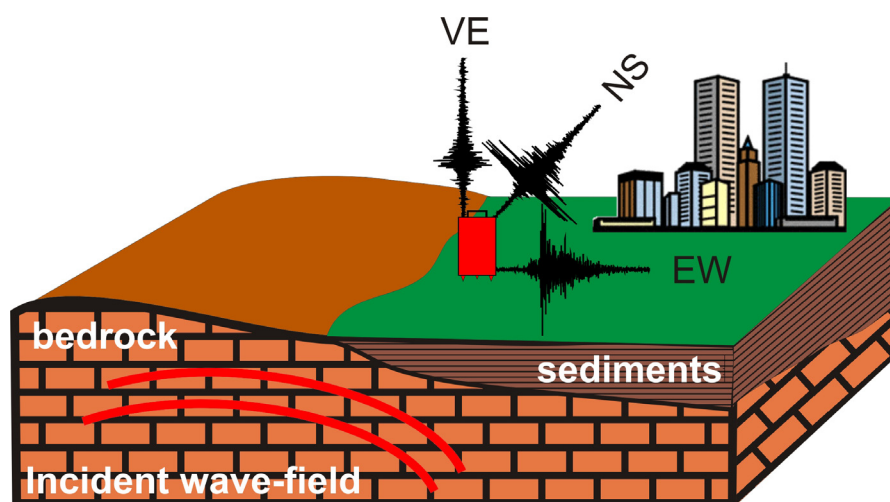
Fig. 1.3 Schematic description of the EHV method.

H/V spectral ratio of earthquake data (EHV)

The H/V spectral ratio technique was introduced by *Langston* (1979) as a method to determine crustal and upper-mantle structure from teleseismic recordings. The basic assumption of the method is that the vertical component of motion is not influenced by the local structure, whereas the horizontal components contain the P-to-S conversions due to the geology underlying the station. Therefore, by deconvolving the vertical component from the horizontal, one could estimate the site response. The technique has been applied in many studies (e.g., *Lermo and Chavez-Garcia*, 1993; *Field and Jacob*, 1995; *Lachet et al.*, 1996; *Bonilla et al.*, 1997; *Parolai et al.*, 2000, 2004; *Parolai and Richwalski*, 2004). In general, it was found that H/V ratios for S waves reveal the overall frequency dependence of the site response, even if the level of amplification, especially at frequencies higher than the fundamental one, can be different.

H/V spectral ratio of seismic noise (NHV)

The analysis of ambient noise has become a very attractive method to study site-response characteristics, because it is rapid and cost effective. In particular, the H/V spectral ratio (*Nogoshi and Igarashi*, 1970; *Nakamura*, 1989) has been widely used, even if its theoretical background is still not clear. In fact, whereas *Nakamura* (1989) assumed that the effect of surface waves can be either eliminated or neglected so that the NHV ratio is a reliable estimate of the S-wave site response, other authors (e.g., *Lermo and Chavez-Garcia*,

1994; *Lachet and Bard*, 1994; *Konno and Ohmachi,* 1998) showed that NHV ratios can be related to the ellipticity of Rayleigh waves. In this case, NHV provides a reliable estimation of the fundamental resonance frequency of the site because the ellipticity is peaked around it due to the vanishing of the vertical component. According to this interpretation, no straightforward relationship should exist between NHV peak amplitude and site amplification. A clear link between NHV shape and ellipticity of the fundamental mode of Rayleigh waves was shown by means of numerical simulations by *Fäh et al.* (2001). Furthermore, they used this evidence to derive S-wave velocity profiles by NHV inversion. In addition, *Arai and Tokimatsu* (2000) showed that the NHV shape is better retrieved when not only the fundamental mode of Rayleigh wave is simulated, but also when higher modes and Love waves are taken into account. *Parolai et al.* (2005), in deriving S-wave velocity profiles, forward modelled NHV spectral ratios by taking into account multiple mode Rayleigh waves and Love waves. Furthermore, Love wave contributions to the wavefield around the H/V peak has been recently investigated also by *Endrun* (2010).

Spectral Intensity

The original spectral intensity (SI) definition is showed below in equation (3) as the area under the pseudo-velocity spectrum (PVS), with 5% damping ξ, between 0.1 and 2.5 even though different integration interval are used to fit each case, which is dependent upon the building stock and the input seismograms,

$$SI = \int_{0.1}^{2.5} PVS(T,\xi)dT \qquad (3)$$

Where *PVS* is the pseudo-velocity spectrum, *T* is the period and ξ is the fraction of critical damping.

As stated above, SI is a stable estimator of the severity of ground shaking, accounting for both its amplitude and frequency content (e.g. *Ueong*, 2009; *Masi et al.*, 2010). Recently, *Chiauzzi et al.* (2010), following the approach and findings of *Housner*, (1952), developed a relationship between SI and Macroseismic Intensity (EMS) using data selected from the Italian accelerometric archive (*Itaca*, n.d.). This allows SI values to be easily used for calculating hazard and risk scenarios when the hazard is expressed in intensity and the vulnerability classes are related to it through fragility curves.

1.4 Earthquake Microzonation studies

The starting point of any microzonation study is generally the acquisition of information about the local geology and results from previous geophysical-geotechnical investigations, if

available, in order to plan in an optimal way the microzonation campaign. In fact, the microzonation level will depend upon, for example, the available budget, the extent of the area to be covered, and the depth of the soft sediments.

In this thesis I propose an approach based on the combination of two layers of information: in the first layer, the site effects at a few calibration points are estimated by analyzing earthquake data or from using other geophysical information (e.g., shear-wave velocity profiles); in the second layer, the proxy for the site effects over a larger areal coverage are estimated by means of single-station noise measurements. The two layers are then merged together, combining the high quality of the first layer with the good spatial coverage of the second. This approach allows us to have a harmonized methodology able to provide a second level microzonation (Figure 1.4).
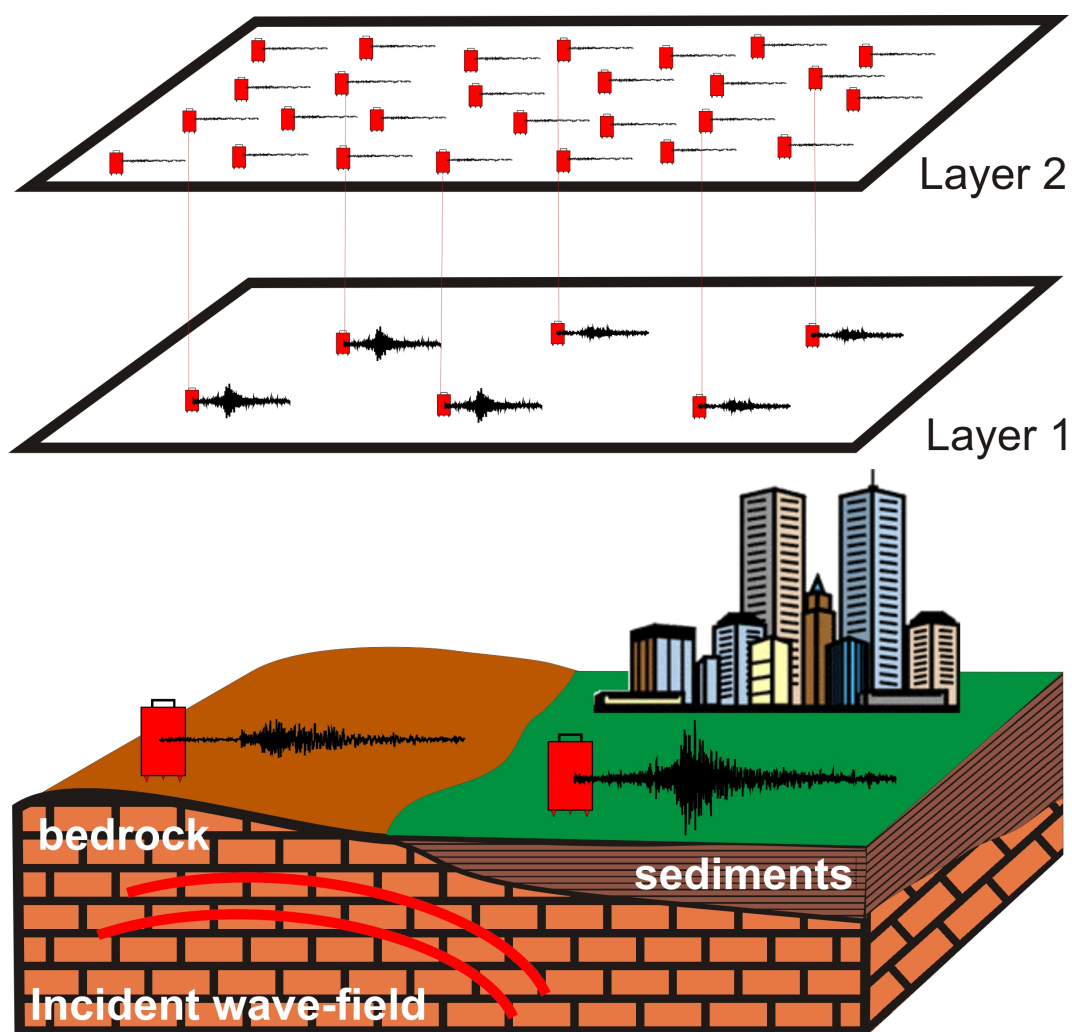
Figure 1.4 Simplified scheme of the approach followed in this thesis: In Layer 1, only a few sites are characterized by means of earthquake data, while in Layer 2, noise measurements ensure a good spatial resolution.

In order to develop the two-layer approach proposed in this work, the methods for estimating site effects previously described have been combined and tested in Potenza (Italy), where a considerable amount of information is available. Following this, a similar approach, combining earthquake and noise data, has been used for the microzonation of two different large cities, namely Istanbul (Turkey) and Bishkek (Kyrgyzstan). For both cities, after having calibrated the fundamental frequencies of resonance estimated from seismic noise with those obtained by analysing earthquakes (first layer), a new fundamental frequency map has been computed using the noise measurements performed within the town (second layer). In the following, the procedure and the main results are summarized.

Earthquake and noise data

In order to characterize the site response of some representatives sites within an urban area (i.e., the calibration points of the first layer, Figure 1.4), earthquake data have been collected either by installing a temporary seismic network, as in the case of Potenza and Bishkek (*Chapters 3* and *5*, respectively) or considering the recordings from already existing permanent stations (Istanbul, *Chapter 4*). Depending upon the availability of data, different methods for assessing the site effects have been applied in the three microzonation studies. In particular, at the Potenza test-site, all of the methods described above (i.e., SSR, GIT, EHV, SIR, figure 1.5) were applied, only SSR and EHV were considered for Bishkek, while for Istanbul, only the EHV was applied at the calibration sites.

A large number of single station noise measurements have been carried within the three cities (about 200 for each one) in order to improve the spatial sampling of the second layer (Figure 1.4). For each noise measurement site, the NHV spectral ratio has been computed. After having checked the reliability of the fundamental frequencies estimated from noise with respect to those computed using earthquakes recorded at the calibration sites, a map for the fundamental frequency of resonance has been computed for each town (Figure 1.6). Moreover, since in Istanbul only a few earthquake recordings were available considering the large area investigated and the geological heterogeneity, S-wave velocity profiles were experimentally derived for 8 sites from seismic noise recordings carried out using micro arrays of sensors (e.g. *Okada*, 2002). Thus, the available "calibration information" was improved and the lack of earthquakes was accounted for *(Chapter 4)*. Also in Bishek, one micro array measurement was carried out in order to have information on the S-wave velocity structure, which was expected to be quite high, along with a very deep basement *(Chapter 5)*.

In Potenza, results from the conventional methods have been compared with the SIR amplification factors (figure 1.5). It was found that the variability of SIR values correlates

well with the results of the SSR and GIT techniques. In particular, when the latter showed large amplifications, higher SIR values were also found.
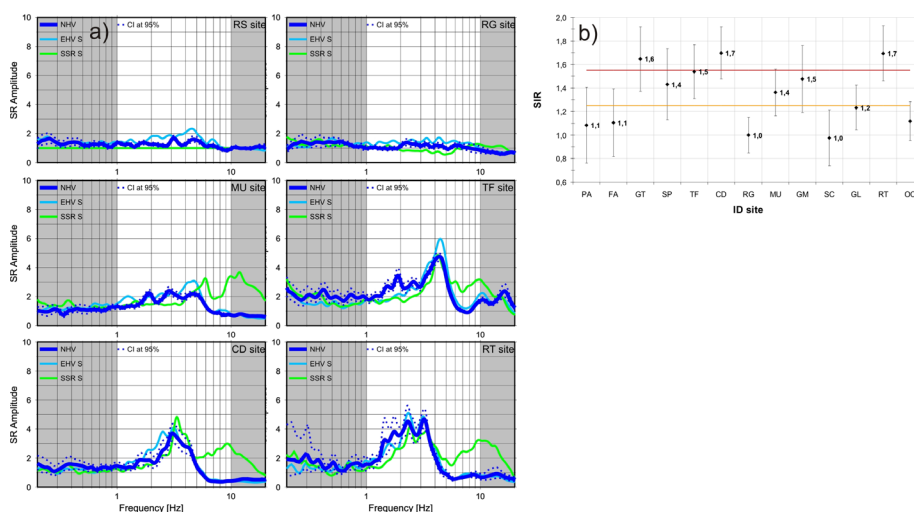
Figure 1.5 a) NHV, EHV and SSR for the Potenza test site; **b)** SIR values
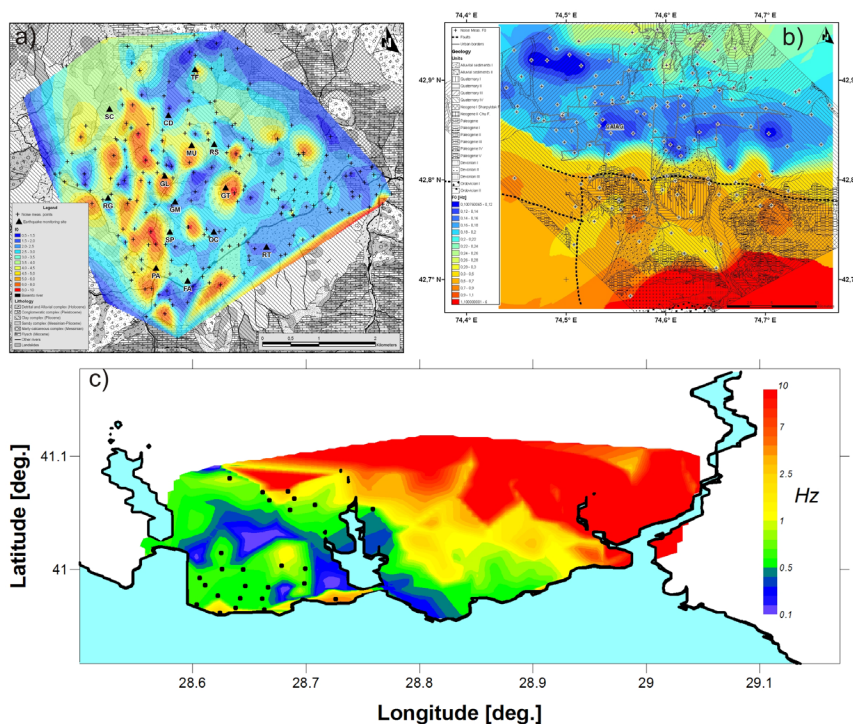
Figure 1.6 Fundamental frequency maps for (a) Potenza, (b) Bishkek and (c) Istanbul.

Combining the two layers (Earthquake and Noise)

Over the last few years, different attempts in correlating the NHV function with the site response have been carried out. Recently, *Bragato et al.*, (2007), following the approach used by *Rodriguez and Midorikawa*, (2002), used NHV functions to identify homogeneous areas in terms of site response by means of cluster analysis, following a Bayesian approach. Similarly,

Cara et al., (2010) used the correlation between NHV functions and local geology to explain the damage patterns of a past earthquake in Palermo (Italy). In both studies, the sites are clustered considering similarity in the NHV function but without associating any site response function to each cluster.

After having evaluated the reliability of the NHV functions and SIR values in representing the site effects occurring at the calibration sites in Potenza with respect to the GIT and SSR results, the NHV functions have been used as a proxy to extrapolate the earthquake-based information (layer 1) and to the noise measurements points. In particular, a correlation procedure described in *Chapter 3* has been developed to associate the two layers. As a final product, a map in terms of SIR amplification factors has been produced (Figure 1.7).
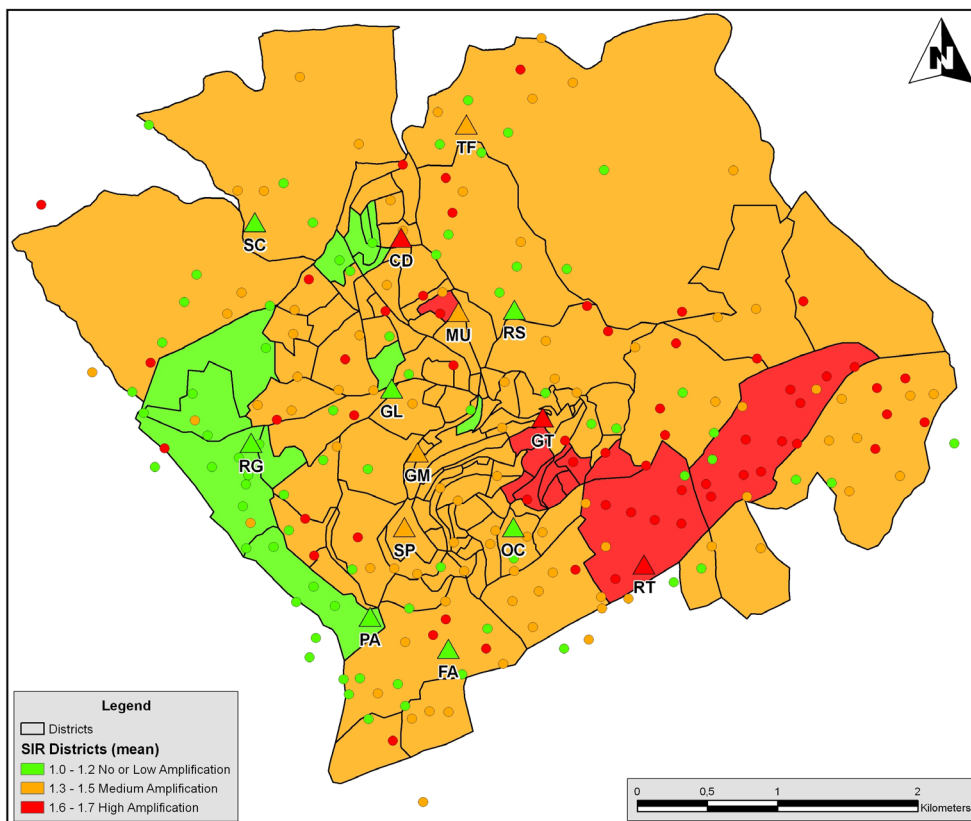
Figure 1.7 Microzonation map of Potenza in terms of spectral intensity ratio.

Considering the difference in the 1st layer data set for Istanbul and Bishkek, the fundamental frequency instead of the full NHV function was used as a proxy. Thus, after having compared the fundamental frequencies at the calibration sites, the fundamental frequency maps were then derived.

The novelty proposed within this work is to use seismic noise as a proxy to connect the two layers of information as indicated in figure 1.4. Thus, independent of the environmental conditions, the completeness of layer 1, or the parameter used to estimate site amplification,

the information can be extrapolated and spread over layer 2. In fact, while recording earthquakes or having detailed geotechnical information from boreholes is quite complicated, seismic noise is available everywhere and at anytime, especially in urban areas.

1.5 Reliability of Noise measurements

It is worth noting that in the three cases explored in this chapter, as well as in most recent work about microzonation, the results are based on ambient noise measurements. This is mainly due to the fact that the use of NHV, also termed the Nakamura technique (*Nakamura,* 1989), is suitable for large urban areas since it is cost effective. Considering the small amplitude of the signal treated, particular care is needed in the selection of the most suitable instrument for recording ambient noise. The results of any analysis performed on noise, such as the NHV spectral ratios, could be severely biased by instrumental noise when the measurements are performed under particular environmental conditions, such as over deep sedimentary basins during periods of weak microseismic activity. For this reason, within this thesis I have investigated the performance of the instruments generally used for noise measurements and provide some general guidelines for their selection.
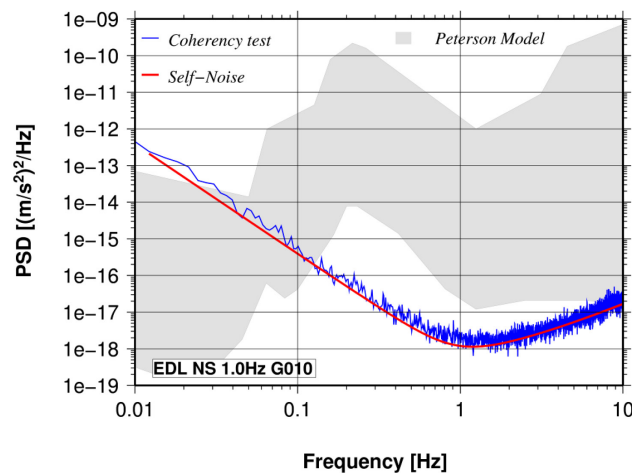
Figure 1.8 Figure showing the self-noise model of the most used configuration in this work. In particular, there is a comparison between estimates of theoretical self-noise (black) and experimental self-noise (grey) from the coherency test. The grey shading indicates the area delimited by the NLNM and NHNM of Peterson (1993).

The importance of the instrumental issue when ambient noise is recorded has been recognized and addressed in recent studies (e.g., *Chavez-Garcia and Tajeda-Jacome,* 2010) Furthermore, during the SESAME European project, some specific tasks were also dedicated to assess the performance of different instruments when used to measure ambient noise (*Guiller et al.,* 2008; *Chatelain et al.,* 2008). In fact, during the SESAME project, particular emphasis was placed on the instrumental issue. However, only empirical observations acquiring noise in different conditions have been showed. In contrast, in this work (*Chapter*

2) the self noise models for all possible configurations used in our noise acquisition have been carried out (Figure 1.8).

Subsequently, the continuous measurement of microseismic activity has been used to assess the reliability of the fundamental resonance frequency estimated by means of the NHV over the 0.1–1 Hz frequency range, using short-period sensors (natural period of 1 s). NHV have been calculated over a long time window and its stability in time evaluated in two alluvial basins with different sedimentary cover thicknesses, namely the Lower Rhine Embayment (Germany) and the Gubbio Plain (Central Italy). The results confirm the reliability of the model proposed in the first part of the *Chapter 2* for predicting the instrumental noise curves. Furthermore, both studies confirmed that, for particular environmental conditions, some instruments and settings could fail to identify the correct frequency of resonance (Figure 1.9).
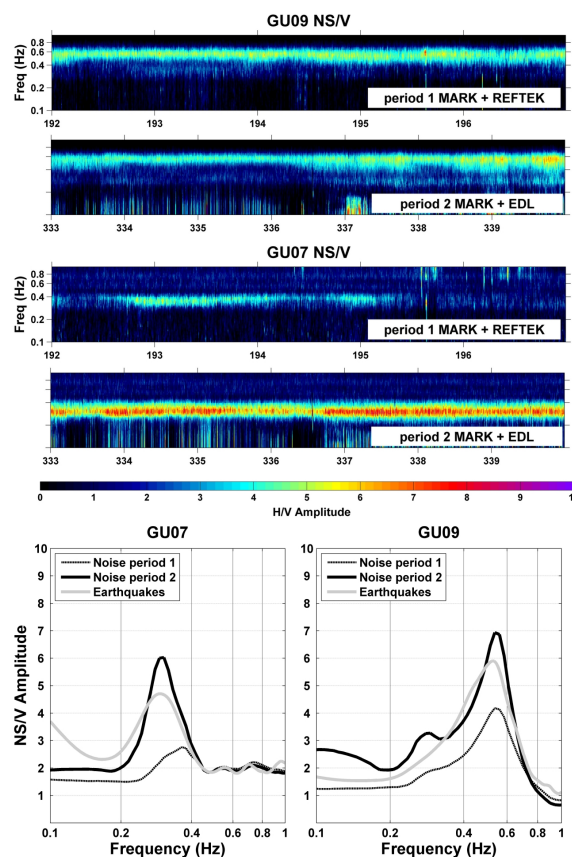
Figure 1.9 Upper part: NS/V spectral ratios for stations GU09 (top panels) and GU07 (bottom panels) over the period 12-16 July and 29 November-5 December, 2005. Average of the same data represented in the upper part. Stations GU07 and GU09 istalled in Gubbio (Italy).

1.6 Conclusions

The research described in this dissertation is concerned with the development of techniques that allow site-effects investigations to be conducted in large urban areas in a relatively short time and for relatively low costs. In particular, different well-assessed standard methods have been nested within an innovative two-level approach that combines

high quality but sparse information (generally based on earthquake or geotechnical data) with simplified site-effect estimators available at a high spatial resolution These two layers have been combined together using a proxy, based on seismic noise, calibrated for the area of interest. The selection of a suitable proxy is problem-dependent and its selection is driven by the environmental conditions, in particular by the amount of information *a priori* known, and depends on which estimator has been selected for quantifying the site effects.

The novelty of the developed approach is the way in which the information provided by each layer is combined together. Within layer 1, the relationship between the *a priori* selected parameter (e.g., spectral intensity ratio for the case of Potenza) and the seismic noise based proxy (e. g., the NHV function) is calibrated for those sites where the site effects can be evaluated with accuracy (e.g., the earthquake monitoring sites in Potenza). Then, using the calibrated proxy, the site effect estimator is evaluated for all the noise measurement points available within layer 2 (Figure 1.4). This approach is based on the assumption that sites with similar NHV functions respond in a similar way with respect to the selected parameter when exited by an earthquake. The approach has been applied for the first time to the Potenza test site (*Chapter* 3). The complex topography and the strong variability of geological conditions over a limited extent, as well as the large amount of available data, allowed us to test the proposed two-layer procedure. The Spectral Intensity Ratio (SIR) was selected to quantify the expected ground motion and its suitability in mapping the site affects has been validated by applying standard reference and non-reference site methods (e.g., SSR and EHV). By means of a correlation analysis between the NHV evaluated at the calibration sites and the same function evaluated at each noise measurements points, site-effects mapping was carried out for Potenza in terms of SIR. The results have been provided in terms of maps matching the requirements of engineers who calculated the impact of a scenario earthquake.

In particular, the scenario study carried out by *Chiauzzi et al.,* (2010) using a regression relationship between spectral intensity (SI) and macroseismic intensity (EMS), confirmed the importance of correctly accounting for site effects within the risk chain. In fact, their introduction in the scenario led to an increase of about 50% in the predicted number of buildings partially or totally collapsed. This application showed the potential of the proposed approach for preparing realistic seismic risk scenarios for large urban areas, providing the input for the vulnerability assessment using either damage probability matrixes or fragility curves. Moreover, this application confirmed that SIR is a suitable parameter to easily include the outcomes from a microzonation study within the seismic hazard evaluated at a regional scale. Finally, it is worth noting that the Spectral Intensity (SI) can be calculated using different period ranges providing specific amplification factors for specific building

typologies (i.e., effectively incorporating a dependence on the frequency of vibration). Moreover, the integration interval can be optimized in order to define SIR intervals that correctly represent the soil amplification coefficients introduced in many building codes. Thus, empirical estimates of site effects can be easily considered by engineers when designing new buildings.

For the first time, a map of the fundamental resonance frequency (f_0) has been computed for Western Istanbul (Turkey) and Bishkek (Kyrgyzstan), following the two-layer approach proposed in this work (respectively in *Chapters 4* and *5*). For these towns, the reliability of f_0 estimated by computing the NHV ratios was first assessed at the monitoring sites from which earthquake recordings were also available. In the next step, the f_0 was evaluated for the whole city using noise measurements. In this case, only f_0 has been mapped instead of SIR but, considering the extent of the investigated area, this is already a quite challenging task. Furthermore, as soon as data dealing with strong historical earthquakes is made available, the full procedure tested in Potenza will also be applied to Bishkek.

The reliability of the results is also strictly related to the reliability of the NHV function. Therefore, *Chapter 2* discusses this issue extensively. The reliability of NHV has been investigated by first calculating the instrumental self noise models for all the instruments widely used in this field. Second, the self noise models have been compared with data collected within two deep sedimentary basins, Cologne (Germany) and Gubbio (Italy). The tests confirmed, even more than what was expected, that in some conditions of acquisition (instrumental and environmental), the NHV function become flat and was therefore not reliable below a certain frequency. Therefore, guidelines have been provided for when dealing with such data, noting that seismic noise must be handled with care, especially when the interest is focused on frequencies below 1 Hz.

Finally, the new approach for earthquake microzonation studies proposed here allows us to obtain at least a second level microzonation for large cities within a reasonable period of time (generally a few months) and at an acceptable cost (a few thousand euro when the instruments are available). Moreover, the extrapolation of the site effects using a proxy based not only on the fundamental frequency of resonance, but considering the full shape of the NHV function allows the provision of microzonation maps in term of different calibrated parameters, which can serve as a suitable seismic input for design purposes, while considering to local or regional seismic regulations.

In conclusion, the approach outlined in this thesis is particularly suitable for microzonation studies in developing countries, performed within the framework of global projects aiming at introducing harmonized approaches for risk assessment.

Chapter

2

Reliability of instruments used for quick noise measurements*

2.1 Suitability of short-period sensors for retrieving reliable H/V peaks for frequency less than 1 Hz

Abstract

Using three different short-period electromagnetic sensors with resonance frequencies of 1 Hz (Mark L4C-3D), 2 Hz (Mark L-22D), and 4.5 Hz (I/O SM-6), coupled with three digital acquisition system, the PDAS Teledyne Geotech, the REFTEK 72A, and the Earth Data Logger PR6-24 (EDL), the effect of the seismic instruments on the horizontal-to-vertical spectral ratio (H/V) using seismic noise for frequencies less than 1 Hz has been evaluated. For all possible sensors - acquisition system pairs, the background seismic signal and instrumental self-noise power spectral densities have been calculated and compared. The results obtained when coupling the short-period sensors with different acquisition systems show that the performance of the considered instruments at frequencies < 1 Hz strongly depends upon the sensor-acquisition system combination and the gain used, with the best performance obtained for sensors with the lowest resonance frequency. For all acquisition systems, it was possible to retrieve correctly the H/V peak down to 0.1-0.2 Hz by using a high gain and a 1 Hz sensor. In contrast, biased H/V spectral ratios were retrieved when low-gain values were considered. Particular care is required when using 4.5 Hz sensors since they may not even allow the fundamental resonance frequency peak to be reproduced.

Introduction

It is well known that subsurface geology can strongly affect both the amplitude and lengthening of the earthquake-induced ground shaking recorded at the Earth surface. The assessment and consideration of local site amplification effects is mandatory for studies aiming at seismic hazard assessment, such as the calibration of ground motion prediction equations (GrMPEs) or the determination of ground-shaking scenarios computed for different levels of source and propagation complexity. Since local geology can vary significantly over distances of only a few hundreds meters, the assessment of site response within large urban areas may require measurements at a large number of sites.

Moreover, the chance of recording seismic events in earthquake-prone urban areas can be small, either due to a low signal-to-noise ratio or to a low rate of seismicity. Therefore, techniques that allow information about site response to be obtained without using earthquake recordings and at a low cost have recently gained popularity. Among these, the Nakamura technique (*Nakamura*, 1989) allows the estimation of the fundamental resonance frequency of a site from the peak in the horizontal-to-vertical (H/V) spectral ratio of microtremor

measurements. The requirement of performing low-cost and rapid measurements therefore affects the choice of the equipment employed. For example, short-period sensors are often preferred to broad-band ones because of their ease of installation, their robust nature and their relatively low-cost. Due to budget limitations, microzonation studies based on seismic noise measurements are also performed by using low-cost, but lower dynamic range, acquisition system.

It follows that when microtremor measurements are used to infer information about the site response, it is necessary to evaluate the contribution to the recorded seismic signal of both the ambient seismic vibrations, that is the signal that carries information about the source generating it and the medium through which it propagates, and of the self-noise of the instruments. In fact, high instrumental noise can limit the exploitability of the seismic noise at frequencies lower than the sensor corner frequency, affecting the estimate of the fundamental resonance frequency of a site from the peak in the H/V.

Nowadays, the Nakamura technique is widely applied for estimating local site effects, especially in engineering seismology. While this technique is quite simple to undertake, many studies suffer from not fully appreciating the many issues associated with instrumental seismology. Therefore, the issue of the reliability of the H/V spectral ratios, and their dependence on the equipment used, must be addressed not only for the interest of people working in engineering seismology, but also to avoid future misinterpretation of the results.

Previous studies were performed either to examine the effect of short-period sensors on the detection of the seismic noise signals at frequencies lower than 1 Hz (e.g. *Riedesel et al.*, 1990; *Rodgers*, 1992, *Rodgers*, 1994) or to test the performance of different kinds of seismic sensors by directly comparing the results obtained from the inferred H/V spectral ratio (*Mucciarelli*, 1998; *Parolai et al.*, 2001). Recently, a comparison of results obtained from different kinds of acquisition system and sensor was carried out by *Guillier et al.* (2008), with an experimental design optimized for investigating the effects in the higher frequency range (> 1 Hz).

In this study the effect of the acquisition system and sensor on the H/V peak, when it is expected to occur at frequencies lower than 1 Hz, is evaluated by considering three different short-period electromagnetic sensors with resonance frequencies of 1, 2, and 4.5 Hz coupled with three different digital acquisition systems. In this work, for each sensor and acquisition system couple, the Power Spectral Density (PSD) of the instrumental self-noise is first calculated and compared with the PSD of recordings from a broad-band station, installed in the area of Cologne (Germany) at a site where the resonance frequency is expected to be about 0.2 Hz (*Parolai et al.*, 2004). Next, the broad-band seismic noise signal is added in the

time domain to the self-noise and the H/V spectral ratios calculated and compared with those obtained by using the original broad-band recordings. Finally, the results are discussed and suggestions for an optimized seismic noise acquisition for H/V spectral ratio calculations are provided. In the following, so as to avoid confusion when using different terms that are synonymous (ambient seismic vibration, seismic noise, microtremor, ambient noise), ambient seismic vibration will refer to the input to our system (digital acquisition system plus short-period sensor). The output will be defined as the background seismic signal, which is the input combined with the instrumental self-noise. Moreover, two acronyms will be used: SPES instead of short-period electromagnetic sensor and DAS instead of digital acquisition system.

Self-noise model and its reliability

Similarly to *Rodgers* (1994), the acceleration power (PSD) self-noise model for a SPES is described by:

$$P_{sn}(f) = \frac{E_n(f) + Q_n}{|H(f)|^2} + S_n \qquad (\text{m/s}^2)^2/\text{Hz} \qquad (1)$$

where S_n indicates the suspension noise, E_n the total electronic noise, Q_n the quantization noise, and $|H(f)|$ is the modulus of the transfer function of the SPES. The signal loss due to the voltage splitting between the coil resistance r_c and the damping resistor r_d is included in $|H(f)|$ using the open circuit generator constant G_g obtained multiplying G_s in Table 1 by: $\left(\dfrac{r_d}{r_c + r_d}\right)$.

The suspension noise term S_n is calculated using:

$$S_n = 16\pi \frac{kT\zeta f_0}{M} \qquad (\text{m/s}^2)^2/\text{Hz} \qquad (2)$$

where k is the Boltzmann's constant, T is the sensor temperature in degrees Kelvin (fixed to 293), ζ is the damping ratio, f_0 is the resonance frequency of the spring-mass system and M is the sensor mass.

The generalized total electronic noise E_n for the DAS considered in this study is

Error! Bookmark not defined. $E_n(f) = 2V_{00}\left(\dfrac{f_{cv}}{f} + 1\right) + I_{00}\left(\dfrac{f_{ci}}{f} + 1\right)r_p^{\ 2} + 4kTr_p \quad \text{V}^2/\text{Hz}$

$$(3)$$

where f_{cv} and f_{ci} are the corner frequencies for the voltage and current noise PSD, respectively. The resistor r_p is the parallel combination of the damping resistor r_d and the coil resistance r_c (all in ohms), V_{00} and I_{00} are the high frequency levels of the operational amplifier (op-amp) voltage and current noise PSDs, respectively, while the factor of 2 is

introduced because the instruments we consider, have two op-amps in the input stage. Therefore, the voltage noise term is doubled.

The power spectral density of the quantization noise Q_n can be defined as:

$$Qn = \frac{\Delta^2}{12}\frac{1}{f_N} \qquad V^2/Hz \qquad (4)$$

where Δ is the quantization interval, also called the least significant bit voltage of the DAS, and f_N is the Nyquist frequency (*Sleeman et al.*, 2006). This formula defines the quantization noise for an ideal analogue-digital converter (ADC) with no over-sampling and no digital anti-alias filtering. When the DASs use ADCs of a sigma-delta type, as in our case, the quantization noise can be empirically calculated using:

$$Qn = \frac{U^2_{peak}}{2}10^{-SNR}\frac{1}{f_C} \quad V^2/Hz \qquad (5)$$

where U_{peak} is the peak input voltage, *SNR* is the full scale signal-to-noise ratio (dynamic range) in dB and f_C is the upper corner frequency of the (digital) anti-aliasing filter, typically $\sim 0.8 f_N$ (*Wesson*, 2004). The signal-to-noise ratio varies with sampling rate, while the peak input voltage is inversely proportion to the gain. Generally, these *SNR* values for a specific sampling rate and U_{peak} values for a certain gain are available from the manufacturers. The Q_n values adopted in this work are for a fixed sampling rate of 100 samples/sec and the extreme values to which the pre-amplifier gain of each recording system can be set.

Short period electromagnetic sensor (SPES) Parameters							
SPES	**Freq.** [Hz]	**G_s** [V/m/s]	ζ	**M** [Kg]	**r_c** [Ohms]	**r_d** [Ohms]	**r_p** [Ohms]
Mark L4C-3D	1.0	276.4	0.70	1.0000	5500.00	8900.00	3399.30
Mark L-22D	2.0	112.0	0.80	0.0728	5470.00	14300.00	3956.55
I/O SM-6	4.5	28.5	0.69	0.0111	375.00	10000.00	361.44

Table 2.1 SPES's parameters.

Digital acquisition system (DAS) Parameters							
DAS	**Gain**	**Amplifier**	**V_{00} [V^2/Hz]**	**f_{cv} [Hz]**	**I_{00} [A^2/Hz]**	**f_{ci} [Hz]**	**Q_n [V^2/Hz]**
EDL PR6-24	1	OP-227	9.00E-18	2.7	1.60E-25	140	7.22E-15
EDL PR6-24	10	OP-227	9.00E-18	2.7	1.60E-25	140	7.22E-17
REFTEK 72A	1	OP-27	9.00E-18	2.7	1.60E-25	140	3.02E-13
REFTEK 72A	32	OP-27	9.00E-18	2.7	1.60E-25	140	2.89E-16
PDAS	1	OP-77	1.00E-16	2.0	6.00E-26	200	2.50E-13
PDAS	100	OP-77	1.00E-16	2.0	6.00E-26	200	2.50E-17

Table 2.2 DAS's parameters.

Figure 2.1 shows the self-noise PSD and the contribution of each term mentioned above when a EDL PR6-24 is coupled with the three SPESs, as well as the area delimited by the

New Low Noise Model (NLNM) and New High Noise Model (NHNM) of *Peterson* (1993) (hereinafter called the Peterson Model).
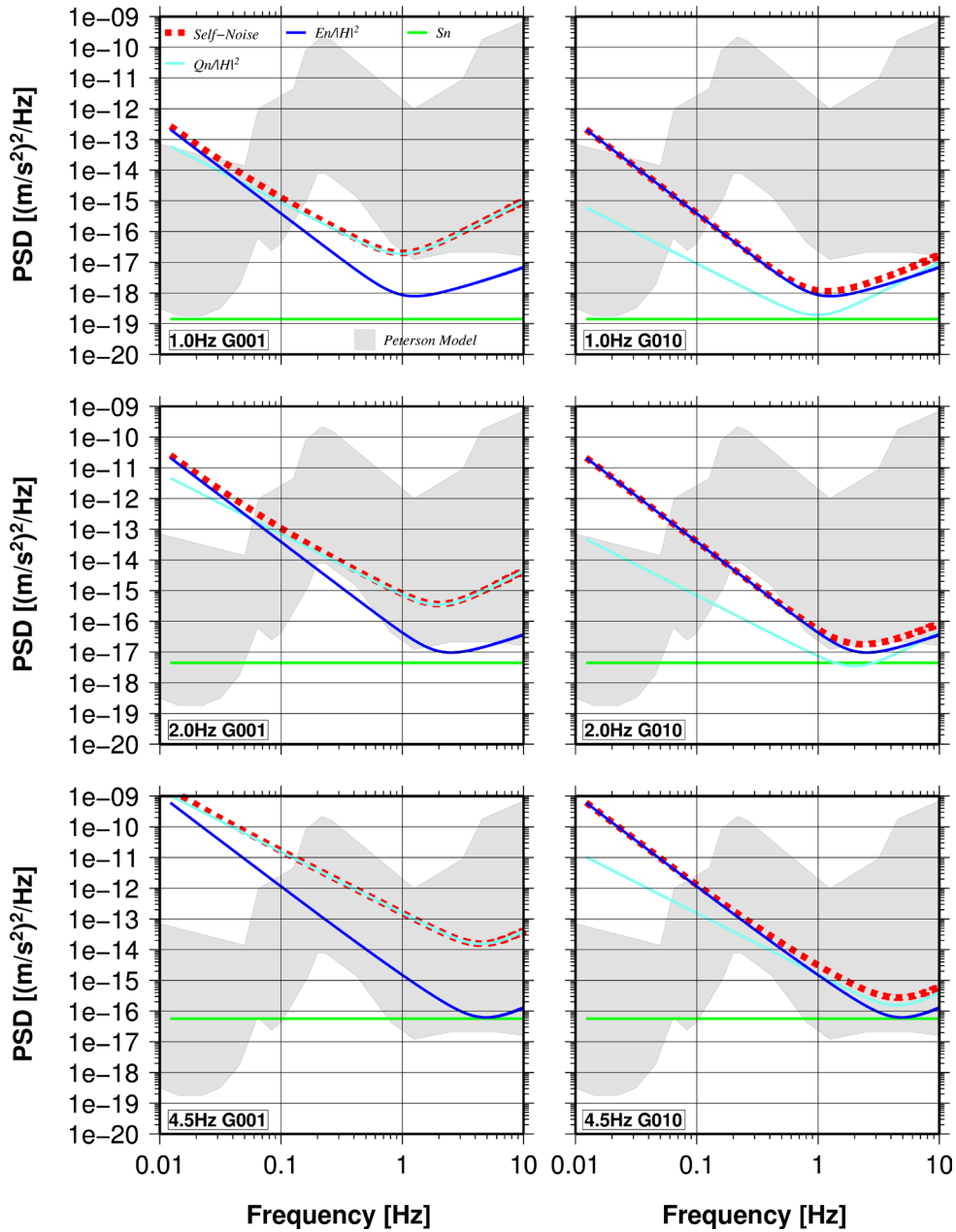
Figure 2.1 Comparison of different components of self-noise for the EDL: Electronic Noise (E_n blue), Quantization Noise (Q_n light blue), Suspension Noise (S_n green) and total self-noise (thick dashed red); the grey shading indicates the area delimited by the NLNM and NHNM of *Peterson* (1993). Left: Results obtained for a gain equal to 1 and different SPESs (1,2 and 4.5 Hz). Right: Results obtained for a gain equal to 10 and different SPESs.

All parameters have been fixed according to Table 2.1 (SPES parameters) and Table 2.2 (DAS parameters). In the case of a gain of 1, the quantization noise Q_n is generally the dominant term for frequencies higher than 0.07, while setting the gain to 10 the electronic noise E_n is dominating especially in the low frequency range. Similarly, we find Q_n provides the larger contribution to the self-noise at low gain, and E_n dominates for high gains, for the REFTEK 72A, which uses the same amplifier as the EDL (Figure A1a, appendix A), and for

the PDAS Teledyne Geotech (Figure A1b, appendix A) which uses a different amplifier. Variability in the results also depends upon the SPES that is connected to the DAS, especially for high gain values.

Due to the strong dependence of the results on the gain used, in the following, the calculations are carried out considering gains of 1 and 10 for the EDL, 1 and 32 for the REFTEK 72A, and 1 and 100 for the PDAS Teledyne Geotech, each representing extreme cases.

In order to validate the self-noise model proposed in this paper, one can obtain a measure of the self-noise by substituting the SPES with an ohmic resistor that has the same resistance as the coil. However, such a resistor will not exactly represent the electric impedance of the unlocked SPES, and therefore this procedure is not meant to precisely measure the electronic self-noise (*Wielandt*, 2002). *Holcomb* (1989), proposed a method based on coherency analysis that requires the recording of background seismic signal using two identical instruments that operate side by side and are exposed to the same input. The main assumption of this method is that the coherent part of the recordings is the ambient seismic vibration, while the incoherent part is related to self-noise (same contribution for each SPES). The limitations of the method are that a relatively quiet location (30-40 dB ambient seismic vibration / self-noise) as well as careful installation are required, since tilt or misalignment could produce additional incoherent noise. In order to verify the reliability of our theoretical estimates of self-noise PSD, that have the advantage of being easily and
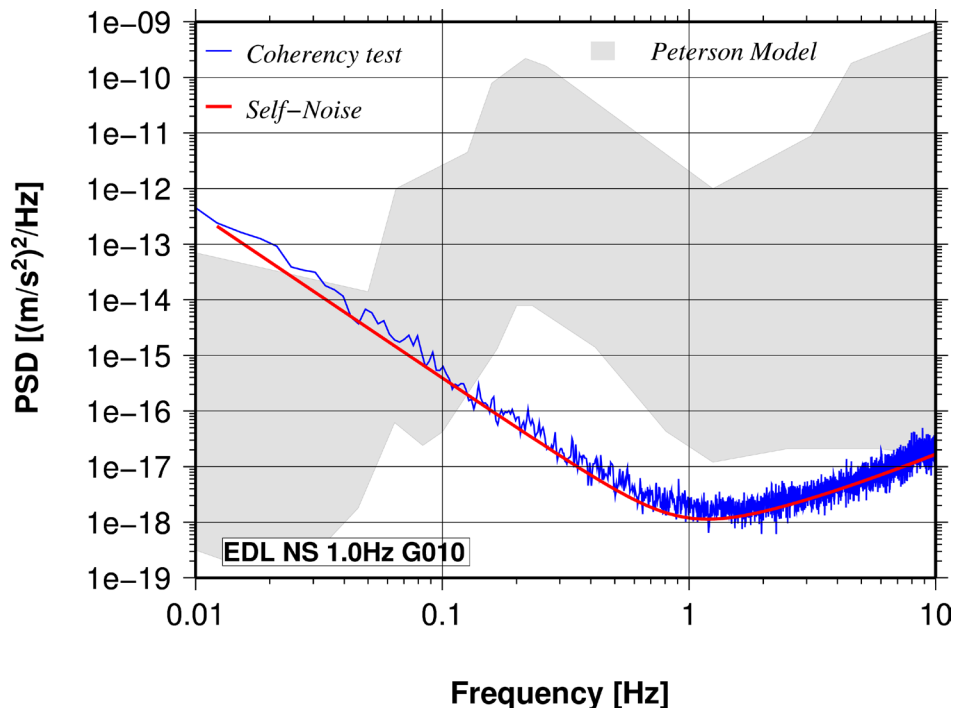
Figure 2.2 Comparison between estimates of theoretical self-noise (red) and experimental self-noise (blue) from the coherency test. The grey shading indicates the area delimited by the NLNM and NHNM of *Peterson* (1993).

rapidly calculated for each possible DAS and SPES couple, the coherency test was carried out using two Mark L4C-3D (1 Hz) connected to a 6-channel EDL PR6-24 (gain=10). The test was carried out in the Geodynamical Observatory Moxa (MOX) where the experimental conditions are optimal for this kind of test (*University of Jena, n.d.*). The corresponding empirical self-noise curve is shown in Figure 2.2 and compared to that obtained from the theoretical approach. The excellent agreement of the results indicates the reliability of our theoretical estimates.

Data and H/V spectral ratio calculation

A network of 44 seismic stations was deployed in the Cologne area between the end of April and the beginning of June 2001, with the aim of recording local and regional seismicity, and ambient seismic vibration (*Parolai et al.*, 2004). In this study we consider 30 minutes of ambient seismic vibration recorded at the station K38 on May 15th starting at midnight. The equipment used was a Güralp CMG-3ESPD seismic acquisition system and a broad-band sensor (all in one). Figure 2.3 (top panels) shows the selected ambient seismic vibration time series.
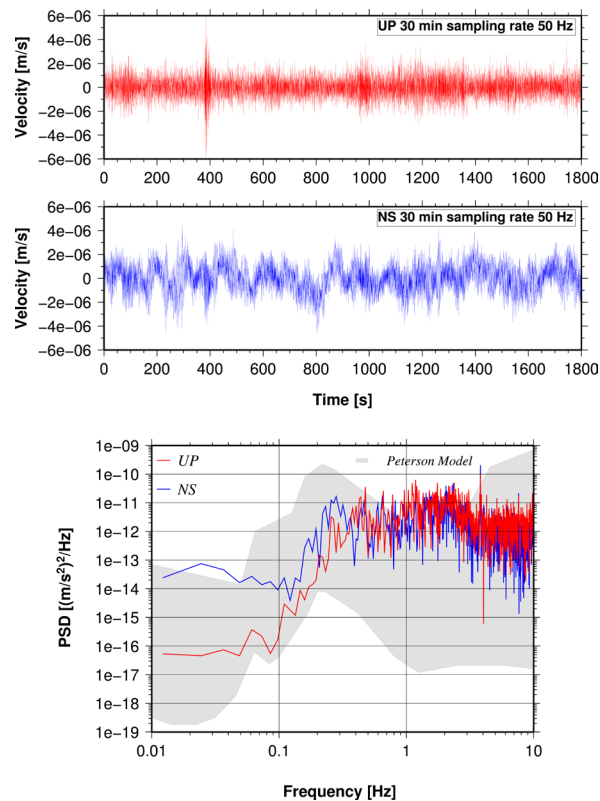
Figure 2.3 (Top and middle) GURALP CMG-3ESPD broad-band recordings of ambient seismic vibration at the station K38 used in this study. (Bottom) PSD of the UP (red) and NS (blue) components of broad-band ambient seismic vibration recordings. Grey shading indicates the area delimited by NLNM and NHNM of *Peterson* (1993).

The 30 minutes of recording are divided into windows of 81.92 seconds without overlapping. For each window, the linear trend in the data was removed and a 5% cosine tapering function was applied to both ends. After applying a Fast Fourier Transform (FFT) to the data the PSD of each window was calculated following *McNamara and Buland* (2004). In this study we consider only the vertical (UP) and north-south (NS) components of ground motion, although similar results can be obtained for the east-west component. Figure 2.3 (bottom panels) shows the UP and NS component PSDs calculated on the first window together with the Peterson Model. Although night recordings were selected, their PSDs exceed the NHNM in the frequency range between 1 and 3 Hz, which is the frequency range generally considered to be strongly affected by anthropogenic activity. This excess can be also related to the industrial activity in the neighbouring city of Cologne (*Plesinger and Wielandt*, 1974). The PSD in the frequency range between 0.1 and 1 Hz is characterized by microseismic activity (*Gutenberg*, 1921; for a recent review, see *Webb* 1998). The major areas for microseisms recorded in Germany had previously been identified as originating from the British and Norwegian coasts (*Gutenberg*, 1921; *Jung*, 1934; more recently, *Friedrich et al.*, 1998; *Essen et al.*, 2003). The surface pressure map of the day of these recordings (e.g. *Wetterzentrale, n.d.*) does not show any strong low pressure system over the North Sea. The absence of strong microseismic activity is also confirmed by values of PSD in the frequency range between 0.1 and 0.7 Hz which approach the NLNM. The behaviour of the lowest frequency part (below 0.1 Hz) of the horizontal component PSD (down to 0.1 Hz) may be related to a tilt effect (*Forbriger*, 2006), due to the non optimal (temporary) installation of the broad-band sensor. However, a peak around 0.02 Hz is mapped also in the time series (Figure 2.3 NS component), which may indicate the presence of infragravity waves (e.g. *Webb*, 1998).

In this work, the background seismic signal from the output of the DAS (output) is computed by summing, in the time domain, the selected ambient seismic vibration (input) window at station K38 with the theoretical SPES and DAS instrumental self-noise (self-noise), which we model using equations (1) to (5). The self-noise signal in the time domain is estimated from the self-noise PSD, assuming a random distribution of the phase. That is, the input is summed to the self-noise in the time domain and then the PSD of the output is calculated. In contrast to the generally adopted simple method of summing the PSDs, this procedure does not require any assumption about the independence of input and self-noise (*Rodgers*, 1992), and takes into account that for the short time windows used, an effect due to the cross-term of the PSD of the resultant signal cannot be excluded. A test we performed (not shown here) showed that the expected PSD computed either directly by summing the PSD of

the input and self-noise, or by computing the PSD of their sum in the time domain, are almost the same, with the most pronounced differences for frequencies where the input and self-noise PSDs cross. Although the tests we carried out showed that our conclusions about the influence of the chosen DAS and SPES on the H/V spectral ratio results are almost independent upon the scheme adopted for computing the expected PSD noise, we preferred to adopt the scheme that better predicted what it is expected for the analysis of actual data. The PSD of the output is then computed for each combination of SPES and DAS. In all, 18 different combinations are considered (three SPESs, three DASs with two different gain values for each). Finally, the H/V was calculated for each PSD and then the logarithmic average of the spectral ratios obtained after splitting the input windows into 20 non-overlapping segments.

Results

The results of all 18 combinations are described in the following. However, for the sake of brevity, only those regarding the EDL and part of those for the REFTEK 72A are shown. The complete set of results is presented in appendix A.

In general the results obtained for the different combinations of short-period SPES and DAS show that the performance of instruments at frequencies below 1 Hz strongly depends upon the combination of SPES, DAS and the gain used.

EDL PR6-24

The PSD expected for a SPES connected to the EDL (Figure 2.4a) with the gain fixed to 1 shows the possibility of a Mark L4C-3D detecting input down to 0.1-0.2 Hz, even if the signal is approaching the NLNM. SPESs with a higher resonance frequency have less chance of correctly identifying input at lower frequencies (Figure 2.4b and 2.4c). In particular, using a 4.5 Hz SPES, the PSD of the input between 0.15 and 1 Hz can be retrieved from the output only when the input level approaches the NHNM. For frequencies below 0.15 Hz, since the self-noise for the 4.5 Hz SPES is larger than the NHNM, the input characteristics cannot be retrieved using this type of SPES. The diminishing signal-to-noise ratio when increasing the resonance frequency of the SPES (Figure 2.4b and 2.4c) has a clear effect on the H/V spectral ratio. While the results obtained with a 1 Hz SPES (Figure 2.4a) agree well with those obtained by broad-band recordings, the H/V spectral ratio from 2 Hz-SPES recordings (Figure 2.4b) show an apparent shift of the resonance peak due to the intersection of the self-noise PSD and the input PSD at about 0.2 Hz, also leading to lower S/N ratios at higher frequencies.

Both a large shift and a strong amplitude reduction of the H/V spectral ratio peak are shown when a 4.5 Hz SPES is used (Figure 2.4c). For the case of smaller spectral amplitudes

(but still well within the NHNM and the NLNM), the H/V spectral ratio of 4.5 Hz SPES would not show any peak at all for frequencies lower than 0.3 Hz.
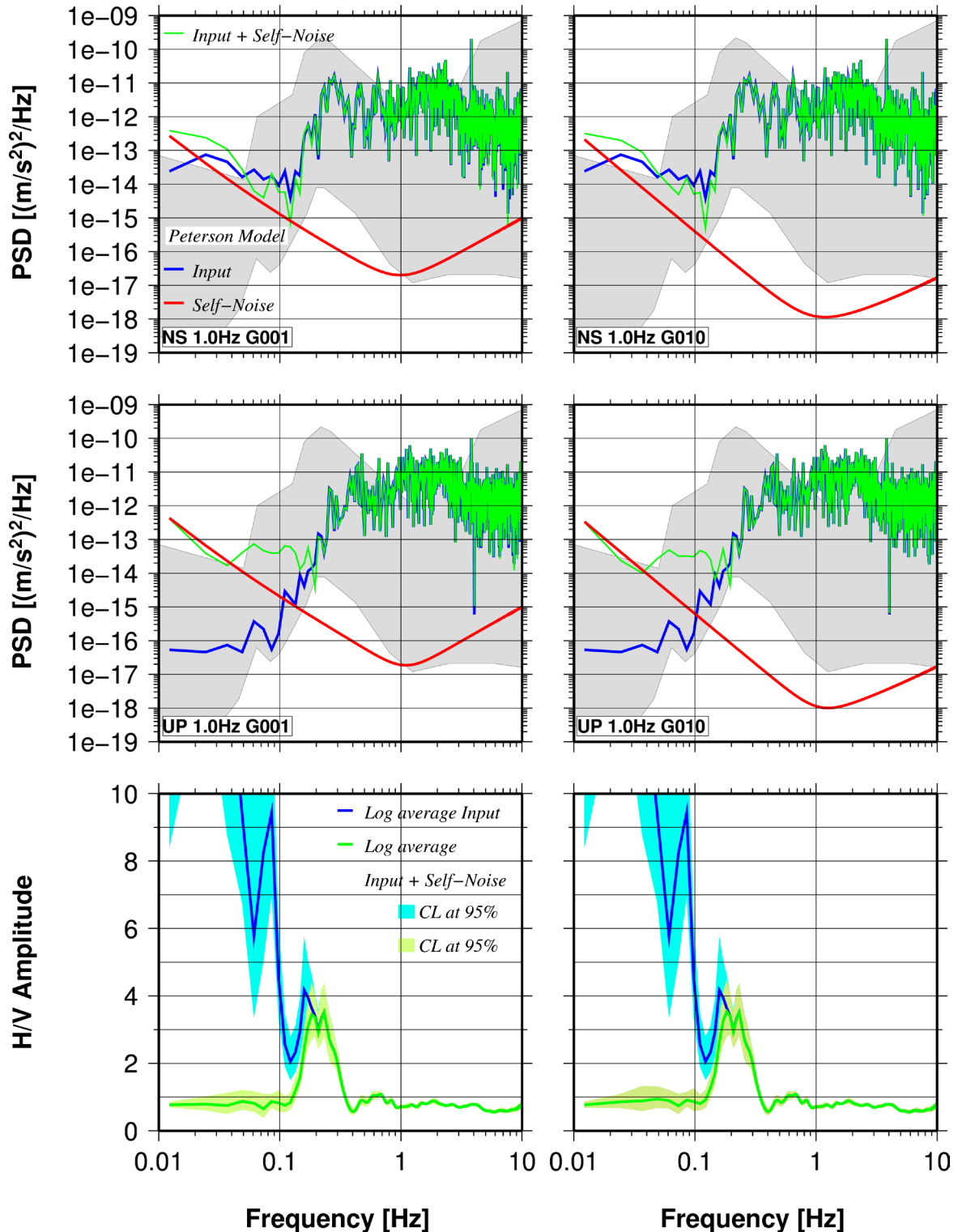
Figure 2.4 Self-noise (red), ambient seismic noise (input) from the broad-band recordings (blue) and input plus self-noise PSD (green) for the EDL DAS with gain=1 (left side) and gain=10 (right side) coupled with the 1 Hz SPES; the grey shading indicates the area delimited by the NLNM and NHNM of *Peterson* (1993). NS components are shown in the top panels while the UP components are in the centre. The bottom panels show the corresponding average H/V spectral ratios of input from broad-band recordings (black) and average H/V spectral ratios of input plus self-noise (grey); for both the shaded area indicates the 95 % confidence intervals (CL).
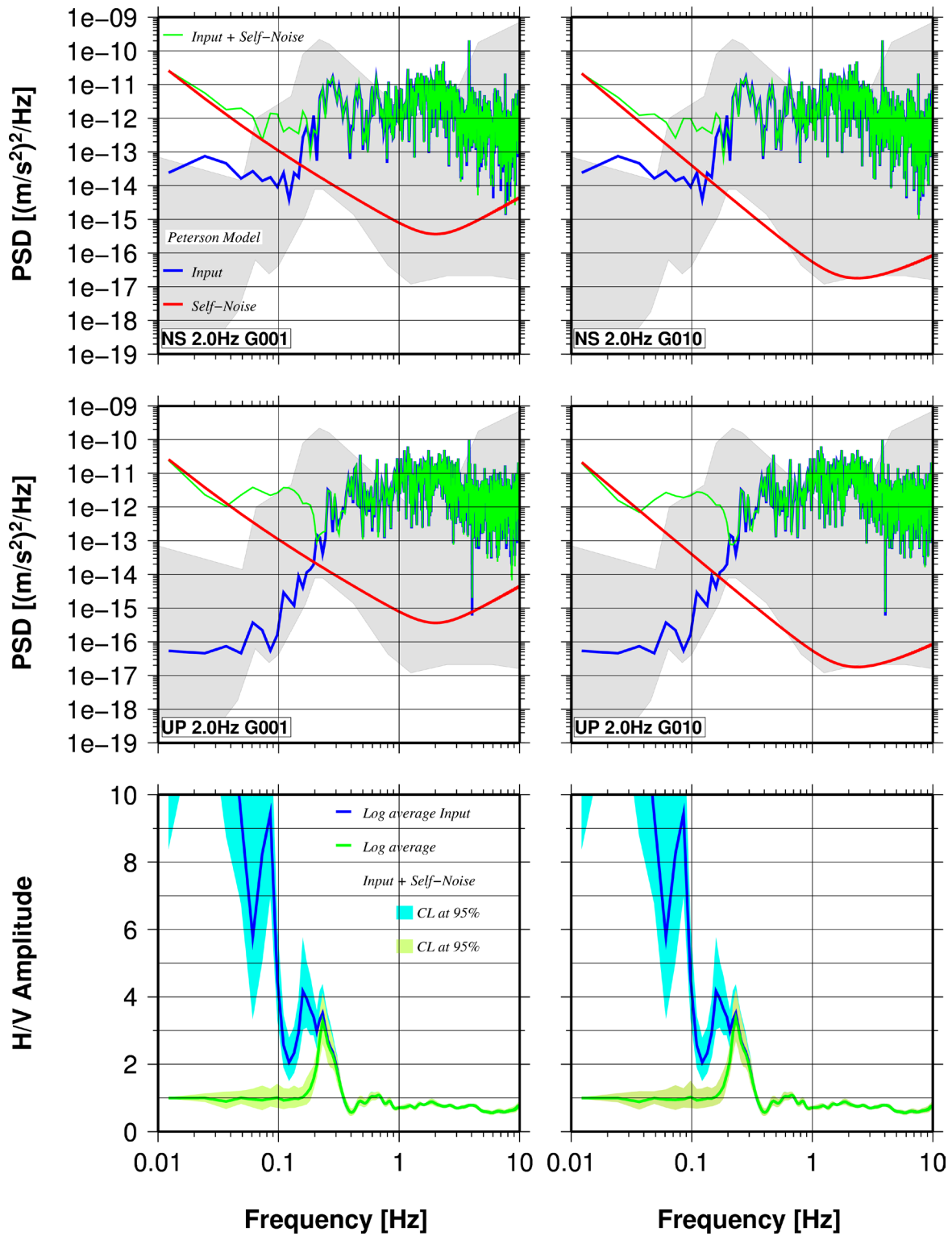
Figure 2.4b Same as Figure 2.4a but for the EDL coupled with a 2 Hz SPES.

Finally, it is worth noting that below 0.1 Hz the H/V spectral ratio of the original broad-band recordings show a strong increase with decreasing frequency. This suggests a likely problem in the installation of the broad-band sensor, with this behaviour probably due to the tilt of the sensor (*Forbriger*, 2006).

Increasing the gain to 10 (Figure 2.4a, 2.4b and 2.4c) improves the ability to detect the spectral peaks in the ambient seismic vibration for the 4.5 Hz SPES, but limitations in

correctly retrieving the H/V spectral ratio peak are still observed for the 2 Hz and the 4.5 Hz SPESs.
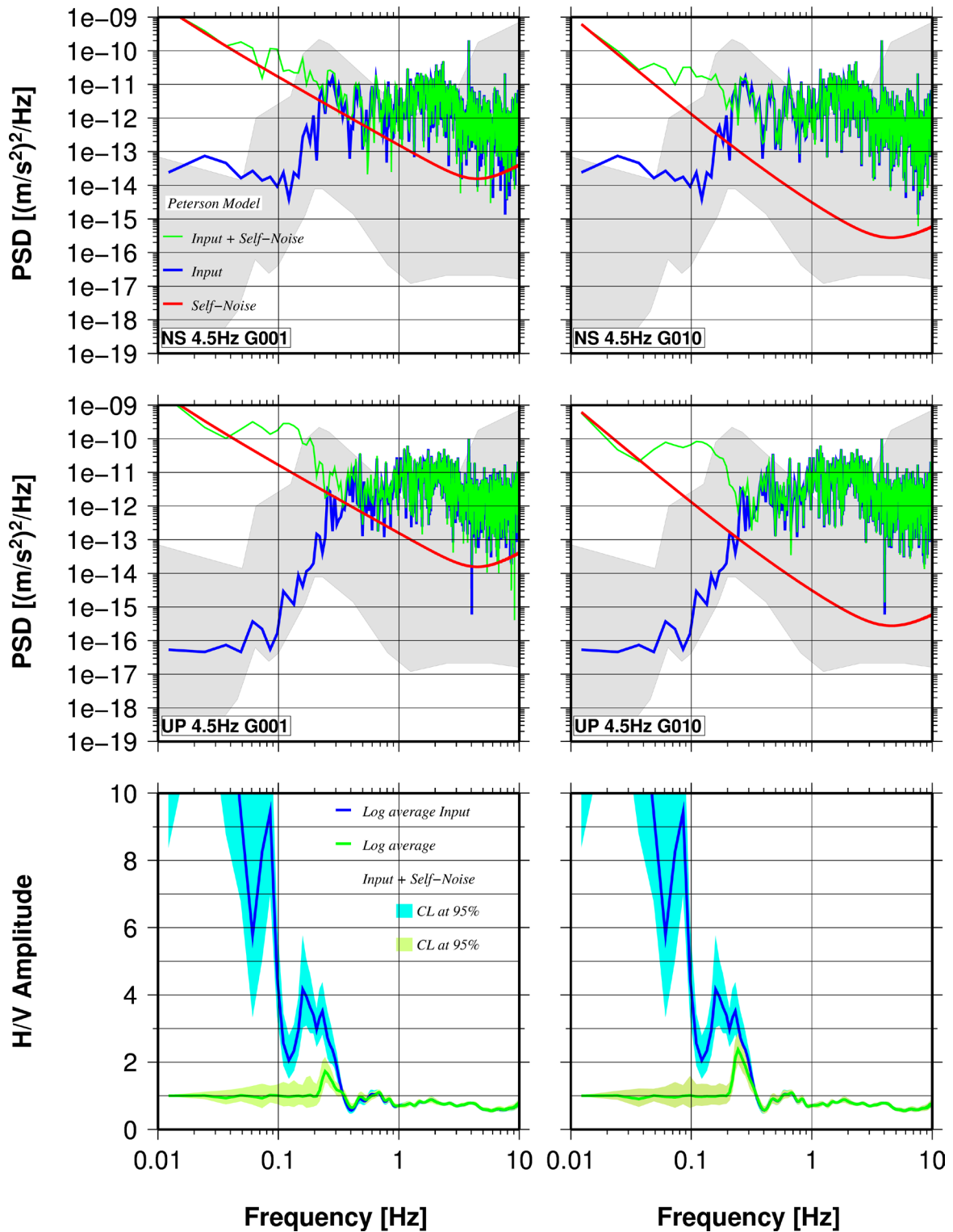
Figure 2.4c Same as Figure 2.4a but for the EDL coupled with a 4.5 Hz SPES.

REFTEK 72A

The combination of the three SPESs with a REFTEK 72A (Figure A2a, A2b and A2c appendix A) while fixing the gain to 1 clearly shows a general worsening of the signal-to-noise ratio when compared to the same SPES and gain for the EDL case. In particular, a slight

shift of the H/V spectral peak also affects the 1 Hz SPES results, while no peak at all is shown when a 4.5 Hz SPES is considered (Figure 2.5).
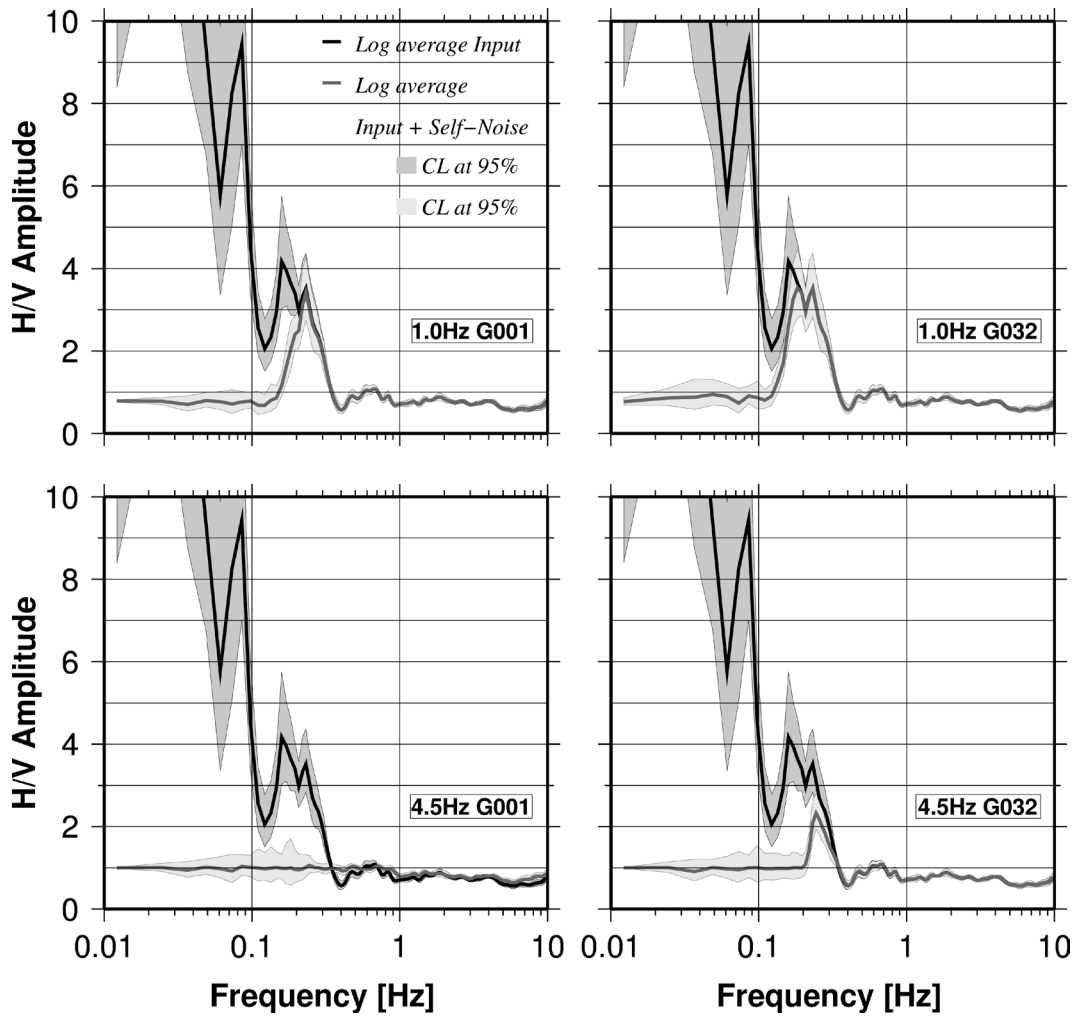
Figure 2.5 H/V spectral ratio results for the REFTEK 72 A and different SPESs. Left: results for gain=1. Right: results for gain=32. Top: results for 1Hz SPESs. Bottom: results for 4.5 Hz SPESs.

Increasing the gain to 32, allows us to obtain results similar to those derived using the EDL with the gain set to 10. This is due to the strong reduction of quantization noise due to the increase in the pre-amplifier gain (Equation (4) and Figure A1a appendix A).

PDAS Teledyne Geotech

Results obtained considering the PDAS Teledyne Geotech (Figure A3a, A3b and A3c appendix A) and fixing the pre-amplifier gain to 1 are nearly identical to those obtained for REFTEK 72A when using a gain of 1. In this case, since the generalized total electronic noise E_n of the two DAS (although having different amplifiers with different f_{cv}, f_{ci}, V_{00} and I_{00}), as well as the quantisation noise Q_n, are very similar, nearly identical self-noise PSD are obtained.

When the gain is set to 100, the PDAS Teledyne Geotech provides results comparable

with those obtained using an EDL and fixing the gain to 10, i.e. the best combination we found. The excellent performance of the PDAS Teledyne Geotech DAS is due to the strong reduction of the quantisation noise determined by increasing the gain (Figure A1b appendix A).

Conclusions

The main results from this study can be summarized as follow:

- 1 Hz SPESs can be used to detect ambient seismic vibration down to 0.2-0.1 Hz, but generally require a large gain. In fact, for the case where the input approaches the NLNM of *Peterson* (1993) and when the gain is fixed to 1, spectral amplitudes below 0.2 Hz can be masked by the self-noise.

- 1 Hz SPESs can be used for estimating the H/V spectral ratio down to at least 0.2 Hz when using the maximum possible gain for the EDL, the REFTEK 72A, and the PDAS Teledyne Geotech, (10, 32, 100, respectively). When the minimum gain for the latter two DAS is used, a slight bias in the peak is observed. The successful use of these SPESs for estimating the H/V spectral ratio at lower frequencies (below 0.2 Hz) strongly depends upon the input amplitude.

- 2 Hz SPESs, combined with REFTEK 72A or PDAS Teledyne Geotech (setting the gain to 1), are not able to resolve ambient seismic vibration features at frequencies lower than 0.3 Hz for the case where the input is less than the average value between the NLNM and the NHNM of *Peterson* (1993).

- 2 Hz SPESs always provide biased H/V spectral ratios (shifting toward higher frequencies the peak) at frequencies lower than 0.3 Hz.

- 4.5 Hz SPESs cannot detect ambient seismic vibration for frequencies lower than 0.6 Hz if the gain is fixed to 1 (Figure 2.4c and A2c and A3c in appendix A). However, if a specially designed pre-amplifier is used, the performance of the 4.5 Hz sensor can be improved, increasing the S/N ratio to about 10 dB.

- The H/V spectral ratio peak at low frequencies obtained by the 4.5 Hz SPES recording is always biased and, for some combinations (e.g. REFTEK and PDAS), may even vanish.

The degree of bias in the H/V spectral ratio due to the DAS and SPES couple estimated in this study can be subject to variations, depending upon the level of the input signal. However, the general tendency that was observed will still be valid. In particular, ambient seismic vibration recorded during periods of strong microseisms might overstep the theoretical self-noise levels that we have calculated. However, we believe that our results provide a clear picture of the problems one can encounter when using certain seismic

instruments. On the basis of these results, we suggest that when ambient seismic vibration of interest is only in the frequency band between 0.1 and 1 Hz, 1 Hz SPESs are preferred instead of 2 and 4.5 Hz SPESs. We also suggest that the ambient seismic vibration measured in the field should be compared with the instrumental self-noise PSD of the SPES-DAS combination, employed especially when high-resonance frequency SPESs are used.

In this paper, we tested 3 SPESs and 3 DASs, all of which are available on the market or still in use. Our results can be extended to SPESs and DASs with similar characteristics and, we hope, may encourage the investigation of the PSD of self-noise of other DASs that we have not considered.

2.2 Empirical spectral ratios estimated in two deep sedimentary basins using microseisms recorded by short-period seismometers

Abstract

In this work, we analyze continuous measurements of microseisms to assess the reliability of the fundamental resonance frequency estimated by means of the horizontal-to-vertical (H/V) spectral ratio within the 0.1-1 Hz frequency range, using short-period sensors (natural period of 1 sec). We apply the H/V technique to recordings of stations installed in two alluvial basins with different sedimentary cover thicknesses, the Lower Rhine Embayment (Germany) and the Gubbio Plain (Central Italy). The spectral ratios are estimated over the time-frequency domain and we discuss the reliability of the results considering both the variability of the microseism activity and the amplitude of the instrumental noise. We show that microseisms measured by short period sensors allow the retrieval of fundamental resonance frequencies greater than about 0.1-0.2 Hz, with this lower frequency bound depending on the relative amplitude of the microseism signal and the self-noise of the instruments. In particular, we show an example where the considered short-period sensor is connected to instruments characterized by an instrumental noise level which allows detecting only fundamental frequencies greater than about 0.4 Hz. Since the frequency at which the peak of the H/V spectral ratio is biased depends upon the seismic signal-to-instrument noise ratio, the power spectral amplitude of instrumental self noise should be always considered when interpreting the frequency of the peak as the fundamental resonance frequency of the investigated site.

Introduction

Since the beginning of instrumental seismology, ambient seismic background noise has focused the attention of many studies. It has been considered not only as an unavoidable disturbance that must be reduced to improve the utility of seismic data or the performance of a seismic network, but also as a useful signal for investigating the effect of the sub-surface geology on ground motion. Since ambient noise measurements can be rapidly performed over large areas, the possibility of linking some features extracted from the background noise recordings to the seismic response of the soil made the ambient noise a suitable tool for many studies aiming at seismic hazard assessment (*Delgado et al.*, 2000). For example, the Nakamura technique (e.g., *Nakamura*, 1989) is generally applied to estimate the fundamental frequency of resonance of the site, in correspondence to the frequency of the first peak observed in the spectral ratio between the horizontal and vertical components (H/V) of noise recordings acquired at a single site. The background noise measurements can be analyzed in several ways for estimating the local site effects. In general, either the fundamental frequency of resonance estimated from single station measurements can be used to map the thickness of the soft sedimentary layer (e.g. Ibs-von *Seht and Wohlenberg*, 1999) or the H/V spectral ratio can be used to unravel the sub-soil structure through an inversion procedure (e.g. *Fäh et al.*, 2003). Other studies exploited the availability of simultaneous measurements of ambient noise at an array of stations to derive a vertical shear wave velocity profile by dispersion wave analysis (e.g., *Scherbaum et al.*, 2003; *Arai and Tokimatsu*, 2005; *Parolai et al.*, 2005; *Picozzi et al.,* 2005). Regardless of the methodology applied, any bias introduced by the adopted instrumental equipments in the background noise measurements can affect the shape of the H/V ratio and therefore corrupt the information on the sub-soil structure. The possibility of obtaining reliable site effects estimation from numerical simulation will be thus limited.

The frequency range of engineering interest generally spans the range 0.1-20 Hz. While frequencies larger than 1Hz are amplified by thin soft sediment layers and correspond to the natural period of most of the buildings, frequencies below 1 Hz are amplified by sediments thicker than about 100 m and are of interest for the response of long bridges and tall buildings (more than 10 stories high, as rule of thumb). Within this frequency range, the sources generating the background seismic noise have different nature (e.g. *Webb*, 1998; *McNamara and Buland*, 2004): while for frequencies larger than about 1 Hz the noise spectrum is related to human activities, in the frequency range from 0.1 to 1 Hz it is characterized by features related to microseism activity, generated by ocean wave energy coupling into motion of the earth (e.g. *Longuet-Higgins*, 1950; *Bromirski et al.*, 2005).

Since the recordings of the background noise for engineering seismology investigations

generally consist of short time measurements (for some minutes to about 1 hour) repeated at several locations over a wide urban area, short-period sensors are more suitable for these field surveys since they are less demanding than broad band instruments by the point of view of installation. However, these sensors damp the signal below their natural frequency (>=1 Hz), and then the signal amplitude may become smaller than the self-noise of the acquisition system. Under these circumstances, the signal-to-noise ratio (here indicating the ratio between the seismic noise signal and the self-noise of the acquisition system) is not improved by removing the instrumental response from the data, since the application of the instrumental correction can only lead to amplification of the self-noise. Following a theoretical approach based on numerical simulations, *Strollo et al.* (2008) evaluated the bias introduced by the instrumental self-noise both on the seismic noise recordings and on the horizontal-to-vertical spectral ratio (H/V) results, considering frequencies less than 1Hz. Here, the suitability of short-period recordings for estimating the fundamental resonance frequency in the 0.1-1 Hz frequency range by H/V ratio is investigated analysing empirical data collected during field experiments carried out in two alluvial basins, the Lower Rhine Embayment (Germany) and the Gubbio Plain (Central Apennines, Italy). In particular data from sites with fundamental resonance frequency less than 1 Hz, as estimated by studies (e.g. *Parolai et al.*, 2004), are considered.

First, the time variability of the power spectra computed for ambient noise, considering high and low microseismic activity periods, and taking into account the effect of self-noise of the instruments is investigated. Second, the Nakamura technique is applied to the recordings to estimate the fundamental resonance frequency of the sites and to investigate the stability of the results against time. The analysis of the results is carried out taking into account both the variability of the microseism activity, and therefore the strength of the seismic noise signal, and the limits introduced by the employed instruments as theoretically predicted by *Strollo et al.* (2008).

Data sets

Cologne data set

We use the dataset of recordings collected within the DFNK (German Research Network for Natural Disasters) project that aimed at the investigation of site effects in the Cologne area (*Parolai et al.* 2001; *Parolai et al.*, 2002; *Parolai et al.*, 2004). A temporary network of 44 stations was deployed between 23 April to 13 June 2001 and continuously recorded background seismic noise as well as regional earthquakes and teleseisms. In the present work, we analyze data from 5 stations of the network, namely stations K13, K25,

K32, K33 and K38 (Figure 2.6). The first four stations were equipped with PDAS TELEDYNE Geotech recording stations connected to a Mark L4C-3D sensor, while a Güralp CMG-3ESPD recording station (all in one) was installed at site K38. Data were recorded with a sample rate of 100 sps at PDAS sites and 50 sps at the Güralp site. The main characteristics of the installations can be found in (*Parolai et al.*, 2004, Table 1).

We selected these five sites because of their fundamental resonance frequency which, for stations K33, K32, K13 and K25, are less than 0.2 Hz, between 0.3 and 0.4 Hz, about 0.5 Hz, and between 0.8 and 0.9 Hz, respectively. Details are given in *Parolai et al.*, (2004, Figure 2.4). The sediment thickness below these stations can be estimated using the thickness versus fundamental frequency relationship derived by *Parolai et al.* (2002) for the study area (i.e. $z=108f^{-1.551}$). For station K33 the estimated thickness is grater than 1.3 km; for stations K32, K13 and K25 the thickness is about 550, 320, and 130 m, respectively.
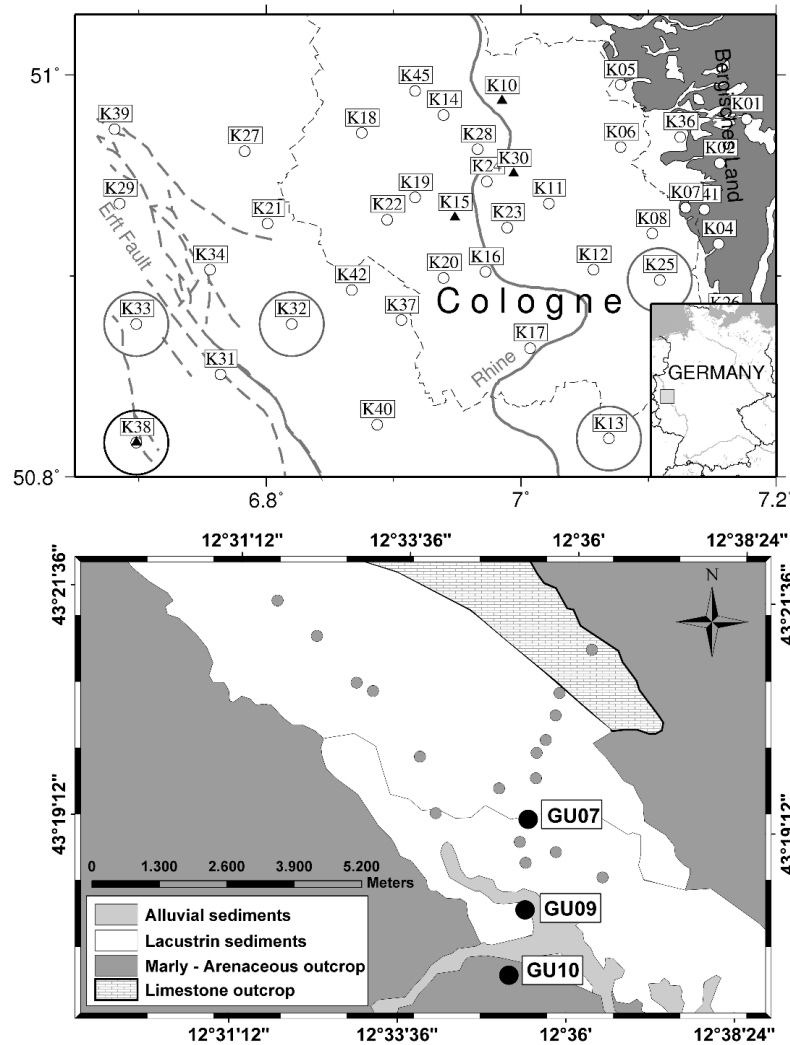
Figure 2.6 Top: The large circles indicate the stations analyzed in the present work (K38, K33, K32, K25 and K13), selected among those analyzed by *Parolai et al.* (2004) in the Lower Rhine Embayment (Germany). Small empty circles are short-period stations; black triangles are broad-band stations. Bottom: Simplified geological map of the Gubbio plain (Central Italy). Grey circles: seismic stations installed within the DPC-INGV project; black circles: stations considered in the present work.

Gubbio data set

We use the recordings from three (GU07, GU09, GU10) of the stations installed in the Gubbio basin (Figure 2.6) by the GeoForshungsZentrum (GFZ) within the framework of a project of the Italian Dipartmento di Protezione Civile (DPC) and the Istituto Nazionale di Geofisica e Vulcanologia (INGV) aimed at computing ground-motion scenarios for some strategic areas in Italy (*INGV DPC-S3, n.d.*).

The selected stations belong to an almost linear array crossing the basin in a north-south direction along the minor axis of the basin, which has an ellipsoidal shape (Figure 2.6). Since station GU10 was installed on outcropping bedrock along the southern basin edge, it is not affected by significant site effects and it can be used as reference station. Stations GU07 and GU09 were placed in the basin and their fundamental resonance frequencies were estimated to be between 0.3 and 0.4 Hz, and between 0.5 and 0.6 Hz, respectively (*INGV DPC-S3, n.d.*). The sediment thickness estimated for stations GU07 and GU09 is 680 m and 420 m, respectively. From June to the middle of September 2005, the sites were equipped with REFTEK 72A recording stations with a Mark L4C-3D sensor, and then until December 2005, the REFTEK digitizers were substituted with Earth Data Logger PR6-24 (EDL) digitizers. Data were recorded with a sample rate of 100 sps.

Data processing

We first investigate the variation of the background seismic noise by computing the Probability Density Function (PDF) for a set of Power Spectral Densities (PSDs), following *McNamara and Buland* (2004). We processed time series T_1 s long, from which we removed the mean and the instrumental response. Each time series is divided into segments of T_2 s, overlapping by 75%, to reduce the variance in the PSD calculation (*Cooley and Tukey*, 1965). The length of the time windows are $T_1 = 900$ s and $T_2 = 300$ s for the Cologne dataset, and $T_1 = 600$ s and $T_2 = 240$ s for the Gubbio dataset. The total power, representing the PSD estimate, is obtained from the square of the amplitude spectrum multiplied by the standard normalization factor $2\Delta t/N$, where Δt is the sample interval and N is the number of samples (*McNamara and Buland*, 2004). The PSD obtained for each T_1 s time series is estimated as the average of the PSDs computed for each T_2 s segments and converted into decibels with respect to acceleration $(m/s^2)^2/Hz$. Following *McNamara and Buland* (2004), we compute a distribution of probability at re-sampled discrete frequencies Fc evenly spaced on a logarithmic scale. Each frequency Fc is selected as the geometric mean frequency within a one octave interval, i.e., Fc = (F1 * F2)$^{0.5}$, where the considered interval extends from frequency F1 to F2 = 2F1. The next Fc is then computed by shifting the interval by one-sixteenth of an octave. Powers

are averaged over ±10% of Fc and grouped into bins 1-dB wide and the frequency distribution at each Fc results from the number of spectral estimates that fall into a bin divided the total number of spectral estimates.

We then use the computed PSDs to investigate the time dependence of the site effects estimated from the noise recordings. The fundamental resonance frequency is estimated as the frequency corresponding to the peak of the Nakamura ratio (*Nakamura*, 1989), computed as the square root of the spectral ratio between the horizontal and vertical (H/V) PSDs.

Analysis of the Cologne dataset

Broad-band station

We use the broad-band station K38, installed in the cellar of the Wissersheim church, as the reference station for analyzing the power spectra characteristics in the Cologne area. Figure 2.7 shows the PSDs computed for station K38, over the period from 4 May to 11 June, 2001. The PSDs (vertical component, V) for T_1 s time series selected at the beginning of each hour are shown. Following *Bromirski et al* (2005), Figure 2.7 shows the PSD normalized to the average PSD computed over the entire time period.
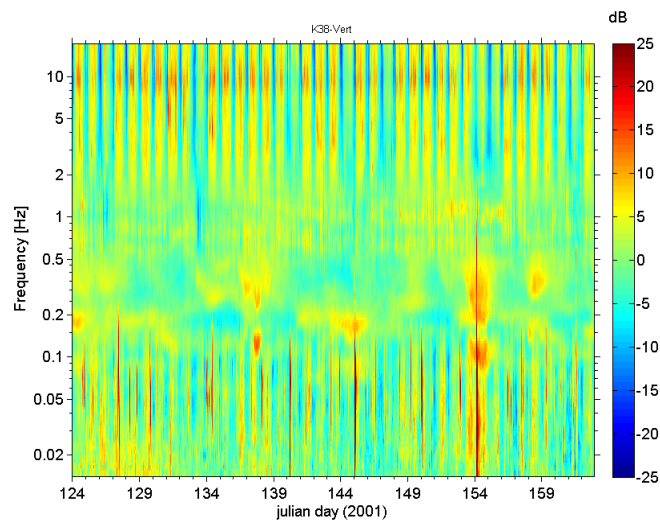
Figure 2.7 Power Spectral Density (PSD) in acceleration for station K38 (Wisserheim church), vertical component. Day 124 is a Friday. For each frequency, the PSD minus the average PSD computed over the entire period is shown.

Several characteristics of the noise spectrum that have been observed worldwide are also recognizable for K38. For frequencies larger than 2 Hz, the background noise is dominated by anthropic sources (e.g., *McNamara and Buland*, 2004) as shown by the daily cycle of the noise spectrum. Spectral levels during the night time are lower by about 40 dB than the day time, when human activities are more intense. A weekly cycle is also recognizable, with lower spectral values during the weekend. The PSDs in the range 0.1-1 Hz do not show such cycles since, in this frequency band, the PSDs are dominated by the microseisms.
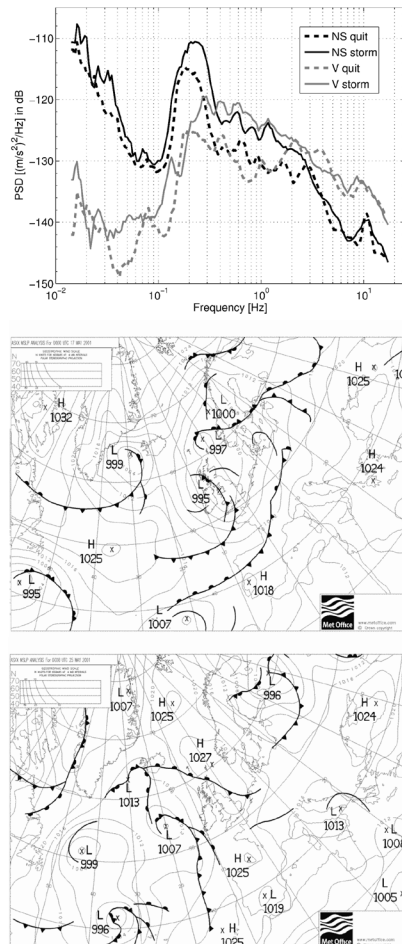
Figure 2.8 Top: PSD computed for station K38, considering the NS (broken line) and V (solid line) components. Black lines: 25 May, 2001 (julian day 145) at high noon; grey lines: May 17, 2001 (julian day 137) at high noon. Middle: Surface pressure chart of May 17, 2001 (julian day 137) indicating unstable weather conditions. Bottom: Surface pressure chart of May 25, 2001 (julian day 145) indicating stable weather conditions.

For stations installed in Germany, the dominant sources are along the British and Norwegian coasts (*Friedrich et al.*, 1998; *Essen et al.*, 2003). This is shown by Figure 2.8 (left), which compares the PSD computed when the microseism activity was intense (May 17, 2001 julian day 137, at high noon) with the PSD of a quiet day (May 25, 2001 julian day 145 at high noon). The surface pressure maps provided by the Met-Office (Figure 2.8) show that larger PSD are observed when a low-pressure system was present in the north Atlantic Ocean (May 17, 2001). In particular, the microseism activity increases both the horizontal (north-south component, NS) and vertical spectral values for frequencies less than 0.5 Hz. The amplitude of the double frequency peak at about 0.2-0.3 Hz is increased by about 8-10 dB and during days of strong microseism activity a primary peak at about 0.15 Hz is also recognizable in the vertical component.

The variability in the spectral levels during the analysed period can affect the H/V spectral ratio and, consequently, bias the H/V peak, leading to incorrect assessments of the local site effects. Figure 2.9 (top) shows the H/V computed for station K38 equipped with a

broad-band sensor. Hereinafter the H/V spectral ratio is computed as the spectral ratio between the NS and V components (NS/V). Since the main conclusions with respect to the aims of the present work, that is the assessment of the influence of the instrumental choices on the reliability of the estimated site effects, are the same when considering also the east-west (EW) horizontal component, we show the results only for the NS component.
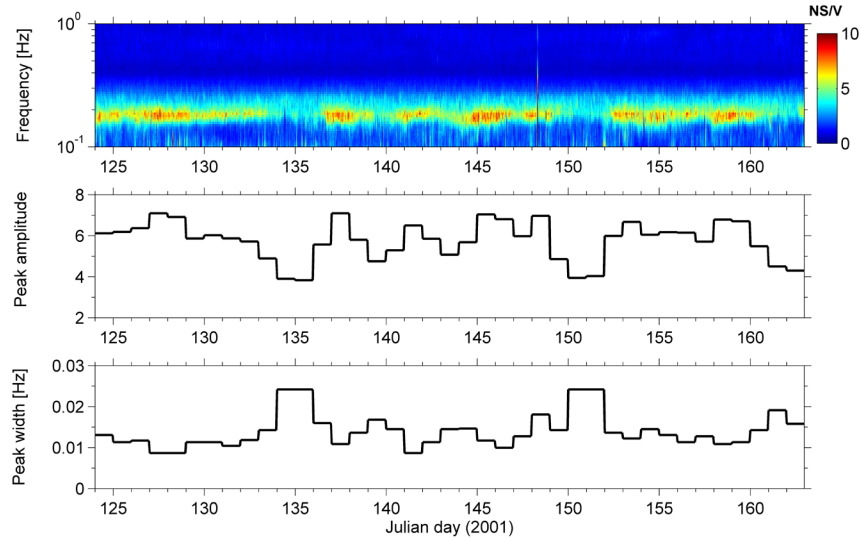
Figure 2.9 Top: NS over Vertical spectral ratios for station K38. Middle: amplitude of the NS/V peak, averaged over one day. Bottom: width at half maximum height of the NS/V peak, averaged over one day.

The distribution of frequencies corresponding to the maximum amplification factor in the frequency range 0.1-1 Hz has mean value of 0.18 and standard deviation 0.01. The mean value is in good agreement with the fundamental resonance frequency estimated by *Parolai et al.* (2001, Figure 12).

The peak of the H/V is generally well recognizable during the analyzed period. In any case, during the days of weak microseism activity (e.g. days 135 and 151) the amplitude of the peak is about half than the amplitude observed during strong microseisms (Figure 2.9, middle panel) and its width at half maximum height increases to about 0.024 Hz, increasing the uncertainty of the fundamental resonance frequency retrieved.

Short-period stations

Since the reduction of the amplitude of the signal level during days of low microseism activity could affect the H/V ratio (*Strollo et al.*, 2008), the next step consists of evaluating the reliability of the H/V spectral ratio computed using recordings from short period sensors.

Figures 2.10 and 2.11 show the results obtained for the stations K33 and K25 in the Cologne area. The figures show the PSD computed over the analyzed period for the NS (top left) and vertical (middle left) components, as well as the corresponding PDFs (top and middle right panels). The bottom panels show the NS/V ratio as a function of time and frequency (left) and the mean +/- one standard deviation of the spectral ratios computed over

the whole period (right). Figure 2.12 shows the NS/V ratios for stations K32 and K13. The frequencies corresponding to the H/V peak are 0.17, 0.49, 0.49, 0.87 Hz for stations K33, K32, K13 and K25, respectively, in good agreement with the results obtained by *Parolai et al.* (2004). The figures show that the NS/V spectral ratios for all stations are quite stable over time, with only the peak for station K33 being not well expressed during days of low microseismic activity (e.g. julian days 135, and between 150 to 153) while the peak of station K13 is partially affected by the strong noise present in the horizontal spectrum at frequencies lower than the fundamental one. The strong peak at 2 Hz in the NS/V ratio of station K13 is determined by a strong industrial source of noise present in the area close to the station (*Parolai et al.*, 2004).
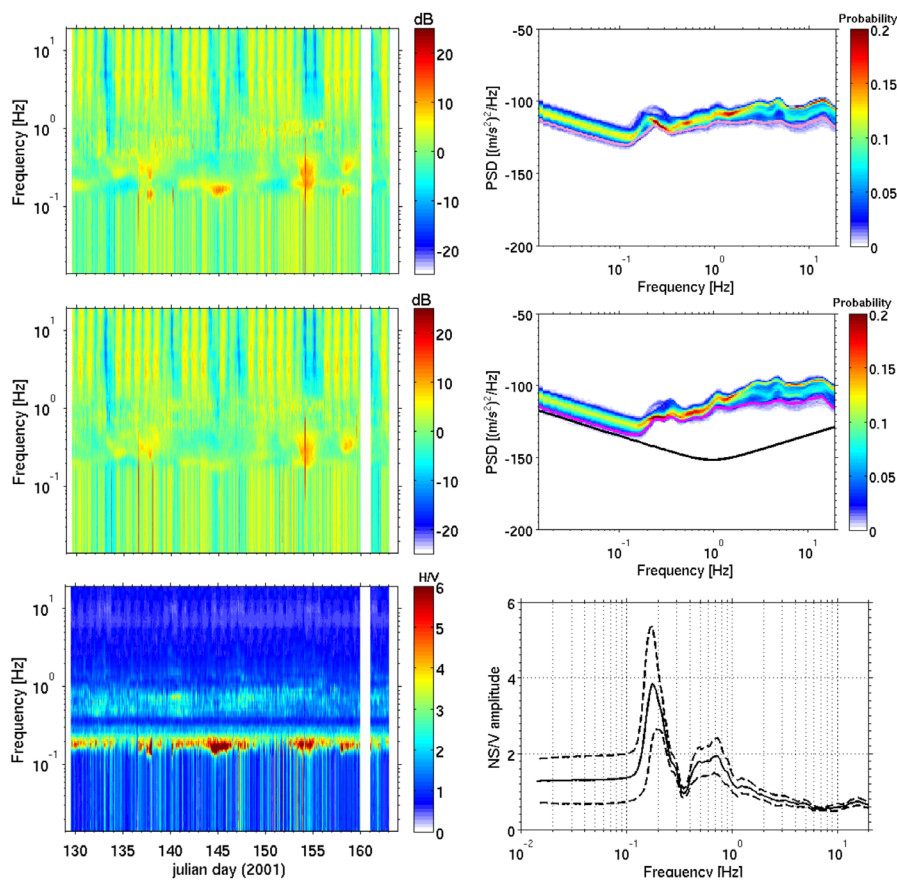
Figure 2.10 Station K33. Top: PSD (left) and Probability Density Function (PDF) (right) for component NS. The 5th percentile of the PDF is also shown (pink curve). Middle: PSD (left) and PDF (right) for component V. The theoretical self-noise PSD (*Strollo et al.*, 2008) (black curve) and the 5th percentile of the PDF (pink curve) are also shown. Bottom: NS/V spectral ratios in the time-frequency domain (left) and average ± 1 standard deviation spectral ratio computed over the whole period (right).

To assess the influence of instrumental noise on the computed ratios, the vertical PDFs are compared to the theoretical self-noise power spectral density, as computed by *Strollo et al.* (2008). Assuming for the sake of simplicity that the self–noise starts to affect the PSD when the difference between the 5-th percentile (pink curves in figure 2.10) of the PDF distribution and the self-noise PSD becomes almost constant for decreasing frequencies, the comparison

shows that the seismic noise spectral levels can also be retrieved for frequencies down to approximately 0.15-0.2 Hz, for the case of a weak microseism activity, confirming that the level of signal is strong enough to permit a reliable estimate of the fundamental resonance frequency for the characteristics of the employed instrumental equipments.
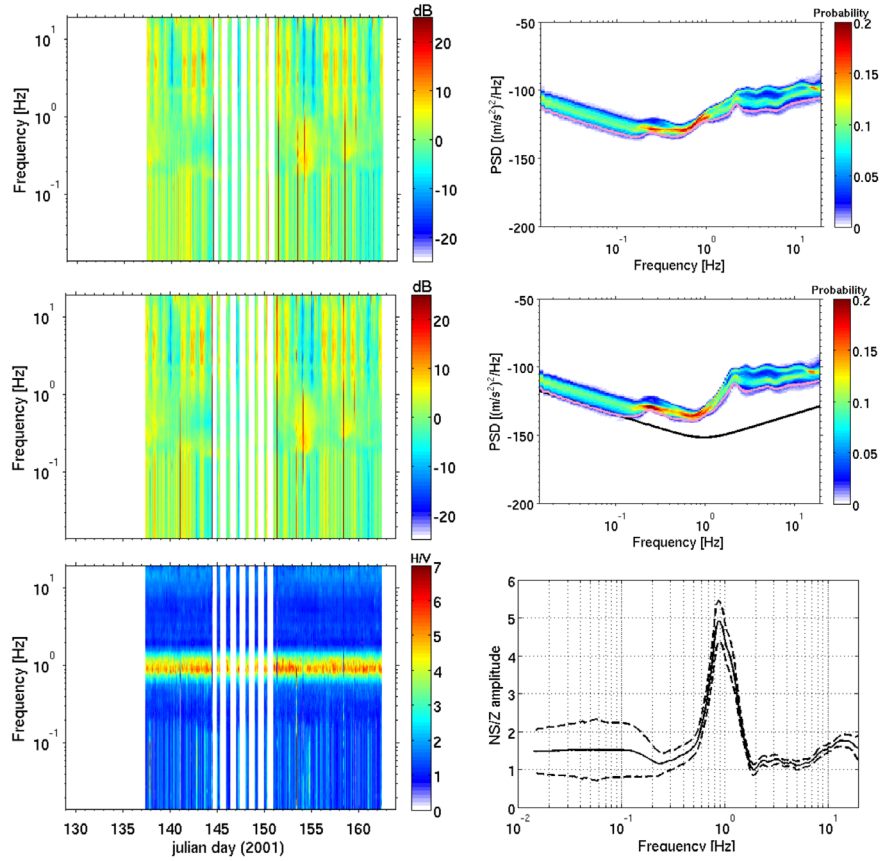
Figure 2.11 The same as in Figure 2.10 but for station K25.
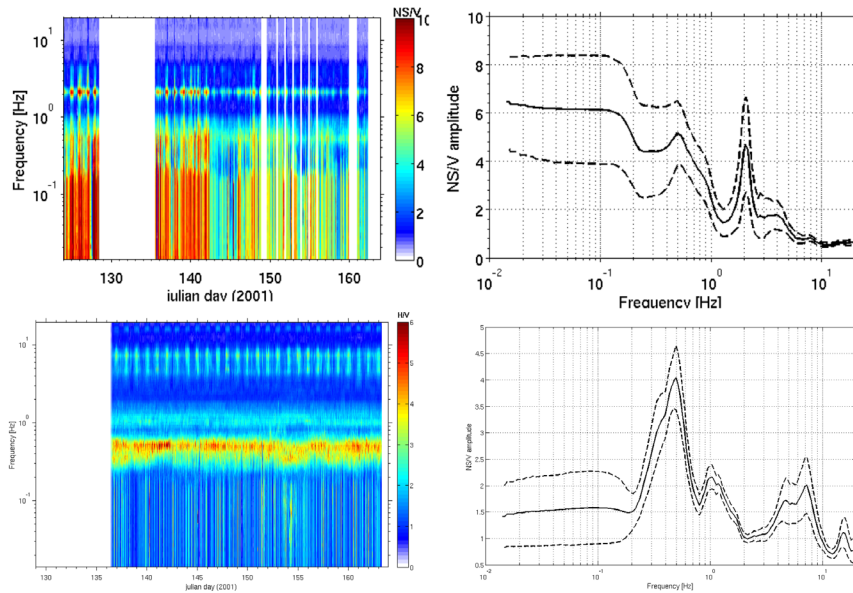
Figure 2.12 NS/V spectral ratios in the time-frequency domain (left) and average ± 1 standard deviation spectral ratio computed over the whole period (right) for stations K13 (top) and K32 (bottom)

Analysis of the Gubbio dataset

The acquisition of seismic data in Gubbio lasted from June 2005 until April 2006. In this work we analyzed data recorded at three stations (Figure 2.6) during two different time periods. The first period was from 12 to 16 July 2005, when microseism activity was weak, while the second period (from 29 November to 5 December 2005) was selected during winter days when microseism activity was stronger.

Figure 2.13 shows the PSD computed for the north-south and vertical components of recordings at stations GU10, GU09 and GU07. Differently from the analysis performed for the Cologne dataset, the PSD in Figure 2.13 are not normalize to the average computed over the entire period, so as to make the comparison between the spectral levels observed within and outside the basin easier. Since station GU10 is installed on the rock outcropping on the southern edge of the basin, its spectral levels are almost free from site amplification effects and the PSD in Figure 2.13 can be used as reference to evaluate the amplifications occurring within the basin.
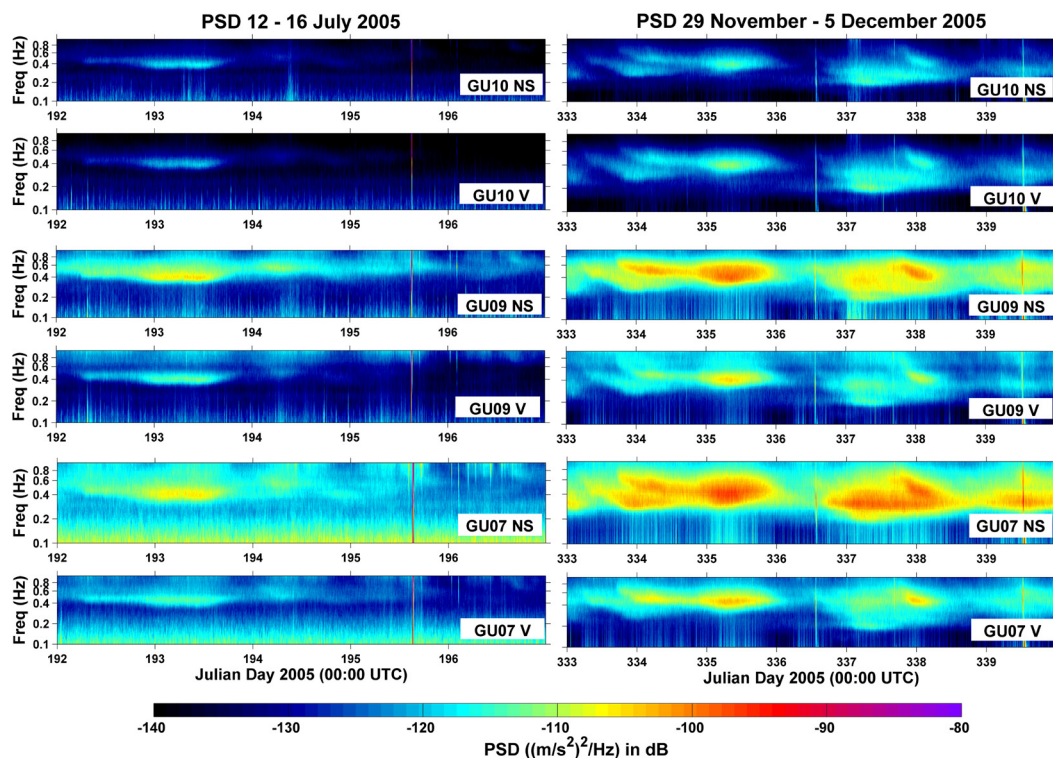
Figure 2.13 PSDs computed for components NS and V recorded at stations GU10, GU09, GU07, from top to bottom respectively. Left: period 1 (12-16 July, 2005). Right: period 2 (29 November-5 December, 2005.

In the first period (left panels), a weak microseism occurs between 192 and 194 Julian day, while strong microseism activity is recognizable in the second period. The difference between the frequency content of microseisms in the second period could be related to the location of the source area (*Stephen et al.*, 2003; *Bromirski et al.*, 2005). Indeed, microseisms

at frequencies larger than about 0.3 Hz are generally observed for events generated in the Mediterranean sea while lower frequencies are affected by microseisms generated in the north Atlantic (*Marzorati and Bindi*, 2006). Figure 2.13 shows that strong amplifications affect both the horizontal and vertical components of stations GU09 and GU07. Note that during the first period a constant high spectral amplitude affects frequencies lower than 0.15-0.12 Hz, hinting to a signal dominated by instrumental noise.

The NS/V spectral ratios for stations GU07 and GU09 are shown in Figure 2.14. The fundamental resonance frequency of the soil column below these stations is about 0.30 and 0.55 Hz, respectively.
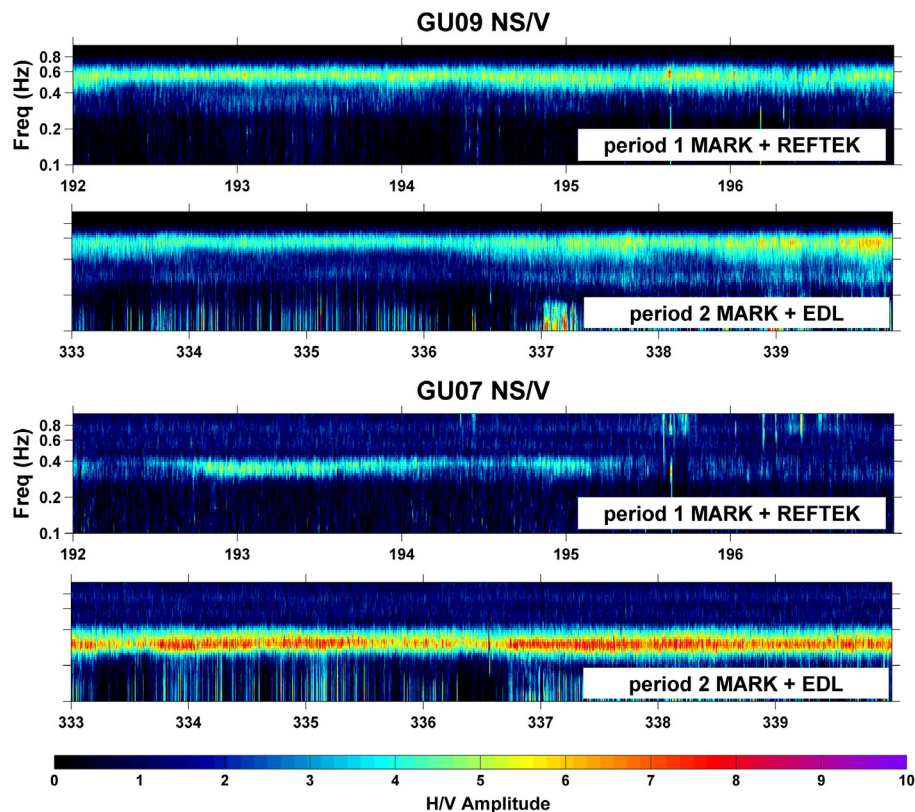
Figure 2.14 NS/V spectral ratios for stations GU09 (top panels) and GU07 (bottom panels) over the period 12-16 July and 29 November-5 December, 2005.

The stability over time of the estimated fundamental resonance frequency is different for the two stations. While for station GU09 it is almost the same for the two periods, the results for GU07 strongly depends upon the level of microseism activity. Although the peak is clear and stable during the whole second period, within the first period it is recognizable only when the microseism activity becomes more intense (julian days from 192 to 194). In particular, the maximum of the peak of amplification obtained for GU07 during the first period occurs at a higher frequency (0.4 Hz) than that obtained during strong microseism activity (0.3 Hz). This is confirmed by Figure 2.15 which shows the average NS/V for stations GU07 and GU09 computed during the two analyzed periods. For station GU09, the

fundamental resonance frequency estimated during the two periods is the same but the average amplitude of the NS/V peak is smaller for period 1. For station GU07, the mean peak of the NS/V ratio during the first period is clearly shifted towards higher frequencies and its amplitude is less than that obtained from the second period recordings. In figure 2.15, the NS/V from background noise are also compared with the average NS/V computed when considering the recording of 27 local earthquakes with magnitudes Ml between 0.8 and 4.7 (*INGV DPC-S3, n.d.*). A better agreement between the peak of the H/V spectral ratio estimated from noise recordings and from the earthquake is obtained using the noise recordings collected during the second period (strong microseism activity).
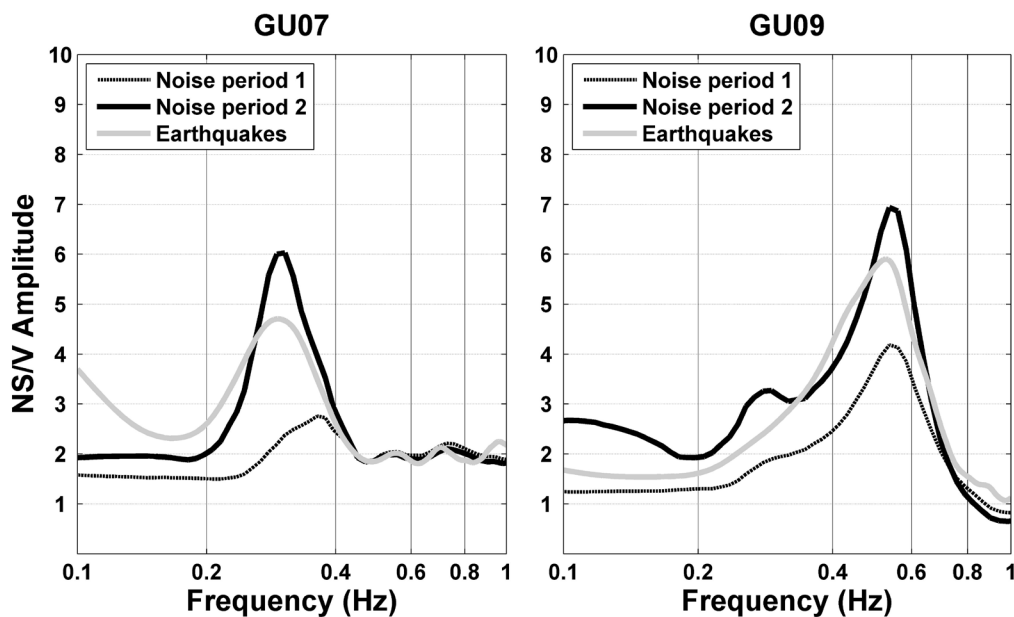
Figure 2.15 Average NS/V spectral ratios computed over period 1 (broken line), period 2 (solid black line) and considering 27 earthquake recordings (red line). Left: station GU07; right: station GU09.

The variability of the results obtained for the stations installed in the Gubbio Plain confirms that the reliability of the amplification peak in the range 0.1-1 Hz detected by NS/V spectral ratios evaluated from short period recordings depends upon the ratio between the signal at frequencies close to resonance and the self-noise of the instrument. Figure 2.16 shows the mean and the 5th percentile of the vertical component PDF distribution for GU07 computed considering days from 192 to 194 during the first period (period 1A), when weak microseism activity was present, from 195 to 197 in the first period (period 1B), when the microseisms activity was very quite, and from 334 to 336 in the second period (period 2), when microseism activity was intense. We recall that during period 2, the station was equipped with a sensor-acquisition system couple having a self-noise level lower than that used during period 1 (*Strollo et al.*, 2008).
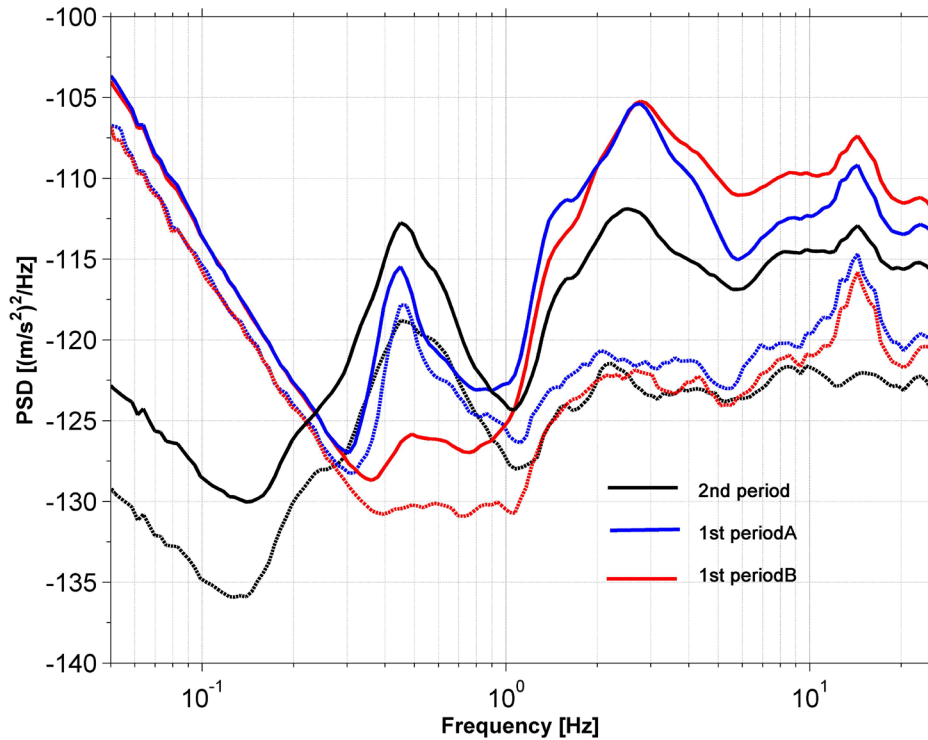
Figure 2.16 Power spectral densities (PSD) for station GU07, vertical component. Broken line: 5th percentile of the Probability Density Function (PDF); solid line: mean PDF. Different colours correspond to different periods. 1st period A: first period with microseisms, julian days from 192 to 194 (i.e. 12 to 14 July 2005); 1st period B: first period without significant microseism activity, julian days from 195 to 197 (i.e. 15 to 17 July 2005); 2nd period: julian days from 334 to 336 (i.e. from 29 November to 5 December 2005), when microseism activity was stronger.

During the second period, the combination of high amplitude signal and low instrumental self-noise allow for the detection of reliable amplification patterns for frequencies greater than about 0.15 Hz, while during periods 1A and 1B, the higher instrumental self-noise limits the exploitable frequency range to those larger than about 0.35 Hz. This limit on the exploitable frequency range explains the results of Figure 2.15 for GU07, where during the second period, the peak around 0.3 Hz could be correctly detected because of the favorable signal to noise ratio (where the signal is the ambient noise and noise is the instrumental noise), whereas during period 1 correct information about site amplification cannot be retrieved below 0.35 Hz. A similar behaviour (apparent shift of the NS/V peak towards higher frequencies with decreasing signal-to-noise ratio) was predicted by *Strollo et al.* (2008) by modeling the instrumental self noise of some short period sensors-digitizer pairs.

Conclusions

In the present work, continuous measurements of microseisms were exploited to assess the reliability of the fundamental resonance frequency detected using short-period sensors

when significant local site effects are expected at frequencies less than 1 Hz. The horizontal to vertical ratio has been computed for stations installed over sediments with different thickness and the stability over time of the results has been investigated.

Following the numerical results provided by *Strollo et al.* (2008), reliable H/V peak can be retrieved only if the signal-to-noise spectral ratio (SNR) at frequencies corresponding to the H/V peak (resonance frequency) is greater than a given threshold (e.g. 3). In the case analyzed here, the SNR is determined by the ratio between ambient and instrumental noise spectral levels. Since the short-period sensor filters the input signal at frequencies lower than its corner frequency (1Hz for the short-period sensor consider in the present work) and the instrumental self-noise spectral level increases for decreasing frequency (e.g. *Strollo et al.*, 2008), the SNR decreases with decreasing frequency and fundamental frequencies of resonance occurring at frequencies below a threshold cannot be retrieved. As shown by the results obtained for station GU07 in the Gubbio basin, this threshold can be lowered by diminishing as much as possible the instrumental self-noise and performing the measurements during hours of strong ambient noise. But, while the self-noise can be partially attenuated by selecting an appropriate set-up for the adopted instrumental equipment (e.g., by increasing as much as possible the gain of digitizers, as suggested by *Strollo et al.*, 2008), the environmental condition are not under the control of the operator. This means that, for a given instrumental choice, the results could be not reproducible, since depending on the input signal, and biased estimates of the fundamental frequency of resonance are obtained. This is the result shown in this article for GU07 when comparing the H/V computed during period 1 (low microseism activity) with the transfer function obtained by analyzing the recorded earthquakes. The peak is clearly shifted towards high frequencies and strongly attenuated (Figure 2.15) and, without any further information, the low amplification of the peak could cast doubts about its reliability. The risk of completely missing the peak of resonance at frequency below 1 Hz is increased if short-period sensor with corner frequencies higher than 1 Hz (e.g. considering the 4.5 Hz geophones, frequently used in microzonation projects) are adopted (*Strollo et al.*, 2008). In conclusion, for a correct interpretation of the amplification peaks at frequencies less than 1 Hz estimated using recordings from short-period sensors, an estimate of the ambient noise-to-instrumental noise ratio must always be considered.

Chapter

3

Microzonation of Potenza (Southern Italy) in terms of Spectral Intensity Ratio using joint analysis of earthquakes and ambient noise*

3   Microzonation of Potenza (Southern Italy) in terms of Spectral Intensity Ratio using joint analysis of earthquakes and ambient noise

Abstract

A temporary seismic network composed of 11 stations was installed in the city of Potenza (southern Italy) to record local and regional seismicity within the context of a national project funded by the Italian Department of Civil Protection (DPC). Some stations were moved after a certain time in order to increase the number of measurement points, leading to a total of 14 sites within the city by the end of the experiment. Recordings from 26 local earthquakes were analyzed to compute the site responses at the 14 sites by applying both reference and non-reference site techniques. Furthermore, the Spectral Intensities (SI) for each local earthquake, as well as their ratios with respect to the values obtained at a reference site, were also calculated. In addition, a field survey of 233 single station noise measurements within the city was carried out to increase the information available at localities different from the 14 monitoring sites. By using the results of the correlation analysis between the horizontal-to-vertical spectral ratios computed from noise recordings (NHV) at the 14 selected sites and those derived by the single station noise measurements within the town as a proxy, the spectral intensity correction factors for site amplification obtained from earthquake analysis were extended to the entire city area. This procedure allowed us to provide a microzonation map of the urban area that can be directly used when calculating risk scenarios for civil defence purposes.

Introduction

The city of Potenza is located in the Southern Apennines (Italy) and has currently 70.000 inhabitants (*ISTAT demographic data*, n.d.). Being the regional capital, during daytime it attracts from neighbouring villages a large number of commuters and students, reaching an estimated daytime occupancy exceeding 100.000 people. Over the last 30 years, 3 damaging earthquakes have affected this area. The M_s 6.9 Irpinia earthquake (1980) reached intensities of VII-VIII MCS inside the urban area of Potenza while the 1990 and 1991 earthquakes (respectively M 5.4 and M 5.1) yielded a maximum observed intensity of VI MCS (*INGV earthquake catalogue*, n.d). Furthermore, the city is located about 20 km from the "Pergola-Melandro" fault (*Moro et al.*, 2007) which is situated between the maximum intensity areas of two of the most destructive earthquakes reported in the Italian seismic catalogue: the M~ 7.0 Val d'Agri earthquakes (1857) and the previously mentioned Irpinia earthquake. This fault is not associated with known historical events and for this reason is currently the subject of

investigations as to whether it constitutes a potential seismic gap, where the probability of future ruptures is higher than in the surrounding regions, also considering the static stress increase caused by the two above mentioned earthquakes (*Lucente et al.*, 2005). Therefore, since the area encompassing Potenza and its surroundings are exposed to moderate to large earthquakes (in the magnitude range from 5 to 7), in the recently issued Italian seismic normative (*INGV Italian Hazard map*, n.d.), it has been included among the areas with the highest hazard level (i.e., classified as zone 1 according to the Italian seismic normative).

The city of Potenza was selected as a test site within the framework of the S3 Italian Civil Defence Department − National Institute of Geophysics and Volcanology 2004-2006 project (*INGV DPC-S3*, n.d.). The aim of this project was to calculate seismic risk scenarios in areas of strategic and/or priority interest in Italy, starting from the maximum credible earthquake generated from surrounding seismogenic faults, and taking into account both site effects and building vulnerability. After the last damaging earthquake (1990), an extensive inventory in term of the vulnerability of buildings was collected within the framework of ENSeRVES project (European Network on Seismic Risk, Vulnerability and Earthquake Scenarios, *Dolce et al.*, 2003). About 4500 data sheets which include all necessary information were compiled through building by building field inspections, providing an additional data set for improved risk analysis.

The effect that the local complex geomorphological features, such as the narrow valleys (covered by different kinds of soft sediments) surrounded by steep hills upon which the city lies, have on ground motion amplification and duration must be taken into account for a reliable hazard assessment. These effects can be empirically estimated in terms of Fourier and spectral intensity amplification factors using both reference and non-reference site methods (*Bard*, 1995). The reference site method (RSM), proposed by *Borcherdt*, 1970, is based on the assumption that the spectral ratio of two recordings at nearby sites is directly related to the relative local site response since the path and source contributions are removed by the spectral division. This method can be generalized by jointly analyzing a set of earthquakes recorded by a local network (e.g., *Andrews*, 1986; *Castro et al.*, 1990; *Bindi et al.*, 2006; *Oth et al.*, 2008). The simultaneous spectral inversion of different earthquakes recorded by different stations, generally referred to as the generalized inversion technique (GIT), allows the separation of the contributions from the site from those of attenuation and the source. In many applications, it has been shown that if a suitable reference site is selected, the results provided by RSM and GIT are consistent (e.g., *Steidl et al.*, 1996; *Parolai et al.*, 2000; *Bindi et al.*, 2009).

Since a reference site is not always available, techniques based on single station

recordings, such as the horizontal-to-vertical spectral ratio (H/V) method, were introduced to estimate site effects. This non-reference site technique was introduced first by *Nogoshi and Igarashi*, (1971), but *Nakamura*, (1989) made it popular. Originally, the method was proposed for interpreting ambient seismic noise measurements (NHV). Only later, *Lermo and Chavez-Garcia*, (1993) applied this technique to the S wave part of earthquake recordings (EHV), showing its capability to estimate the seismic resonance frequency of a site. Over the last few years, several studies have compared site responses obtained using reference and non-reference site techniques (e.g., *Field and Jacob*, 1995; *Parolai et al.*, 2004; *Haghshenas et al.*, 2008). Most of them agree that RSM and EHV generally provide consistent estimates of the fundamental resonance frequency. However, the level of amplification, especially at frequencies higher than the fundamental one, might disagree. Also, the NHV method generally provides reliable estimates of fundamental frequency but not of the amplification of ground motion (*Parolai et al.,* 2004).

Recently the engineering community has focused its attention on the spectral intensity (SI) (*Housner*, 1952) as a tool to describe the severity of ground shaking. It has been shown that it is a stable estimator accounting for both the amplitude and frequency content of ground shaking (e.g. *Ueong*, 2009; *Masi et al.*, 2010). Recently, *Chiauzzi et al.*, (2010), following the approach of *Housner*, (1952) developed a relationship between spectral intensity (SI) computed on data selected from the Italian accelerometric archive (*Itaca*, n.d.) and macroseismic intensities (EMS). This allows that the SI values can be easily used for calculating hazard and risk scenarios. Furthermore, when a reference site is available, the Spectral Intensity Ratio (SIR) with respect to a reference site can also be used as a description of the local site amplification (*Pergalani et al.*, 1999; *Marcellini and Pagani*, 2004; *Pergalani et al.*, 2008). Importantly *Marcellini and Pagani*, 2004 showed that the SIR range of variability is comparable with the range of soil correction coefficients prescribed by several seismic codes. In particular, with respect to the standard engineers practice in Italy, the design soil coefficient "S" (*Rey et al.*, 2002) is directly comparable with SIR.

In this work we first describe the geological setting of the investigated area and the data set acquired during the field surveys. Afterwards, by applying both reference and non reference site techniques, we estimate the site response at sites where the earthquakes were recorded (henceforth referred to as the calibration sites) in order to assess the reliability of the NHV results. Spectral Intensities and the relative ratios with respect to the reference site have been also calculated and compared with amplification functions obtained from RSM methods for each calibration site. Using as a proxy the results of the correlation analysis performed between the NHV calculated for 233 single station noise measurements spread in the

investigated area and those obtained for the 14 calibration sites, the SIR factors are exported to all measurement points. Finally, a microzonation map in terms of SIR is provided for Potenza.

Geological setting

Potenza is located in Southern Italy, along the Apennines chain. It shows the typical features of villages and cities that have developed along this chain, with the old historical part located on the top of a hill and is surrounded by the more recent urban areas where the industries are generally located. In terms of seismic risk, the areas where the new settlements are developing are characterized by the largest exposure indexes, both in terms of population density and the presence of critical facilities. Figure 3.1 shows a simplified lithological map of Potenza, which has an extent of about 16 km^2 and elevation variations of about 200 m within the town.
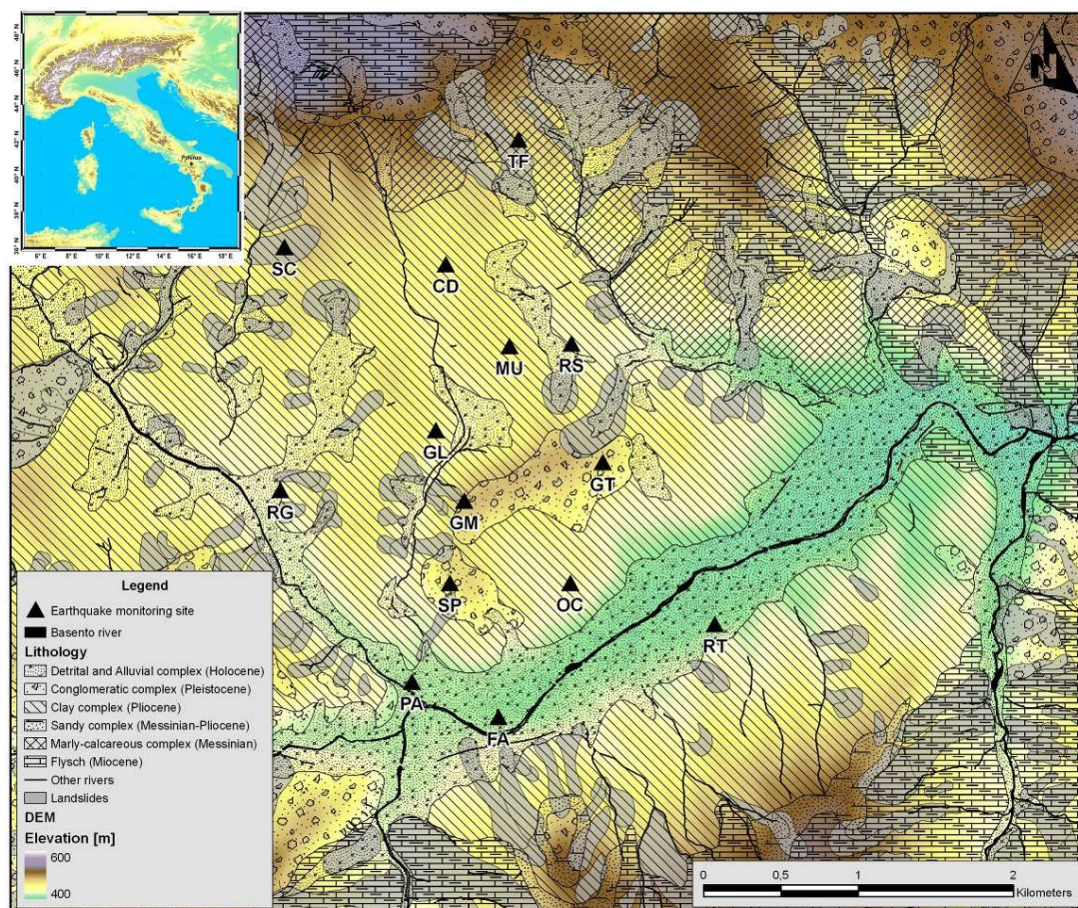
Figure 3.1 Simplified lithological map. The black triangles indicate the location of the selected earthquake monitoring sites.

Six different lithological units outcrop in the urban area. The basement of the most recent units dates back to upper Miocene, the period when the Apennine chain started forming. The flysch and the marly-calcareous complex are part of this basement and mainly belonging to

the Lagonegresi unit (*Di Nocera et al.*, 1988). These units surround the urban area and are essentially made up of layered calcarenites and varicoloured clays. The Plio-Pleistocene units lying on the basement and outcropping in the central part of the map belong to the Altavilla and Ariano units, and are mostly made up of sands, grey-blue silty clays and conglomerates. The uppermost sediments (Holocene), referred to as detrital and alluvial complexes in the simplified geological map above consist of mainly silty and clayey alluvial debris and deposits. In Figure 3.1, the location of landslides is also indicated, showing that, as discussed in *Caniani et al.,* (2008), about 30% of the urban territory is prone to slope instability. It is worth nothing that almost all the landslides detected are located inside the clay complex (Ariano Unit) and within the flysch and the marly-calcareous complex (Lagonegresi unit) at the detachment interface between layered calcarenites and varicoloured clays.

Data set

A seismic network composed of 11 stations was installed in Potenza and operated from October 2004 to May 2005. The number of investigated sites was increased to 14 (shown as black triangles in Figure 3.1 and 3.2) by moving some stations to different sites during this period.
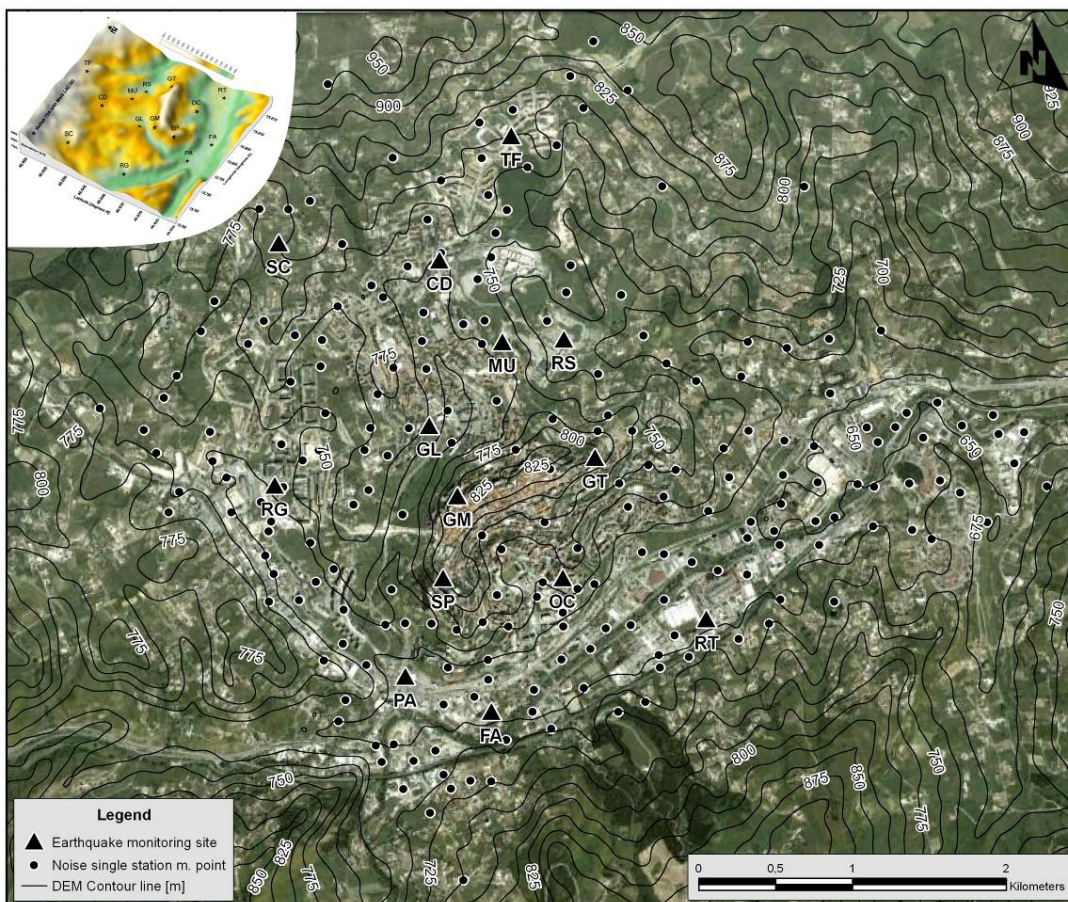
Figure3.2 Seismic stations (triangles) and single station noise measurement points (circles) locations within the city of Potenza. The inset shows the 3D digital elevation model.

In particular, one station was moved, after one month of acquisition, from the SC to GL sites (Figure 3.1) and moved again from GL to OC two months before the end of the experiment. A second station was moved from site PA to RT, after an acquisition period of four months. The monitoring sites were selected with the aim of sampling different characteristic units from both geological and geomorphological points of view. Particular attention was dedicated to areas damaged by past earthquakes. The stations, installed always in the ground floor of buildings, were equipped with a 24 bit digital acquisition system, a 1 Hz natural frequency calibrated geophone, and GPS antenna for synchronous time and position recording. The sampling rate was fixed to 100 sps and recording was continuous mode. During the monitoring period, about 250 earthquakes, including local, regional and teleseismic events, were recorded. The recordings from 26 local earthquakes with signal to noise ratios greater than 3 over the frequency range 1-10 Hz were selected for evaluating site effects in Potenza. The selected earthquakes span the local magnitude range from 2.2 to 3.8 and the distance range from 8 to 92 km. For each earthquake recording, a pre-event noise window of 30 minutes was also stored. In Figure 3.3, the recordings from the three components at 5 different stations of a M=2.8 earthquake located ~55 km from the network are showed. It is worth noting the relative amplification of the peak ground velocity at sites CD and TF with respect to RS.

Vp [km/sec]	h [km]
3,0	1,0
3,5	2,0
4,5	5,0
5,2	10,0
6,0	30,0
8,1	halfspace
Vp/Vs fixed to 1,73	

Table 3.1 Seismic velocity model used for locating the local events showed in figure 3.4

In order to perform the following analysis, for the local subset of events, P- and S-phase arrivals were identified and used to re-locate the selected earthquakes using Hypoellipse (*Lahr*, n.d.). Since the aperture of the network was not enough large to provide satisfactory locations (Figure 3.4), arrival times from 13 permanent stations deployed in the region that belong to the INGV-MedNET network (*INGV-MEDnet*, n.d.), were also considered. The model used for the location is outlined in Table 3.1.

During the working period of the network, 233 single station noise measurements were carried out within the urban area of Potenza (Figure 3.2), sampling different lithologic and topographic conditions. For each site, 30 minutes of ambient noise was recorded using a 24 bit digital acquisition system with an embedded 4.5 Hz three component geophone. The

sampling rate was set to 100 sps.
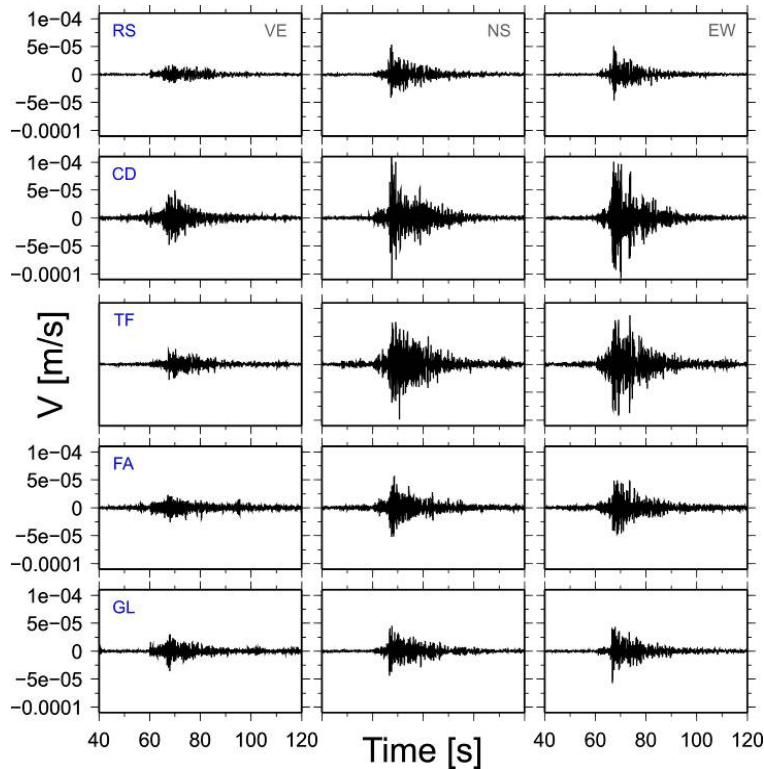
Figure 3.3 Example of recordings of a Ml 2.8 earthquake that occurred at ~55 km from the network (Figure 3.4). In the left middle and right panels are represented the vertical, north-south and east-west components, respectively. The station code (Figure 3.1) is provided within each frame in the left column.
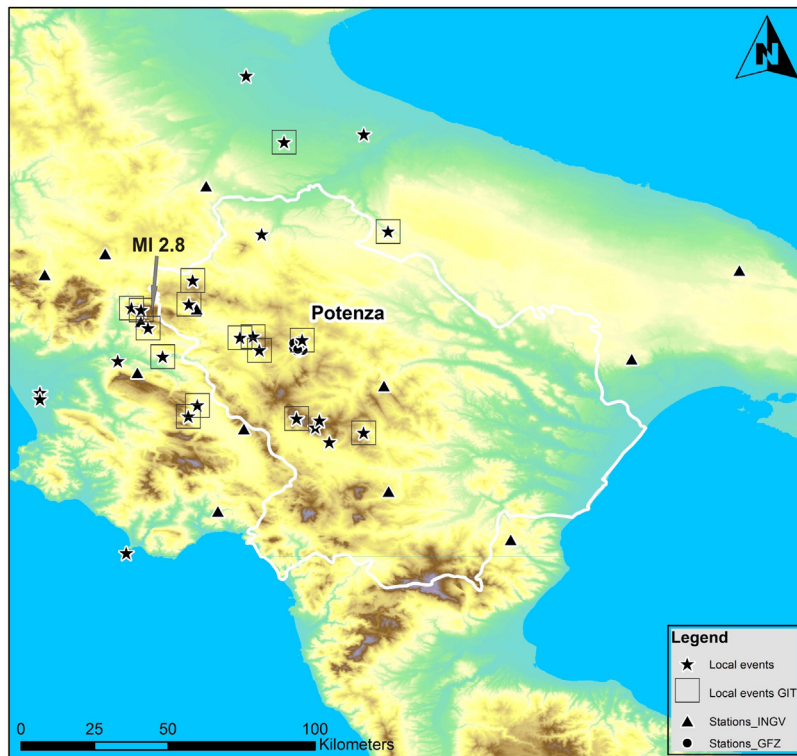
Figure 3.4 The temporary seismic network in Potenza (circles); the local events used in this study are represented with the star while only those with the black square have been used for GIT. Triangles indicate the INGV-MedNET permanent stations used for re-locating the events. The gray arrow indicates the epicentre of the event showed in Figure 3.3.

Earthquake Horizontal to Vertical spectral ratio (EHV)

The EHV method belongs to the class of so-called non-reference site methods (Bard, 1995). It is based on the assumption that the vertical component of ground motion is not affected by amplification effects during the propagation through the soil layers and that it is similar to the horizontal component at the bedrock. The spectral ratios were carried out considering windows selected with the criteria that they contain 90% of the energy content for both P and S phases. The largest duration among those obtained for three components has been considered to have the same length over the three components. For local events, the P-wave window ended 1 second before the S-wave arrival (if the 90% of energy is not reached yet) while the maximum duration for the S-wave windows was fixed to 90 seconds. Each window has been cosine tapered (5%) and Fourier transformed. Instrumental corrections have been applied and the spectral amplitudes smoothed using a *Konno and Ohmachi*, (1998) window. The parameter b, which determines the degree of smoothing, was fixed to 40, ensuring the smoothing of numerical instabilities while preserving the major features of the spectra. Finally, the root-mean-square of the two horizontal components has been computed and, for each station, the geometrical mean of the horizontal-to-vertical spectral ratios for different recordings has been evaluated. Depending upon the period of operation and gaps in the functioning of the stations, the number of events considered for computing the Horizontal to Vertical Spectral ratios varies from 6 (station SC) to 26 (station RS, see Figure 3.1).

Figure 3.5 exemplifies the EHV for 6 stations that are representative of the results obtained for the calibration sites in Potenza. The results show that EHV obtained for RS and RG stations (Figure 3.5, first row) are almost flat. These stations were installed over the silty-clay complex (Figure 3.1), the most common lithology within the city, and where the S-wave velocity has been estimated to be higher. Moreover, since station RS was installed within the draining tunnel of the university, at about 6 meters below ground level, good quality recordings are available for this station for almost all the considered events, due the less noisy environment with respect to the other stations. For all the above reasons, in the following analysis station RS is used as the reference station. The others stations shown in Figure 3.5 (MU, TF, CD and RT) show significant peaks in their amplifications in the frequency range from 2 to 5 Hz, with a good agreement between the results obtained for P- and S-wave windows. The results for the remaining stations, as well as the signal to noise ratio, are shown in the Appendix.
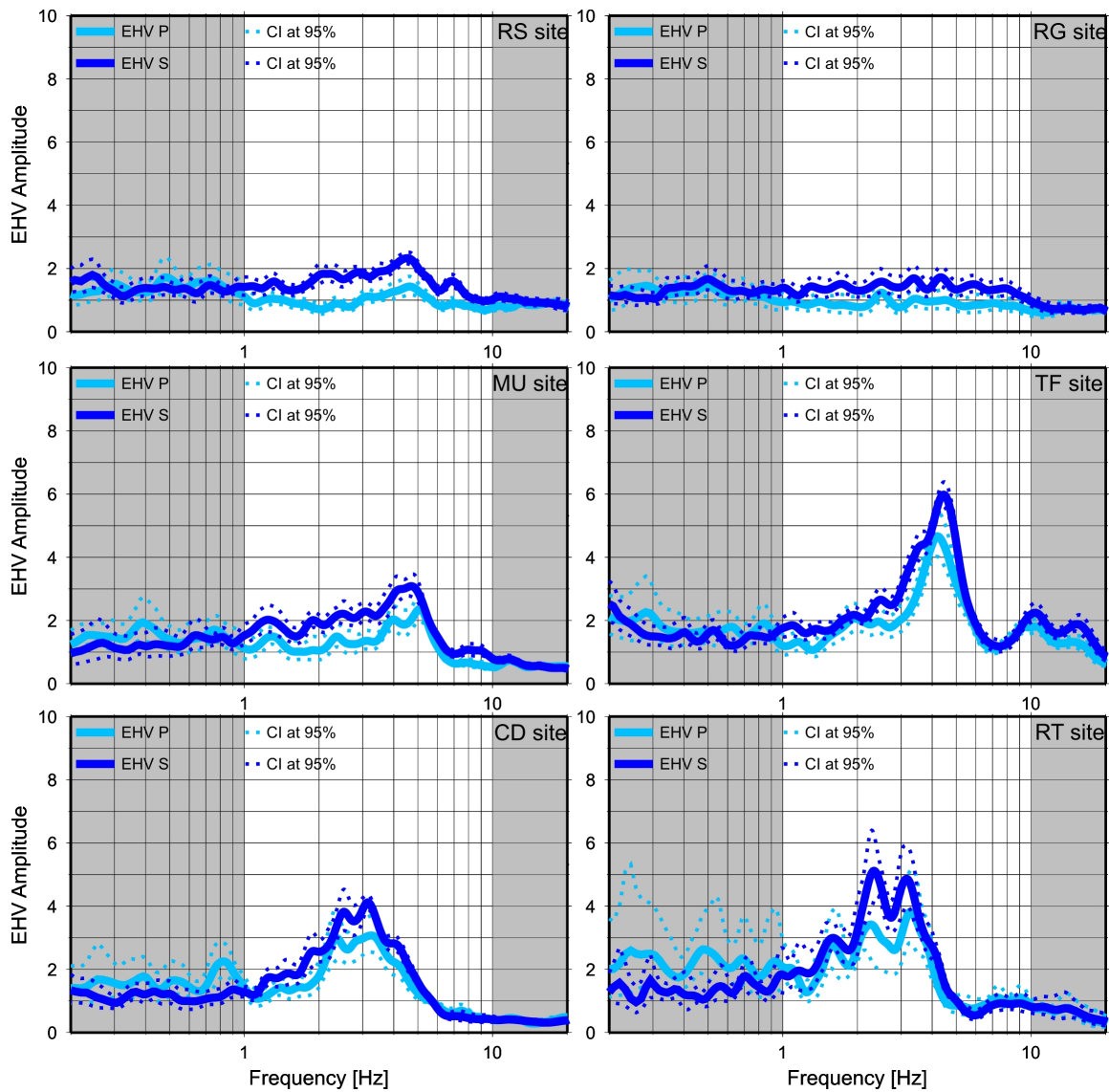
Figure 3.5 EHV for 6 different sites. The blue and the light blue lines represent the EHV calculated using the S phase and P phase windows, respectively. The two thin dotted lines represent the 95% confidence interval. The gray shadowed areas indicate the frequency band where the signal to noise ratio is smaller than 3.

Standard Spectral Ratio (SSR)

The SSR technique is also a reference site method (*Bard*, 1995). In fact, once a reference site has been chosen, the spectral ratios between all the other stations and the reference are calculated for each component of ground motion. In this work, we compute the SSR with respect to station RS and analyze the same S-wave windows used for computing the EHV. In Figure 3.6, the SSR for the horizontal components of 5 representative stations are shown (the same sites as in Figure 3.5, but without RS). The remaining sites are presented in the Appendix. A general good agreement between the EHV (Figure 3.5) and SSR results is observed, both in terms of the locations of peaks and the amplification levels. In particular, the SSR results confirm that RG has an almost flat amplification function, while stations TF, CD and RT show peaks in their amplification in the frequency range between 2 and 5 Hz. The shift of the frequency corresponding to the amplification peak observed in the SSR for station

MU with respect to the EHV is related to the amplification affecting the vertical component, as shown in Figure 3.6.
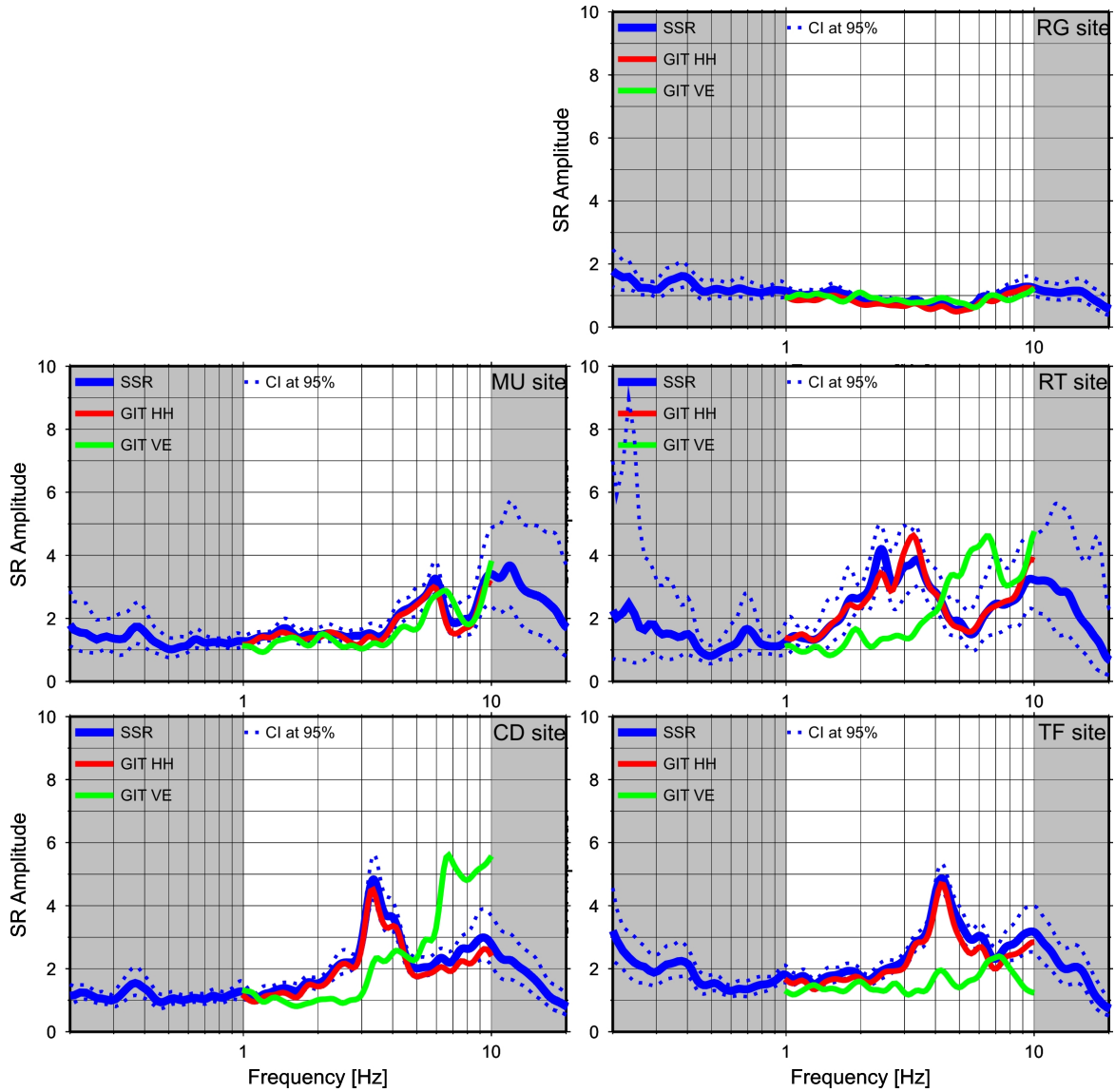
Figure 3.6. SSR and GIT results for 5 sites (the name of the site is indicated in the upper-right part of each panel). The blue lines represent the SSR with its 95% confidence interval while the red and the green lines represent the GIT for the horizontal component, and for the vertical component, respectively. The gray shadow indicates the frequency band with a signal to noise ratio smaller than 3.

Generalized Inversion Technique (GIT)

In the GIT method, the site response of all stations are simultaneously separated from the source spectra and attenuation function by performing a matrix inversion (e.g., *Castro et al.*, 1990; *Parolai et al.*, 2004; *Oth et al.*, 2008) The natural logarithm of the spectral amplitudes $U_{ij}(f,r)$ for an event *i* observed at a recording site *j*, can be described as:

$$\ln U_{ij}(f,r) = \ln S_i(f) + \ln Z_j(f) + \ln A_{ij}(f,r) \qquad (1)$$

where $S_i(f)$ is the source spectrum, $Z_j(f)$ is the site response, $A_{ij}(f,r)$ is a function accounting for attenuation along the path, *f* is the frequency and *r* is the distance. For all events and all stations, equation (1) describes a linear system of the form $Ax = b$, which can be solved by

using suitable inversion algorithms. In order to avoid *a priori* parameterization of the attenuation term $A_{ij}(f,r)$, the inversion is generally performed in two steps (*Castro et al.*, 1990). In the first step, the inversion is carried out to separate the source and attenuation effects. The trade-off between attenuation and source is resolved by requiring that the attenuation assumes an *a priori* value at a given distance, irrespective of frequency. In the second step, the inversion is carried out for the source function and the site responses, using residuals obtained for correcting the observed data for the attenuation results. The undetermined degree of freedom of the second inversion is resolved by constraining the logarithm of the site amplification of the reference station to 0, irrespective of frequency.

Since the distribution of recordings versus distance does not allow a reliable seismic attenuation function to be derived over the analyzed distance range, in this study we carry out only the second step of the inversion after having corrected the observed spectral values, relevant to the 16 earthquakes for the attenuation effects (*Luzi et al.*, 2005). We considered a regional model previously derived for the studied area (*Castro et al.*, 2004) that follows the form:

$$A(f,r) = \frac{1}{R} e^{-\frac{\pi f R}{Q \beta}} \tag{2}$$

where R is the hypocentral distance, f the frequency, β the shear wave velocity (assumed to be 3.5 km/sec), and $Q(f)=32.1f^{1.7}$ is the frequency dependent quality factor. Previous studies (e.g. *Parolai et al.*, 2000) have shown that this choice does not affect the site response estimation.

The GIT inversion has been carried out over the frequency range 1-10 Hz where the signal-to-noise ratio is greatest. The site responses for the horizontal components obtained for stations RG, MU, TF, CD and RT are shown in Figure 3.6. Since for the GIT the amplification function of RS site was constrained to 1 irrespective of frequency, the good agreement between SSR and GIT results shown in Figure 3.6 confirm that RS is a suitable reference site, almost free from significant amplification effects. The GIT transfer functions obtained for all the stations are shown in the Appendix.

Seismic Noise Horizontal to Vertical spectral ratio (NHV)

The horizontal-to-vertical spectral ratio method was also applied to ambient noise recordings (NHV). Differently from the EHV, SSR and GIT methods, the analysis of noise was carried out using the seismic noise recordings from both the calibration sites and from the other 233 sites selected within the urban area. For each of these sites, we analyzed 20 non-overlapping signal windows with a duration of 60 seconds. Each window was tapered at both

ends with a 5% cosine taper and its Fast Fourier Transform (FFT) calculated. The FFT have been smoothed using a Konno-Ohmachi window (*Konno and Ohmachi*, 1998) fixing the parameter b to 40. For each 60 second window, the NHV was computed and the logarithmic average of the NHV estimated. The good agreement between the NHV, EHV and SSR results shown in Figure 3.7 for the sites RS, RG, MU, TF, CD and RT confirm that, through the analysis of ambient noise, it is possible to capture the main features of the amplification effects over the considered frequency band.
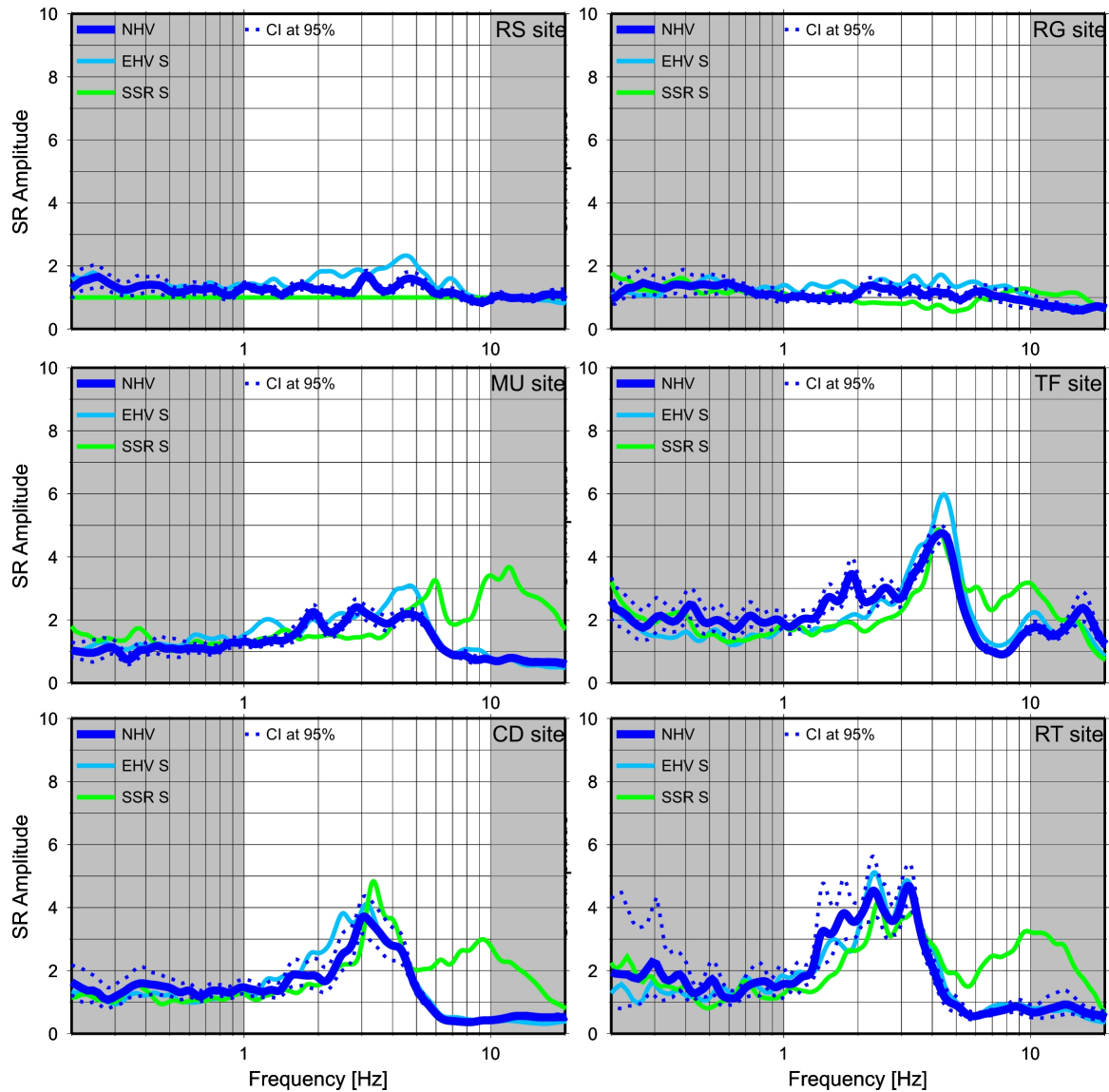
Figure 3.7 NHV results (thick blue line) with their 95% confidence interval (dotted blue line). . EHV and SSR results are showed in light blue and green, respectively. The gray shadowed areas indicate the frequency band with signal to noise ratios (for EHV and SSR) smaller than 3.

Spectral Intensity Ratio (SIR)

In order to calculate the SIR for each site with respect to the reference one, spectral intensities (SI) have been calculated for each local event. Although in the original definition

of *Housner*, (1952) the SI is calculated as the area under the pseudo-velocity spectrum (PVS) between the periods of 0.1 and 2.5 seconds, in this paper, following *Gavarini and Gruppo di lavoro*, (1999), a different integration interval (0.2-2 seconds, according to equation 3) was used in order to take into account both the frequency band with sufficient signal to noise ratio for the recorded events and the period of vibration of modern building stock.

$$SI = \int_{0.2}^{2} PVS(T,\xi)dT \qquad\qquad (3)$$

In fact, considering the characteristics of the Italian buildings, it was shown that SI calculated within this interval provides a better correlation with the building damage grade in terms of EMS Intensity scale (*Gavarini and Gruppo di lavoro*, 1999). Response spectra were calculated considering a 5% damping of the critical. For each earthquake, the maximum between the ratio of the two horizontal components with respect to the SI evaluated for the reference site has been retained as being representative of the site. Finally, for each calibration site (i.e., where earthquakes have been recorded), the SIR factor has been computed as the median of the distribution of values obtained considering different earthquakes (Figure 3.8). The largest SIR values are obtained for those stations affected by significant amplification effects over the frequency range 0.5-5 Hz (corresponding to the period interval used in equation 3), such as stations RT and CD (Figure 3.7). The obtained SIR coefficients are in turn used to group the stations into three classes of amplification (low, medium, and high) using a cluster analysis (*Tryon*, 1939), as shown in Figure 3.8.
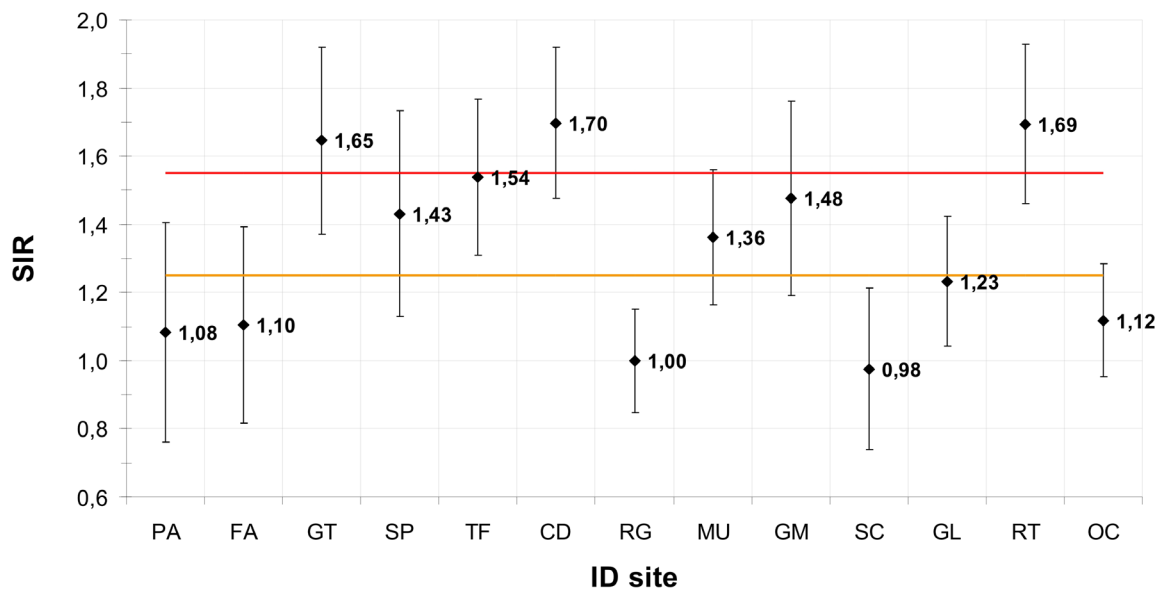
Figure 3.8 Spectral intensity ratios (SIR) obtained for the 13 calibration sites with respect to station RS. The median ± one standard deviation is shown for each station,. The orange and the red lines separate the SIR values into three classes with respect to the amplification level.

Correlation analysis and microzonation map

Recently, different attempts to correlate the NHV function with the site response have been carried out. *Bragato et al.*, (2007), following the approach used by *Rodriguez and Midorikawa*, (2002), used NHV functions to identify homogeneous areas in terms of site response by means of cluster analysis, following a Bayesian approach. Similarly, *Cara et al.*, (2010) used the correlation between NHV functions and local geology to explain the damage pattern of a past earthquake in Palermo (Italy). In both studies, the sites are clustered by considering similarity in the NHV function, but without associating any site response function calculated using earthquake data to each cluster.

In the previous sections, the reliability of the NHV functions and SIR values in representing a proxy for separating areas affected by different site effects occurring at the calibration sites in Potenza was assessed through direct comparisons with GIT and SSR results. In particular, independent of the shape, sites showing similar SSR results also share similar NHV curves. It follows that the NHV functions can also be used as a tool that allow the extrapolation of the SIR values computed at the calibration sites to all the other sites in Potenza where the ambient noise has been measured.

In this work, we applied a correlation approach to NHV following two main steps:

1) The degree of similarity between the NHV functions estimated at noise measurement points with the calibration sites is quantified by considering the product between the Pearson cross-correlation coefficient *"r"* (equation 4) (*Davis*, 1986) and the degree of fit *"f"* (equation 5):

$$
r_{jk} = \frac{cv_{jk}}{\sigma_j \cdot \sigma_k} = \frac{\left(\dfrac{\sum_{i=1}^{n} (x_{ij} - \overline{x}_j) \cdot (x_{ik} - \overline{x}_k)}{(n_i - 1)} \right)}{\left(\sqrt{\dfrac{\sum_{i=1}^{n} (x_{ij} - \overline{x}_j)}{(n_i - 1)}} \right) \cdot \left(\sqrt{\dfrac{\sum_{i=1}^{n} (x_{ik} - \overline{x}_k)}{(n_i - 1)}} \right)}
\tag{4}
$$

$$
f_{jk} = \frac{1}{\sqrt{\dfrac{\sum_{i=1}^{n} (x_{ij} - x_{ik})^2}{n_i}}}
\tag{5}
$$

In these equations, *i* represents the number of frequencies selected over the range 1 -10 Hz

(740 samples), j is the number of noise measurement sites (233), k is the number of calibration sites (14) and the vector x represents the NHV functions. The selected frequency range accounts for both the limits of the instruments (i.e. 4.5 Hz geophone) used for measuring ambient noise (e.g., *Strollo et al.*, 2008) and the range of variability of the fundamental frequency of resonance computed in the previous sections for Potenza. Moreover, the upper limit was fixed to 10 Hz in order to avoid strong and very local high frequency sources of noise that are quite common in urban and industrial environments.

A cross-correlation matrix CC is then evaluated as

$$CC = r \cdot f \tag{6}$$

where the matrix CC has dimension [233x14].

In order to identify at which calibration site the noise measurement point is closer in terms of NHV similarity, a threshold of positive values of *CC* larger than 0.3 has been chosen (existence condition). Moreover, a difference in amplitude of at least 10% between the two largest values in the matrix CC for each noise measurement site was required in order to identify uniquely the corresponding calibration site (uniqueness condition).

2) In the second step, the noise measurement points that did not satisfied the uniqueness condition were associated with one of the possible selected calibration sites by considering a hierarchical scheme based on considering the largest value of the *CC* coefficient, the lithological properties and the distance to the calibration sites with the higher *CC* values. In particular, among the calibration sites showing *CC* values within the 10% of the highest one, the noise measurement point is associated with the closest one that shares the same lithology. If the closest among these calibration sites are within 10% of the max *CC* value and share the same lithology at a distance larger than 1 km, the noise measuring point is excluded.

Figure 3.9 exemplifies the results for two different noise measurement points. In each panel, the NHV evaluated for the site (blue line) and those relevant to the calibration points with both the largest (light blue line) and smallest (gray line) cross-correlation coefficients are shown. The example shown in the left panel represents a case corresponding to one of the largest cross correlation obtained (*CC*=3.6) while the example in the right panel correspond to a cross-correlation value equal to the threshold select for the existence condition (*CC*=0.3). Figure 3.9 show that also in the case of the minimum adopted threshold value a fair agreement between the NHV curves is observed.

By applying the two-step cross correlation scheme, SIR values have been successfully associated with 213 sites in Potenza, allowing us to produce a map of 227 SIR values spread within the town (Figure 3.10).
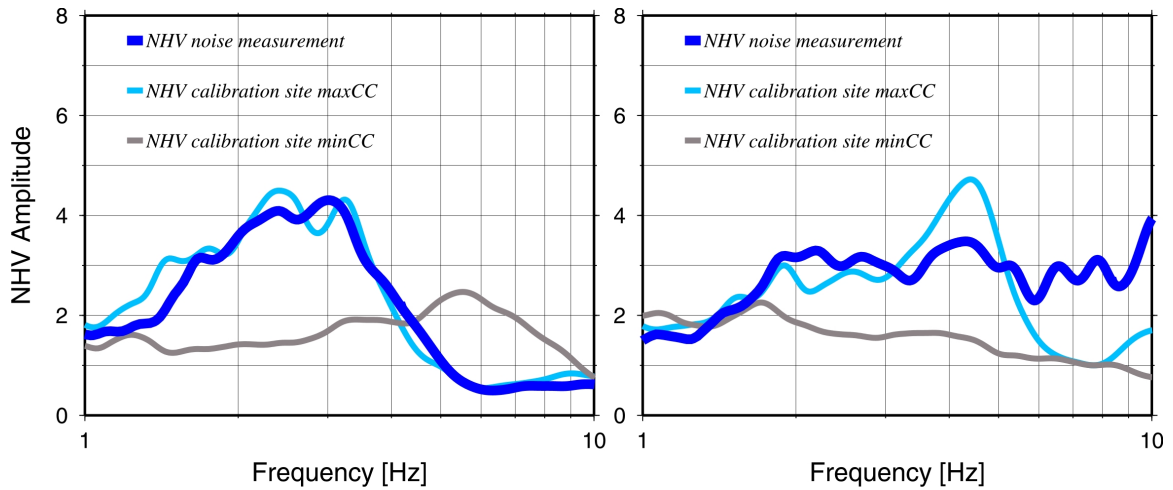
Figure 3.9 Two examples of correlation (points n. 202 (left) and 125 (right) indicated in figure 3.10): NHV of the noise measurement point in blue and NHV for the associated calibration site in light blue. The grey line represents the NHV of the calibration site with the lowest correlation coefficient. Left and right panel have been selected respectively between the maximum and minimum values of correlation coefficients. The NHV of the calibration sites having the max CC values for the two measurements, 202 and 125 are respectively RT and TF, while the min CC values are respectively SC and SP.
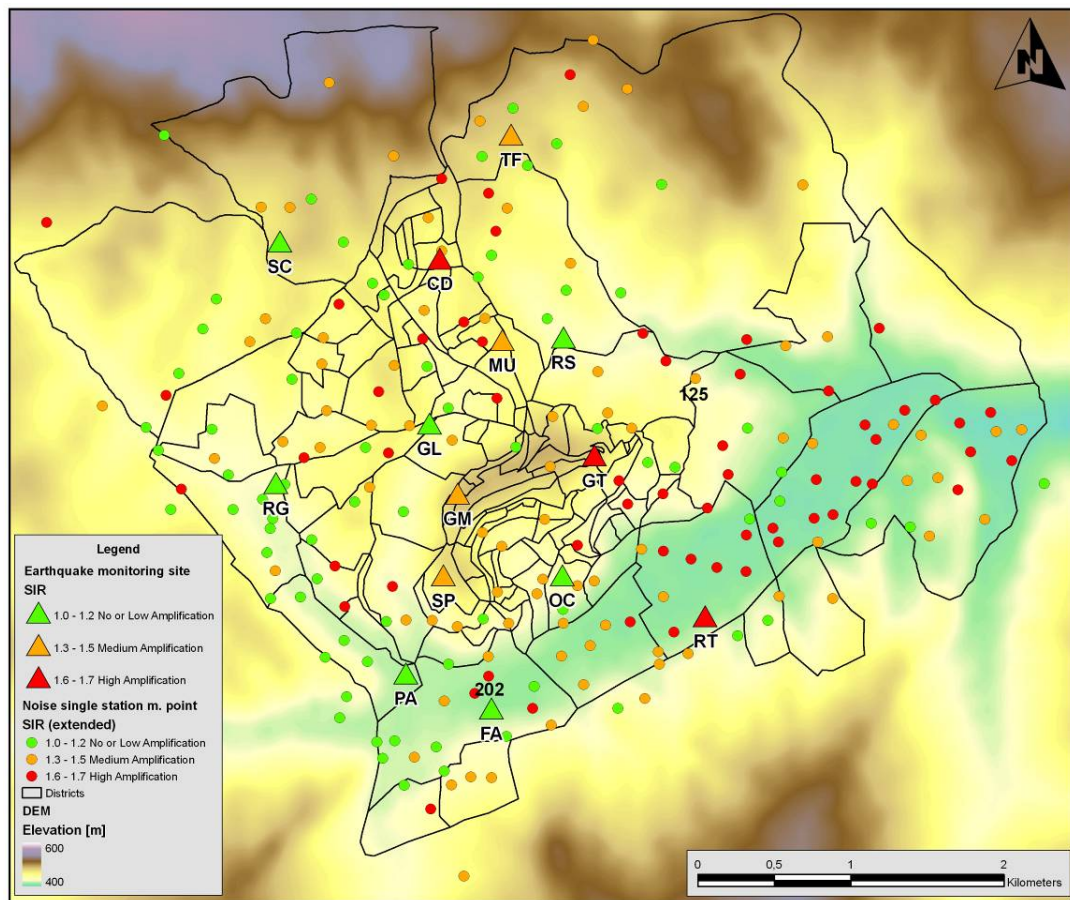
Figure 3.10 Distribution of SIR values for both earthquake monitoring sites and those used for the noise measurements points.

Finally, since for engineering applications such as land-use planning or risk scenario computations, the identification of homogeneous macro-areas within an urban territory with respect to the level of expected ground motion is required, the 227 SIR values were interpolated (Figure 3.11a) and macro areas identified. Furthermore, in order to be consistent with the spatial coverage of the existing vulnerability data, the SIR values have been averaged within the cells representing the districts of the city (Figure 3.11b). The SIR values are represented in the maps according with the three classes identified by means of the cluster analysis (Figure 3.8).
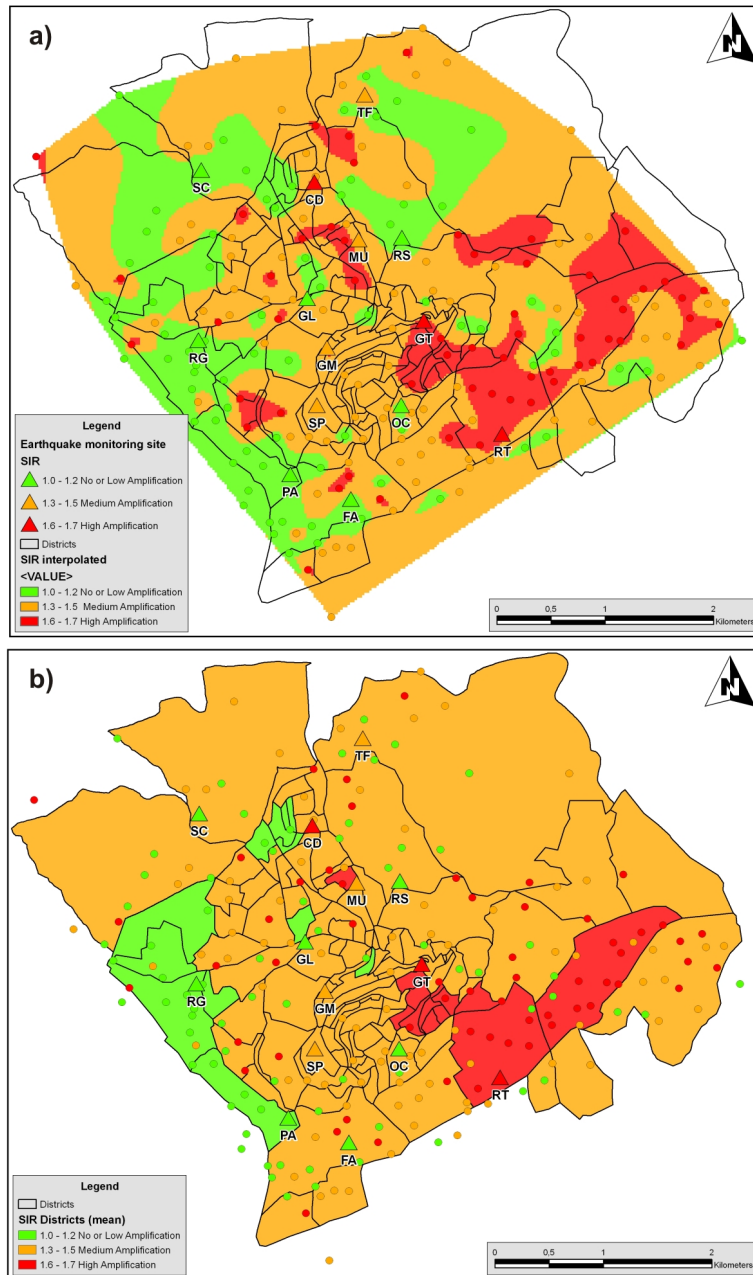
Figure 3.11 a) Natural neighbours interpolation of the SIR values. **b)** District map in terms of SIR**.**

Discussion and conclusions

Within the framework of the seismic microzonation of the town of Potenza (Southern Italy), we have introduced a procedure to extrapolate and link the acquired information, calibrated at a small number of high-quality recording sites, to a larger number of points within the town.
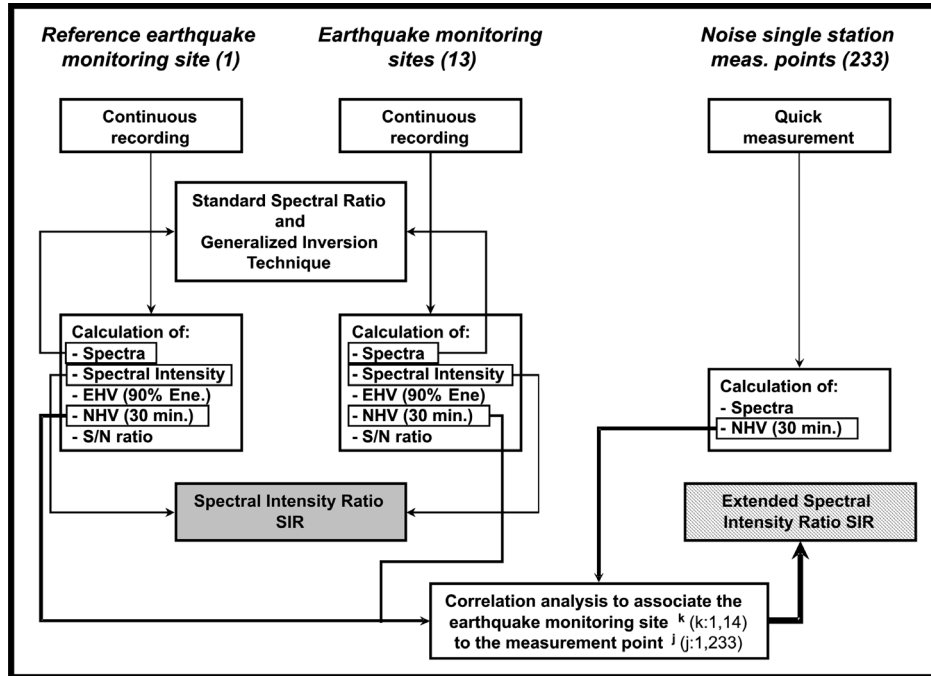
Figure 3.12 Flow-chart of the procedure applied in this study to provide a microzonation of Potenza in terms of Spectral Intensity Ratios.

The approach followed in this work can be described in three steps as follows (Figure 3.12). In the first step, the site transfer functions of 14 sites (calibration sites) in the town, where a temporary seismic network was installed, have been computed using the recorded earthquakes. We applied different techniques to the spectra of S-wave computed for both horizontal and vertical components. A good agreement was obtained between the results of the horizontal-to-vertical spectral ratio technique (EHV) and the site response evaluated by computing the spectral ratios with respect to a reference rock site (SSR and GIT methods). In Potenza, the fundamental frequency of resonance varies within the frequency range from 2 to 6 Hz, with amplifications of up to 6. Differences observed for a few sites (e.g. station MU) can be ascribed to amplifications affecting the vertical component. Moreover, the good agreement between EHV calculated using P and S waves suggests that S-to-P phase conversion could contaminate the wave-field of the horizontal component within the selected P window as showed by *Parolai and Richwalski,* (2004).

In the second step, a single parameter (i.e., spectral intensity ratio) that captures the amplification over the frequency range of interest and well correlates with macroseismic

intensity has been introduced to describe the site effects at the calibration sites. The reliability of SIR as a measure of site amplification effects has been assessed by comparing the spatial variation of the SIR values with that of the site response. We observed that sites showing larger amplification (4-6) also have larger SIR values (1.6-1.7) and that the SIR values vary with the amplification functions.

Finally, in the third step, a procedure to extrapolate and link the SIR values to other sites in Potenza, where recordings of earthquakes were not available, was proposed. Since ambient noise has been recorded at 233 sites in Potenza, we first assessed the suitability of the horizontal-to-vertical spectral ratio of ambient noise (NHV) as tool to estimate the site amplification variability. This task has been accomplished by computing the NHV at the monitoring sites and comparing the results with those of SSR. The good agreement shown by the results obtained from the analysis of noise and earthquakes confirmed that the NHV method is a suitable tool (at least in Potenza) to capture the significant features of site responses and their spatial variability. Then, we used the NHV as a proxy to extrapolate amplification factors (SIR) estimated at the calibration sites to a large number of sites within the town where only noise recordings were available. We developed an approach based on cross-correlation applied to NHV to identify, for each considered site, the calibration site closest in term of site response. Following this approach, we were able to generate a microzonation map (Figure 3.10) for Potenza in terms of Spectral Intensity Ratio values.

This map shows increasing amplification factors along the main valley, starting from nearly no amplification surrounding the RG site at its apex and increasing towards the RT site where the valley is widening (Figures 3.2 and 3.10). The amplification factors reach a maximum in eastern side of the investigated area where detrital and alluvial complexes reach their maximum thickness. Medium amplification factors can be assigned to the remaining part of the urban area except for the two green spots with low amplification located between the GL and SC sites and the red area with high amplification south of the GT site. These variations in amplification are related to lateral changes within the clay complex that is composed of clays with different grades of consolidation. The SIR zonation (Figure 3.11b) shows a fair correlation with the main features of the lithological map (Figure 3.1), indicating that the general of the variations in ground motion are related to lithological changes. The largest amplifications were also observed to correspond to the area covered by the new settlements, industries and strategic facilities (south-east part of the town). Site effects must be therefore taken into account when assessing the seismic risk for this strategically important area.

Finally, we proposed a method for seismic microzonation, based on combining two

different layers of information. The first layer includes detailed but sparse information obtained from the analysis of earthquake data, such as site responses and SIR amplification factors. The second layer includes NHV functions of the elements included in the first layer as well as a large number of additional points to improve spatial resolution. Subsequently, the two layers are linked through similarities in the NHV functions.

Importantly we should remark that the SIR correction factor (accounting for site amplification effects) has been easily included in the hazard scenarios generated for assessing seismic risk in Potenza, improving the spatial resolution and ground motion estimation. In fact, in a first attempt at producing a complete scenario for damage assessment in Potenza using a scenario earthquake, (*Chiauzzi et al.*, 2010) used relationship between Spectral Intensity (SI) and Macroseismic Intensity (EMS) for generating the seismic input. This was in turn locally modified using our site specific coefficients. The results show that, considering site effects, the estimation of unusable buildings in the event of the scenario earthquake increases by 50%. This confirms the potential of the proposed approach for improving seismic risk scenarios for large urban areas.

Chapter

4

Site characterization by seismic noise in Istanbul, Turkey*

4   Site characterization by seismic noise in Istanbul, Turkey.

Abstract

Single station seismic noise measurements were carried out at 192 sites in the western part of Istanbul (Turkey). This extensive survey allowed the fundamental resonance frequency of the sedimentary cover to be mapped, and identify areas prone to site amplification. The results are in good agreement with the geological distribution of sedimentary units, indicating a progressive decrease of the fundamental resonance frequencies from the north-eastern part, where the bedrock outcrops, towards the south-western side, where a thickness of some hundreds meters for the sedimentary cover is estimated. The particular distribution of fundamental resonance frequencies indicates that local amplification of the ground motion might play a significative role in explaining the anomalous damage distribution after the 17 August 1999 Kocaeli Earthquake.

Furthermore, 2-D array measurements of seismic noise were performed in the metropolitan area with the aim of obtaining a preliminary geophysical characterization of the different sedimentary covers. These measurements allow the estimation of the shear-wave velocity profile for some representative areas and the identification of the presence of strong impedance contrast responsible of seismic ground motion amplification. Comparison of a theoretical site response from an estimated S-wave velocity profile with an empirical one based on earthquake recordings strongly encourages the use of the low cost seismic noise techniques for the study of seismic site effects.

Introduction

Istanbul is a megacity of 12 million inhabitants, who are exposed to a significant earthquake hazard. Moreover, the considerable rate of urbanization combined with uncontrolled land use makes such hazard even higher (*Erdik et al.*, 2003).

The main factor controlling the earthquake hazard for Istanbul is undoubtedly the proximity of the North Anatolian Fault, which in the Marmara Sea region forms a complex fault system (*Erdik et al.*, 2003). From an analysis of the available earthquake records performed by *Ambraseys and Finkel* (1991), the city is estimated to be affected by a medium intensity (epicentral intensity of VII-VIII) earthquake with an average return period of 50 years.

During the Izmit and Düzce 1999 earthquakes, this scenario was worsened by the recognition of site amplifications that were observed to locally modify the ground motion inside the metropolitan area. In particular, as shown by several studies (e.g., *Ozel et al.*, 2004;

Ansal et al., 2004) the Avcilar district in the western part of Istanbul suffered significant damage, largely due to the amplification of the earthquake ground motion. In fact, for this area, an intensity of VII (MSK) was assigned, while in the other districts of the metropolitan area an intensity of VI (MSK) was generally observed (*Gruenthal*, 1998; *Ozmen*, 2004). The anomalous amplification of the ground motion observed in the western part of the city is considered to be mainly related to the presence of soft sediments overlaying a competent seismic bedrock. In fact, the thickness and the velocity of the sedimentary layers, as well the impedance contrast between the sediments and the underlying bedrock, are the main parameters affecting the frequency band of the seismic motion that may be strongly amplified by the local conditions. Therefore, recent studies (e.g., *Ergin et al.*, 2004; *Sørensen et al.*, 2006) have focused on estimating possible site effects in the metropolitan area of Istanbul, and in particular in its western part.

A suitable characterization of local site effects can be performed by estimating local S-wave velocity profiles, or by determining the resonance frequency of the soft soil layers. Often, information is obtained through invasive techniques, such as drilling, down/cross-hole measurements, etc.. However, due to their expensive nature, the widespread application of such techniques is only able to be performed after coming to a compromise with respect to cost, resulting in a limited exploration depth. In fact, microzonation works are frequently based on the use of the average shear wave velocity in the uppermost 30 m (Vs30), which is adopted by the National Earthquake Hazard Reduction Program (NEHRP) classification in the USA. However, several works (e.g., *Wald et al.*, 2000; *Mucciarelli and Gallipoli*, 2006) have showed that in a number of geological-geotechnical and morphological contexts, the Vs30 classification is not always a suitable tool for site effect estimation. Also for this reason, non-invasive and cost effective passive seismic techniques have recently become an attractive option for seismic site-effect studies.

Especially in the last decade, environmental noise recordings performed by single-station methods to estimate *horizontal-to-vertical* (*H/V*) spectral ratio curves (e.g., *Fäh et al.*, 2001; *Arai et al.*, 2004) and by 2D micro-array techniques to estimate surface wave dispersion curves (e.g. *Scherbaum et al.*, 2003) have provided very promising results.

Parolai et al. (2001, 2004), showed that the seismic noise *H/V* curves exhibit a good agreement with the *H/V* from earthquake recordings, especially with regard to the value of the fundamental resonance frequency of the sedimentary cover. Therefore, performing a large number of noise measurements over a region of interest allows a map of the fundamental frequencies to be obtained, which provides an overview of the distribution of both the sedimentary cover thickness and, most importantly, of those areas where the amplification of

the seismic motion in the frequency band of interest for buildings behaviour is expected.

Concerning 2D arrays, it has been shown (e.g., *Tokimatsu et al.*, 1992; *Parolai et al.*, 2006) that by using Rayleigh wave dispersion curves, the characterization of the local *S*-wave velocity profile can be obtained with a good accuracy, especially when a priori information about the total sedimentary cover thickness is available in advance. Further improvements are obtained by applying the joint inversion of phase velocity and *H/V* ratio curves (*Scherbaum et al.*, 2003; *Parolai et al.*, 2005; *Arai et al.*, 2005) which allows the trade-off problem between the model parameters that hampers the separate inversion of these curves to be overcome. The application of this inversion scheme has also had success in estimating the S-wave velocity profile for sedimentary covers hundreds of meters thick (e.g., *Parolai et al.*, 2005). Although for the engineering-geotechnical community the lack of high resolution in the S-wave velocity profile can be considered a drawback, from the site-effect point of view, passive techniques, especially in the case of sedimentary cover thicker than 30 to 50 m, provide estimates of the local transfer function that are in very good agreement with both the empirical ones (*Picozzi et al.*, 2007; *Parolai et al.*, 2007) and those obtained by 1D techniques (e.g. SASW, MASW) that allow the reconstruction of the shallower part of the S-wave velocity profile with a higher resolution *Richwalski et al.*, 2007).

In this work, as a preliminary activity for the microzonation characterization of Istanbul, 192 single station measurements (Figure 4.1a) for the estimation of the *H/V* curves were carried out in the western part of the metropolitan area, in order to estimate the fundamental resonance frequency of the sedimentary cover. In particular, 42 of these noise measurements were performed at sites where accelerometers belonging to the permanent and temporary networks operated by the Kandilli Observatory and Earthquake Research Institute (KOERI) are located. Thus, for 29 sites of the considered accelerometric stations, the *H/V* curves from noise recording were compared with those calculated using weak motion recordings. This comparison of the results provided by the different methods was in fact directed towards performing a calibration of the passive seismic techniques in the area investigated, allowing a preliminary validation for the reconstructed sediment-bedrock interface geometry and the site-effects estimates.

In addition, in order to provide additional useful information for site effects and microzonation studies, a series of eight 2D micro-array measurements utilizing short-period sensors and high dynamic digitizers were carried out in selected sites of the study area. The extended spatial autocorrelation technique (ESAC; *Ohori et al.*, 2002; *Aki*, 1957; *Okada et al.*, 2003), and frequency-wavenumber analysis (maximum likelihood method; *Capon*, 1969; *Horike*, 1985) were used for the estimation of the Rayleigh wave dispersion curves and

wavefield analysis. For the first time, the resulting dispersion curves were used together with the H/V curve in a joint inversion scheme for the estimation of the S-wave velocity profiles in a megacity. Finally, theoretical site responses were calculated from the S-wave velocity profiles obtained from the micro-array data using the propagator matrix method for a 1D-layered medium (*Parolai et al.*, 2006).

Geological Setting

The western part of Istanbul is characterized by two main geological settings; the northern and northeastern sections that are dominated by Paleozoic bedrock, and the southern and western parts that are mainly covered by geologically softer sediments (Figure 4.1b, *Birgören and Özel*, 2006). The Paleozoic basements consist of Devonian limestone formations (Trakya, Dolayoba). The upper Miocene sediments and sedimentary rocks that extend over the Paleozoic bedrock are divided into the following units:

- the Bakirköy formation of the upper Miocene, consisting of alternating white, porous, chalky and medium to hard limestone, marl and clay layers;

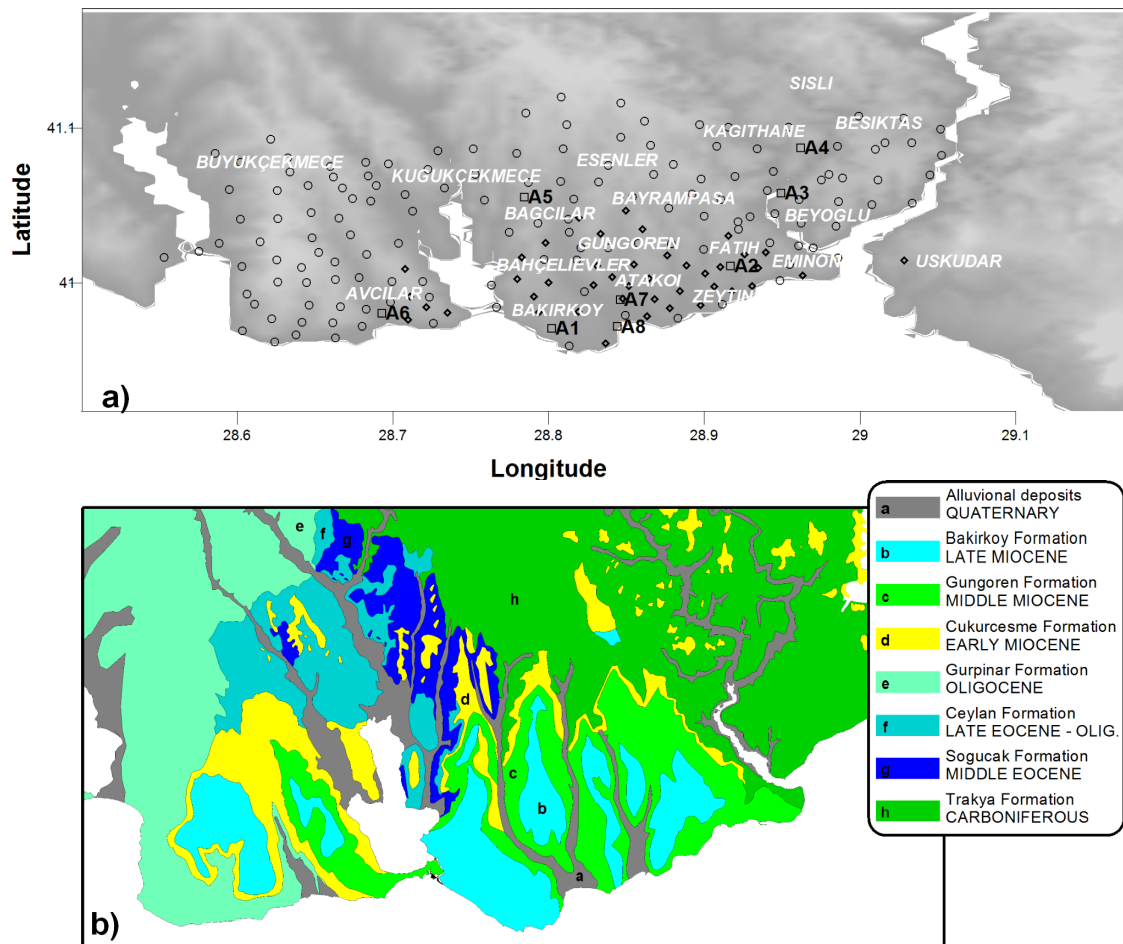

Figure 4.1 Western part of Istanbul. a) Single station noise measurements at free field sites (dots), IERRS stations (rhombus, name of stations with earthquake recordings is indicated), and 2D array measurements (squares). b) Geological map.

- the Güngören formation of the middle Miocene, composed of green coloured fissured clay, highly plastic, thin laminated clays, marl and clayey siltstone;

- the Cukurcesme formation, which contains dense to very dense sand, silty sand, clayey sand, gravel and clay;

- the Late Quaternary Kusdili formation, which consists of clay with molluscs, sand, silt and mud, covering the southern coast of Kucukcekmece Lake and the Golden Horn;

- the Alluvial deposits of Quaternary age, consisting of unconsolidated sediments composed of gravel, sand, silt and clay, which overlay the other formations and are the result of fluvial activity;

- anthropic construction material, overlain by a layer of gravel of a few decimeters, and filled with about half a meter of soil. All of these materials overlie the alluvium and the other formations in some part of the city, reaching a total thickness of approximately 2 m.

Alluvial deposits and other sediments and softer sedimentary rocks represent the most important geological units from the point of view of site effects. In fact, due to the contrast between their generally poor mechanical characteristics and those of the Paleozoic bedrock, strong site amplification of the ground shaking can be expected.

Single station measurements

H/V spectral ratio – data analysis

From June 24 to July 15 2007, an extensive survey of single station seismic noise recordings was carried out over the western metropolitan part of Istanbul. In total, 192 sites were investigated, 42 of which were performed at the accelerometric sites of the Istanbul Earthquake Rapid Response System (IERRS) operated by the Kandilli Observatory and Earthquake Research Institute of Bogazici University, and 8 carried out using data collected at 2D array sites (see section 4). Seismic noise measurements were carried out using seismic stations equipped with the EDL 24 bit digitizer connected to a Mark L-4C-3D 1 Hz sensor with GPS timing. All the sensors were calibrated, and, as showed by *Parolai et al.* (2001), can be used to reliably analyze frequencies lower than 1 Hz. Following *Strollo et al.* (2008), the maximum possible gain for the digitizer (i.e. 10) was used in order to reduce instrumentation self-noise effects. This allows the estimation, also in the case of the most unfavorable scenario where seismic noise approaches the minimum new low-noise model (NLNM) of *Peterson* (1993), of unbiased fundamental frequencies down to at least about 0.2 Hz. Sensors were installed so as to obtain a good coupling between the instrument and soil, and where possible, avoiding asphalt. Moreover, sensors were covered in order to reduce any interference caused by wind. Ambient seismic noise was recorded at 100 Hz sampling rate for about 20 minutes,

which guarantees the statistical stabilization of the signal (*Picozzi et al.*, 2005).

The *H/V* spectral ratios (*Nakamura*, 1989) were computed using 20 non-overlapping time windows of noise recording signal, each window 60 seconds long and tapered with a 5 per cent cosine function before the computation of the spectra. The Fourier spectra were computed for each noise component and smoothed using a Hanning window of 10% relative bandwidth. This ensures the reduction of numerical instabilities while preserving the major features of the spectra, especially the flanks of the *H/V* ratios maxima. The resulting spectral ordinates relative to horizontal components were geometrically averaged and divided by the vertical spectral ordinate to compute the *H/V* function. Moreover, the time-stability of the spectral ratios over the recording length was verified in order to avoid the presence of spurious *H/V* peaks. Whenever *H/V* ratios determined by transient signals were observed, the relevant portions of recordings were rejected. Although this procedure does not bias the average *H/V*, it reduces the variability of the confidence interval (*D'Amico et al.*, 2004). Finally, *H/V* ratios obtained by considering the resultant time windows (i.e. between 10 and 20) were then averaged to compute the final *H/V* curve along with the relevant 95% confidence interval (Figure 4.2).
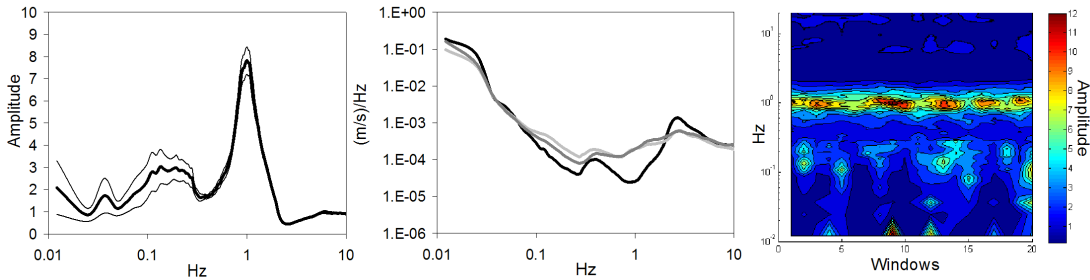
Figure 4.2 *Left)* *H/V* spectral ratio curve +/- 95% confidence interval. *Middle)* Ground motion amplitude spectra for the vertical component (black), the north-south component (dark grey), and the east-west component (light grey). *Right)* Contour plot of the *H/V* spectral ratio time stability.

Event	Latitude	Longitude	Depth (Km)	Mw/ML	Moment (dyne·cm)
05/16/2004	40.868	29.268	16.7	4.2/4.3	2.07E22
09/29/2004	40.780	29.020	12.4	4.1/4.0	1.73E22

Table 4.1 Location, magnitude and source parameters of the earthquakes discussed in this work.

H/V analysis of small earthquake recordings

Recordings of 2 local earthquake events with magnitude ML of 4.1 and 4.2 (Table 4.1) were available for 29 accelerometric station sites of the IERRS (*Harmandar et al.*,2006). The Fourier spectra of the events were computed using zero-baseline corrected and cosine tapered acceleration recordings of the three components. Therefore, 5 sec time windows starting 0.5

sec before the S-onset (*Birgören and Özel* , 2006) were selected. The spectral amplitudes from the two horizontal components were then combined by finding their root-mean square average. Finally, the *H/V* spectral ratio of the earthquake data (*EHV*) were computed.

Figure 4.3 compares for some representative sites the *H/V* spectral ratios estimated from seismic noise recordings (*NHV*)from seismic stations and following the procedure previously described, and those obtained using the two earthquake recordings. It is worth noting that, although the number of available earthquake records is limited, the two data sets show a general agreement in the estimation of the fundamental resonance frequencies, *fo*, including in some cases their amplitudes as well. Therefore, it is reasonable to have confidence in the reliability of the *fo* estimated by the *NHV* curves.
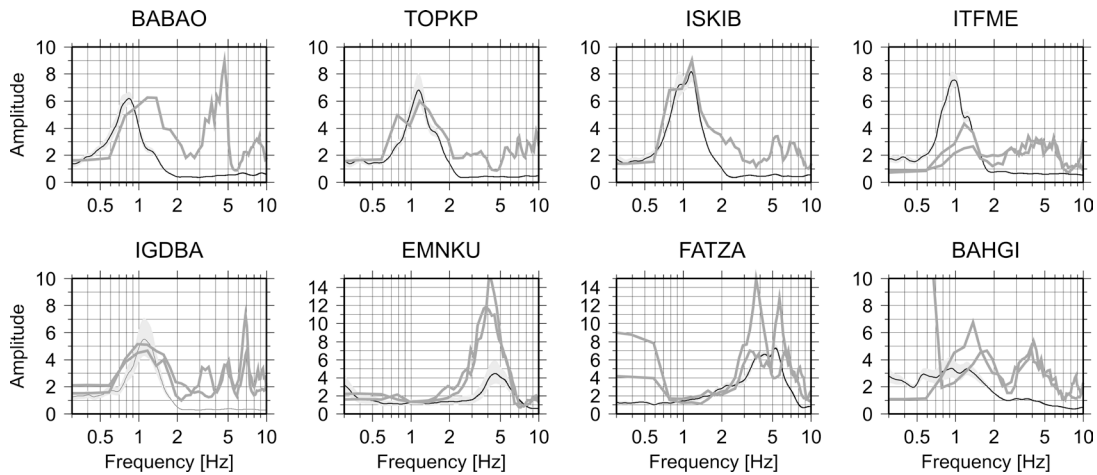
Figure 4.3 Average *H/V* spectral ratios of noise (black line) +/- 95% confidence interval (grey area) and *H/V* spectral ratios (dark grey lines) of one earthquake with M ~ 4 recorded by IERRS stations BABAO, TOPKP and ISKIB, and two earthquakes with M ~ 4 by IERRS stations ITFME, IGDBA, EMNKU, FATZA, and BAHGI

H/V analysis to map soft soil fundamental frequencies

The single station seismic noise measurement dataset was used with the aim of assessing the fundamental resonance frequency *fo* of soft sedimentary cover. Moreover, the lateral variability in *fo* also allows lateral variations in sedimentary thickness and its dynamic properties to be inferred.

Only in one case was the *H/V* ratio curve severely affected by low frequency disturbance, most likely due to bad soil-sensor coupling and wind. Therefore, a map of *fo* using information from 191 measurement sites was obtained. It is also noted in the western part of the investigated area that for a large number of measurement sites, multiple peaks in the *H/V* curves were observed, in particular, those sites that typically show a first maximum in the frequency range between 0.15 Hz up to 0.3 Hz, and a second one at frequencies higher than 0.5 Hz (Figure 4.2). The presence of multiple peaks is interpreted as indicating the presence of multiple impedance contrasts at different depths. In this paper, while drawing the map of resonance frequencies we considered the higher frequencies (i.e. with *H/V* maxima in

the frequency range from 0.5 Hz to 10 Hz) to be related to a shallower impedance contrast than those at very low frequencies (Figure 4.4a). In fact, the shallower impedance contrasts probably determine the amplification in a frequency band closer to the fundamental resonance frequencies of buildings, and would be a better indicator of the local increase in damages.

Considering the effect of instrumental self noise in biasing the *H/V* shape, as showed by *Strollo et al.* (2008), the resulting fundamental resonance frequencies were considered reliable at least until 0.2 Hz, since in the favourable condition of a level of seismic noise higher than the NLNM, the instrumentation used allows the estimation of reliable H/V values down to nearly 0.15 Hz.
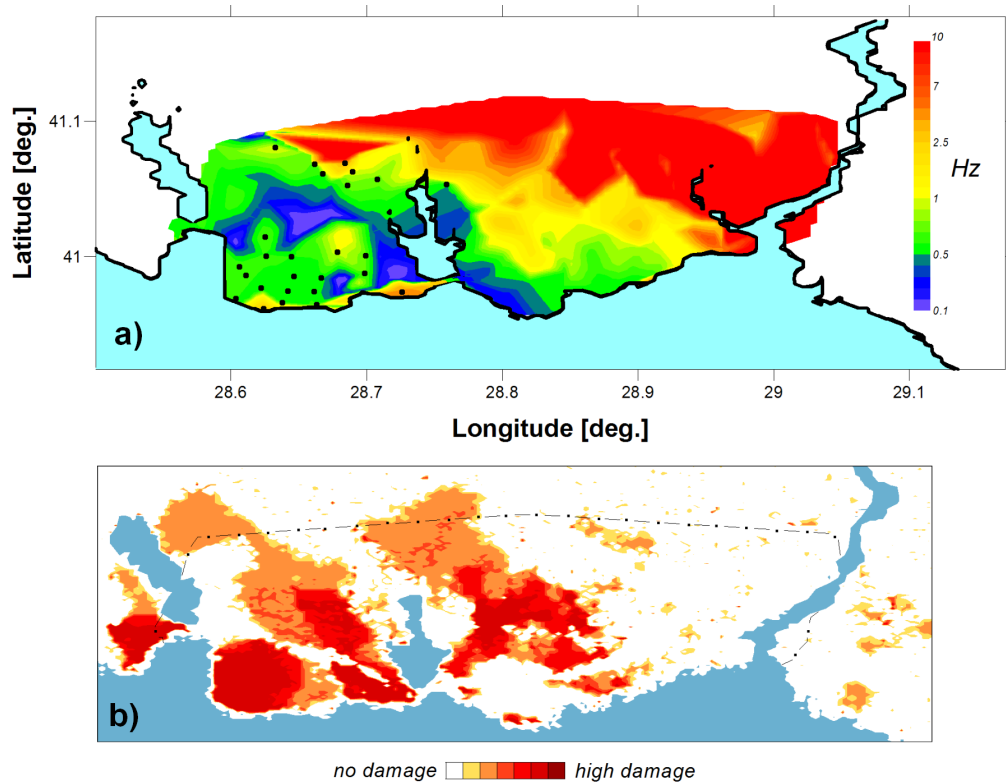
Figure 4.4 *Top)* map of the resonance frequency of the soil cover in the study area estimated by seismic noise recordings. Measurements where multiple peaks are observed (black dots) and array-2D locations are also indicated (squares). *Bottom)* Distribution of damage in Istanbul 17 August 1999 Kocaeli Earthquake (*redrawn after Istanbul Governorate Disaster Management Centre*). The dotted broken line bounds the investigated area.

Analysing the resulting map of resonance frequencies (Figure 4.4a), it is straightforward to identify some general characteristics of the investigated area:

- the isoline of *fo* equal to 10 Hz indicates that the area with very thin sedimentary cover or outcropping bedrock is mainly on the eastern and northern part of the city;

- the central-southern area (e.g. Atakoy, Bakirkoy, Gungoren, etc.) is characterized by *fo* decreasing in a northeast-southwest direction from 10 Hz to about 0.3 Hz;

- the westernmost area shows more irregular *fo* features. In fact, in Avcilar, the *fo* are well above 0.5 Hz whereas most are about 1 Hz, while in the north, *fo* decrease until least 0.2 Hz,

then increases again.

A comparison between the distribution of *fo* and the geological map (Figure 4.4a and Figure 4.1), clearly highlights the agreement between the fundamental frequencies and geology. In particular, the *fo* limit of 10 Hz reproduces well the outcropping area of the Trakya and Dolayoba limestone formations. Other significant geostructural characteristics indicated by the *fo* map are as follows:

- for the central part of the investigated area, the very low *fo* (< 0.5 Hz) in the Atakoy and Bakirköy districts (Figure 4.4a) appears related to the presence of thicker segments of the Bakirköy formation;

- for the western part of the urban area (Avcilar district) *fo* values around 1 Hz are observed, that could be related to the impedance contrast due to the contact between the soft Güngören and Cukurcesme formations overlying the stiff Bakirköy formation.

Several studies (e.g. *Hagshenas and Bard*, 2008) have shown that the amplification factor estimated from seismic noise H/V curves is not a reliable proxy for estimating the experimental amplification of a site, since often the seismic noise H/V fundamental frequency amplitude is lower than that estimated from earthquake recordings. Moreover*, Picozzi and Albarello* (2005) showed for a well constrained test site that, while higher harmonics in the experimental and theoretical site response function can have higher amplitudes than the fundamental resonance frequency, this information is always missing in the seismic noise H/V curves. For these reasons, the lack of detailed statistically significant comparisons between seismic noise and S-wave site response amplification, mean that the fundamental resonance amplifications are not taken into account.

Figure 4.4b shows the distribution of damage after the 17 August 1999 Kocaeli Earthquake (*after Istanbul Governorate Disaster Management Centre*). As observed in several previous studies (e.g., *Ozel et al.*, 2004; *Ergin et al.*, 2004; *Sørensen et al.*, 2006; *Cranswick et al.* 2000; *Kudo et al.*, 2002) the role of site effects in the damage distribution in the western part of Istanbul was considerable for this event. Although a discussion of the observed damage after the 17 August 1999 Kocaeli earthquake is beyond the scope of this microzonation study, since information about the vulnerability of the structures in question is not available, we will consider a qualitative comparison between the *fo* map and the distribution of damage. In particular, the boundary between the "no damage" and "consistent damage" areas in the eastern and northern parts of the study area corresponds quite well to the isoline for the 10 Hz *fo* map. Thus, at a first glance it is clear that the most damaged areas are located in the part of the city mainly covered by geologically softer sediments, where *fo* spans the frequencies of interest for buildings (i.e. from 0.5 to 10 Hz). Local differences may, of

course, be due to vulnerability variations. Therefore, we believe that the *fo* map provides a valuable tool for identifying areas of a city that could experience heavier damage from future earthquakes due to the unfavorable geological conditions.

Array measurements

The S-wave velocity profiles were experimentally derived from seismic noise recordings carried out using arrays of sensors (e.g., *Okada*, 2003). Considering the high geological heterogeneity characterizing the investigated area, sensor arrays were installed at sites with different surficial geology (Figure 4.1 and Table 4.2). The 2D array geometries were slightly variable due to practical restrictions. The inter-station distance chosen ranged between a minimum of 5 and 10 m, and a maximum between 100m and 150m, depending on the site. These ranges allow the analysis of a range of wavelengths that guarantee large depths to be investigated, but with still sufficient (i.e. from 5 to 10 m) shallow resolution (*Okada*, 2003). A good azimuthal and inter-station distance coverage was guaranteed by the applied geometry (Figure 4.5).

Code	Name	Latitude (GPS Position)	Longitude (GPS Position)
A1	Saruzian Sokak	40°58'15.00"N	28°48'07.00"E
A2	Fatih	41°00'40.00"N	28°55'00.00"E
A3	Miniaturk	41°03'29.00"N	28°56'57.00"E
A4	Kagithane	41°05'14.00"N	28°57'43.00"E
A5	Bagcilar	41°03'20.00"N	28°47'04.00"E
A6	Refinery Esenyurt	40°58'50.00"N	28°41'34.00"E
A7	Atakoy	40°59'21.00"N	28°50'46.00"E
A8	Military Base Bakirkoy	40°58'19.48"N	28°50'39.05"E

Table4.2 Location of the 2D array. The GPS position is for the central sensor of the array.
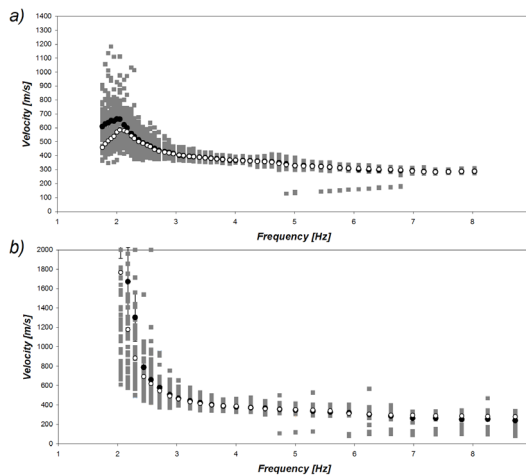
Figure 4.5 *a)* ESAC dispersion curve for seismic noise recordings of array A2 using singular time-windows analysis (grey dots) and average values (black dots), and from the classical approach following Ohori *et al.*(2002) (white dots). *Inner inset)* array configuration for A2. *b)* singular time-windows analysis for the same data set similar to *a)* but for MLM analysis (grey and black dots), and from the classical approach following Capon (1969) (white dots).

The arrays located in the Atakoy district (A7) and in the "Military area" (A8) consisted of 12 stations equipped with a 24 bit digitizer RefTek connected to a Mark L-4C-3D 1 Hz sensor with GPS timing. The stations recorded for more than 1 hour at 100 Hz sampling rate. For A7, due to instrumental malfunctions , data from two stations could not be used. All other arrays consisted of 13 stations equipped with the EDL 24 bit digitizer and the same sensors of the previous array. Ambient seismic noise was recorded at 200 Hz sampling rate and the stations were operated continuously for about 2 hours. Before the analysis, all recordings were corrected for the instrumental response, considering the calibration parameters of each sensor. The *H/V* curves were computed for all stations of each array, following the procedure described previously.

Phase velocity analysis

For estimating dispersion curves of Rayleigh waves, a total of 120 non-overlapping signal windows of vertical component recording, each window being 30 s long, where considered. In this study, the Extended Spatial AutoCorrelation (ESAC; *Ohori et al.*, 2002; *Aki*, 1957; *Okada*, 2003) and the Frequency-Wavenumber (FK), specifically the maximum likelihood method (MLM; [31,32]), methods were adopted.

Computing the Rayleigh wave dispersion curve by the ESAC procedure (*Ohori et al.*, 2002), we followed both the procedure described by *Parolai et al.* (2006), and a different approach that allowed us to estimate the statistical uncertainties for the average phase velocity. Accordingly, the spatial correlation coefficients estimated for each singular time-window were fitted with Bessel functions. In this way, for each frequency, the average phase velocity is obtained from the resultant 120 velocity samples. As shown in Figure 4.5a, the two approaches provide equivalent average estimates, but the redundancy of information of the second approach allows the 95% confidence interval for the average phase velocity to be evaluated.

The MLM-FK analysis (*Capon*, 1969; *Horike*, 1985) is performed by a coherence matrix evaluation, which is used for computing the FK power spectral density function (PSDF). The location of a peak in the PSDF provides information about both the apparent propagation velocity and the azimuth of the signal recognized from the array. It has been shown (e.g., *Richwalski et al.*, 2007; *Okada*, 2003) that FK techniques show a tendency to overestimate the phase velocity with decreasing frequency with respect to ESAC. However, the FK estimates, differently from ESAC, allow the direction from which the main sources of energy originate to be resolved. This is especially important in urban area, where the sources of microtremors may not be randomly distributed, and therefore the basic assumption of the

ESAC method not verified. Moreover, MLM-FK may help to discriminate between the contributions of higher modes of surface waves to the wavefield.

The array response and PSDF contour plots of different frequencies were computed for all the arrays. The comparison of these plots allows us to identify secondary peaks due to spatial aliasing (e.g. see 10 Hz in Figure 4.6), and to verify the microtremor source distribution (Figure 4.6).
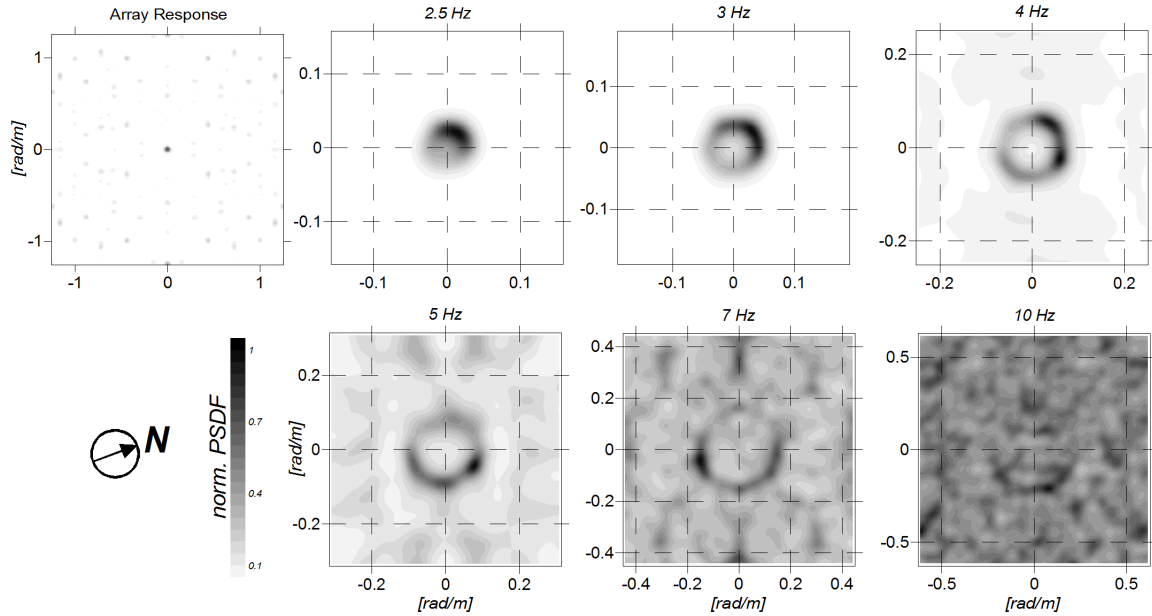
Figure 4.6 Results from applying the MLM to the seismic noise recordings of array A2. Array response and contour plots showing for some representative frequency the normalized frequency-wavenumber power spectral density function. The symbol indicates the north direction.

In most of the analyzed array recordings, the maximum frequency that could be analyzed was around 10 Hz. Also for the MLM method, the velocity analysis was performed by following both the classical strategy, where the averaged PSDF is analysed (e.g. as proposed by *Horike*, 1985), and by estimating the PSDF of each singular time-window (*Wathelet*, 2005). The two approaches provided nearly equivalent results (Figure 4.5b), with the second preferred as it allows a statistical uncertainty to be evaluated. Figure 4.7 shows Rayleigh wave dispersion curves derived by array measurements. In general, the variable trends of the dispersion curve reasonably reflect the variable geological conditions existing at the different sites (Figure 4.1). In particular, A1, A2, A5, A6, and A7 were installed on surficial deposits where the phase velocity increases almost regularly with decreasing frequency between 2 and 10 Hz. On the other hand, the dispersion curve at A4, which was located on outcropping bedrock, shows a Rayleigh wave velocity of about 2000 m/s, while a low Rayleigh wave velocity (100-200 m/s) and a steep increase at lower frequencies were estimated at the A3 and A8 arrays, indicating that close to the coast, very soft sediments overlie stiff bedrock.

In the cases (e.g. array A2, A3, A6 and A7) where the basic assumption of a uniform

distribution in space of the stationary and stochastic seismic noise sources is verified, and the wavefield is dominated by the Rayleigh wave fundamental mode, as indicated by the frequency wavenumber PSDF (not shown), the ESAC and MLM curves are in good agreement (Figure 4.7).
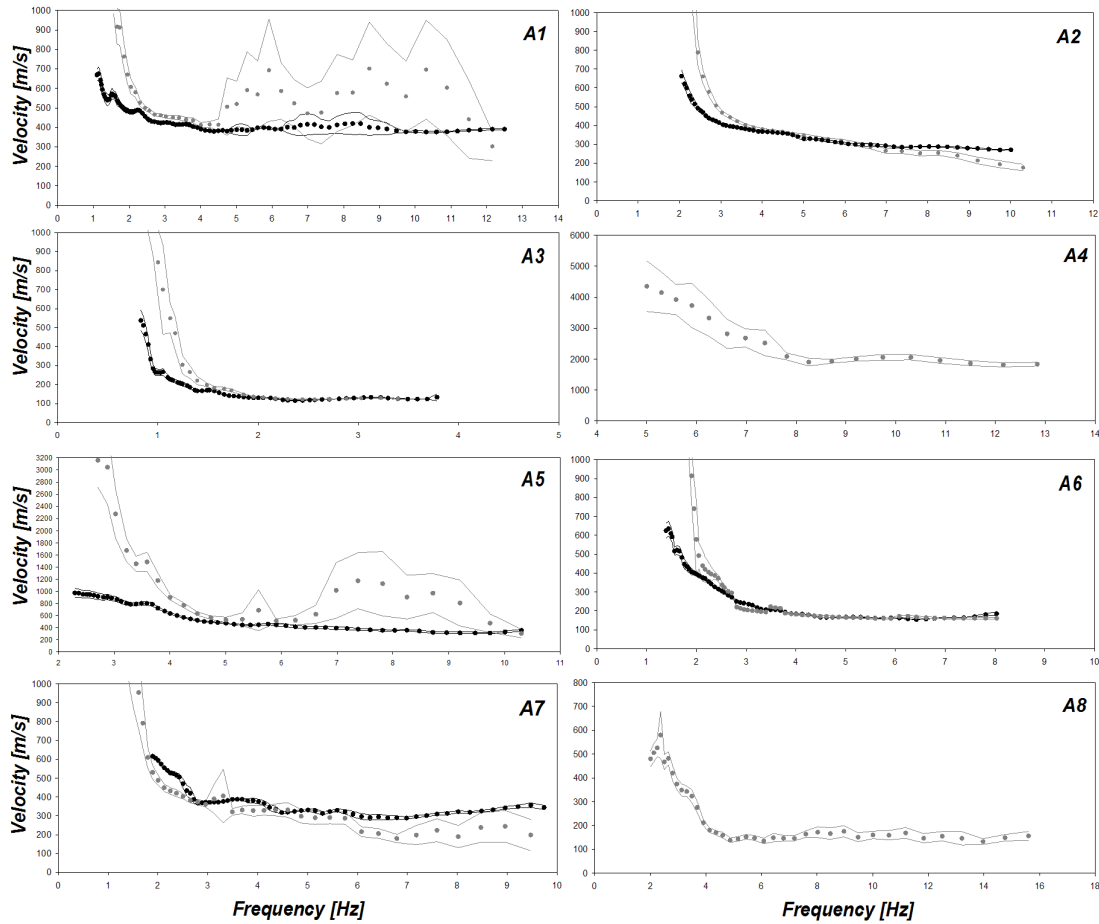
Figure 4.7 ESAC (black dots) and MLM (grey dots) Rayleigh wave dispersion curves and relative +/- 95% confidence interval (thin lines).

However, in the low frequency range, the MLM curves exhibit, as usual, larger velocities than ESAC. For arrays A1 and A5, at frequencies higher than about 4 Hz, MLM provides phase velocities considerably higher than those from ESAC, that are characterized by a larger uncertainty. This suggests that the wavefield is not dominated by surface waves and the MLM estimation is very sensitive to local spurious maxima in the single record PSDF. In contrast, the ESAC method, with the procedure of fitting the spatial correlation coefficients with a zero-order Bessel function, seems to be more robust in extracting the contribution of dispersive waves. A more detailed investigation of this evidence is well beyond the scope of this paper, but will certainly be taken into account in future methodological studies.

Finally, for arrays A4 and A8, only the MLM method provides coherent dispersion curve results, probably because the basic assumptions of the temporal and spatial noise sources being stationary for the application of the ESAC method were not verified.

Inversion

For the sites where both high-quality Rayleigh wave dispersion and *H/V* ratio curves were derived, a joint inversion scheme (*Parolai et al.*, 2005) was used to estimate the local S-wave velocity profile. In particular, the joint inversions of dispersion and *H/V* curves were performed following the scheme proposed by *Picozzi and Albarello* (2007). This scheme uses a combination of genetic algorithms and generalized least-squares methods to obtain the global minimum of the non-linear solution fitness. In fact, the genetic algorithm allows a non-linear inversion analysis to be performed that does not depend upon an explicit starting model and allows the identification of the parameter's search space where the global minimum of the inversion problem lies. However, it may only provide a solution close to the global minimum and in some cases be unable to reproduce the experimental data satisfactorily. Therefore, the minimum misfit model from the genetic algorithm inversion can be used as the starting point for the linearized inversion carried out with the generalized least-squares algorithm. Here, the genetic and the generalized least-squares algorithm, respectively proposed by *Yamanaka and Ishida* (1996) and *Arai and Tokimatsu* (2005), were used. The forward modeling of Rayleigh wave phase velocities and H/V curves was performed using the modified Thomson-Haskell method proposed by *Hermann* (2002) and following the suggestions of *Tokimatsu et al.* (1992) and *Arai and Tokimatsu* (2004), under the assumption of vertically heterogeneous 1D earth models. The validity of this assumption is investigated by computing the *H/V* curve for each station of the array. Whenever the *H/V* curves provide the same estimate of the fundamental frequency and the main peak exhibits a good level of shape similarity, it is reasonable to assume that the geological structure underneath the array does not change significantly. Thus, in these cases, the resulting average *H/V* curve can be safely considered as being representative for the volume underneath the array.

The modeling of both the dispersion and *H/V* ratio curves during the inversions was not restricted to the fundamental mode only, but included higher modes. During the inversion, the two data sets are weighted in a balanced way by the cost function used by *Herrmann et al.* (1999). Nevertheless, when the two data sets differ considerably in quality, their relative influence is controlled by a weighting parameter. Obviously, when one of the two experimental curves cannot be used (e.g. because of the presence of industrial noise signals) the proposed inversion scheme can still be applied using only one of either the dispersion or *H/V* curves.

Results of the inversion analysis and discussion

The results of the inversion analysis for all array measurements are shown in Figures

4.8 and 4.9. For most of the arrays, (i.e. A1, A2, A5, A6, A7, and A8), it was possible to perform a joint inversion analysis using dispersion and H/V curves of equivalent quality. Only for arrays A3 and A4 were the inversions performed using the dispersion curve alone. In fact, for A3, the *H/V* curves at different sensors were perturbed close to the *fo* by the presence of spurious, probably industrial, signals, while A4 was executed in the northern part of the city where the Paleozoic bedrock outcrops and, thus, the *H/V* curve is flat (Figure 4.8).
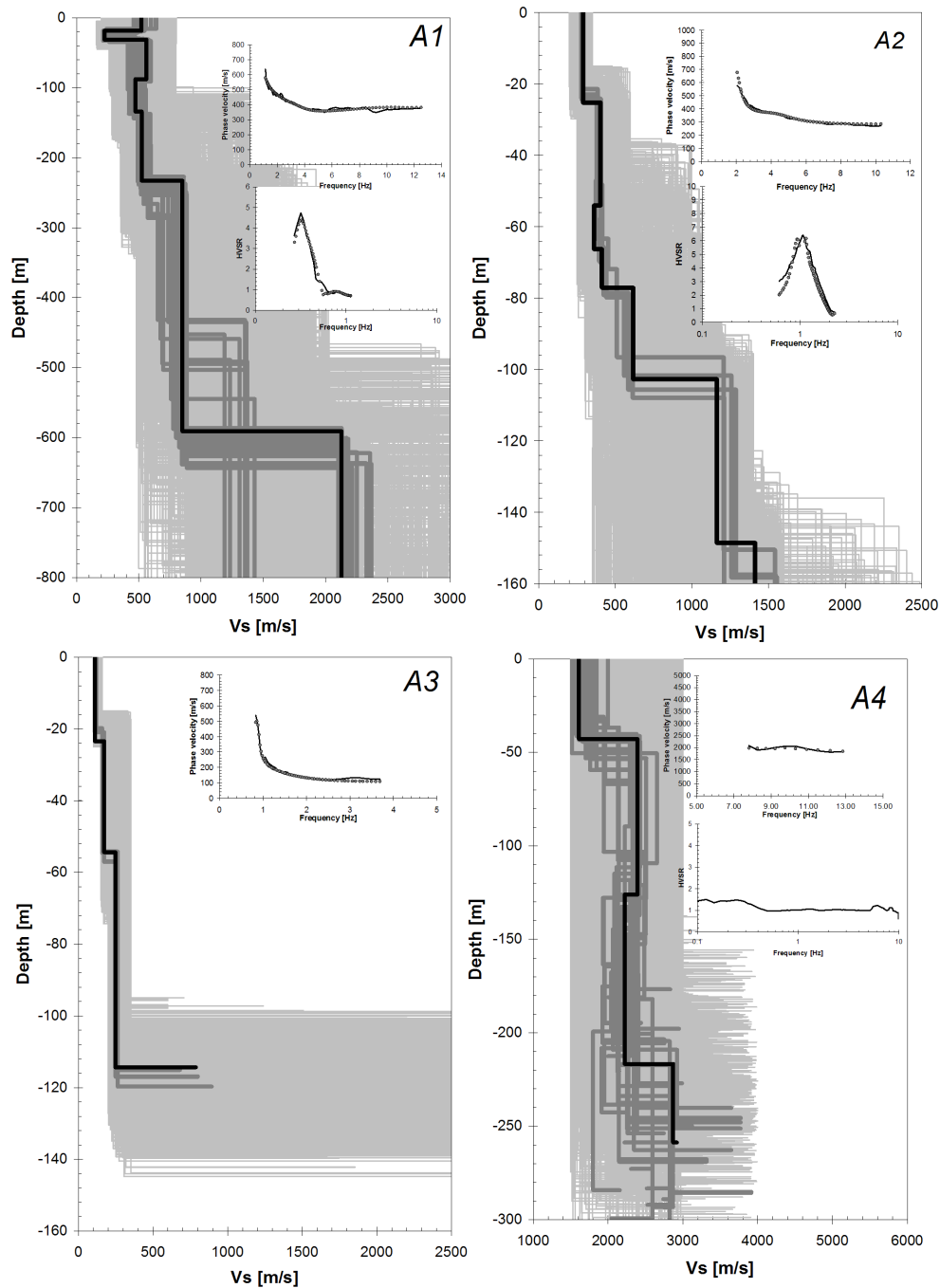
Figure 4.8 Inversion results and fit to the dispersion and *H/V* ratio curves (insets) for the arrays A1, A2, A3 and A4. All four figures show tested models (thin grey lines), the minimum cost model (black line), and models lying inside the minimum cost +10% range (thick dark grey lines). Top inset: Observed phase velocities (black line) and the phase velocities for the minimum cost model (grey dots). Bottom inset: Average observed *H/V* ratio (black line) and the *H/V* ratio for the minimum cost model (grey dots).
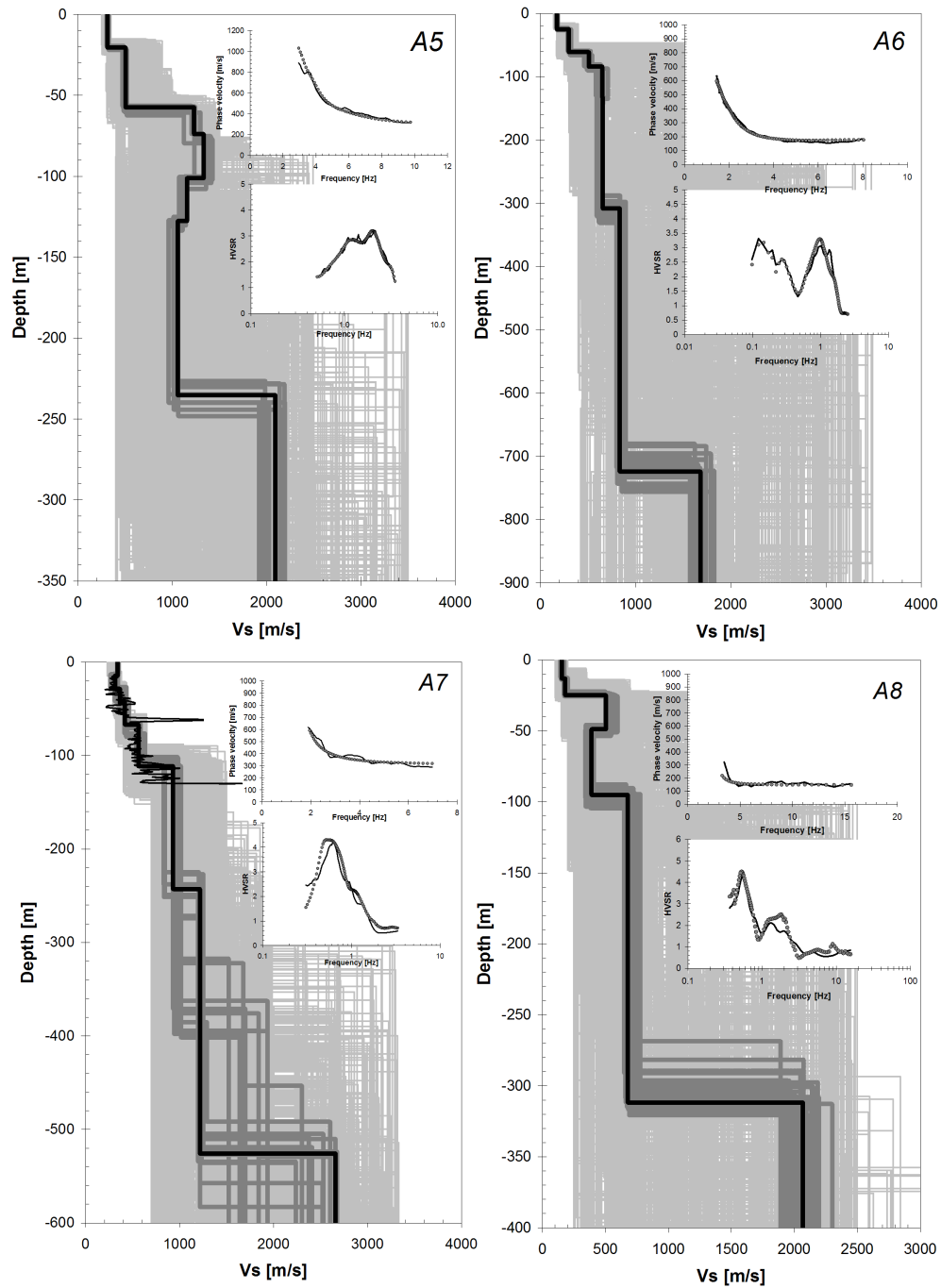
Figure 4.9 Same as for Figure 4.8, but for arrays A5, A6, A7 and A8. For array A6, the S-wave velocity profile from *Kudo et al.* (1999) (thin black line) is also reported. For array A7, the S-wave velocity profile (thin black line) determined from Suspension PS Logging testing performed at Borehole SK-3 at the Atakoy Vertical Array Site (personal communication) is also reported.

Both the theoretical dispersion and *H/V* curves fit the observed values well. The reliability of the inversion results is influenced not only by the quality of the input data, but also from the frequency range spanned by the *H/V* and dispersion curves. For A2, the two experimental curves are partially superimposed in frequency and, therefore, both the final best-fit S-wave velocities and the impedance contrast at about 100 m of depth (in the range of wavelengths covered by dispersion and *H/V* values) are very well constrained. Similar

considerations also hold for A5, which exhibits two high impedance contrasts at about 50 m and 250 m. On the other hand, for A1, A6, A7 and A8, the dispersion and *H/V* curves occupy different frequency ranges (i.e. the fundamental resonance frequency is well below the frequencies of the dispersion curve). In these cases, they carry information for different depth ranges, with the dispersion curve being what mainly constrains the velocity in the surficial part of the model, and the *H/V* curve providing information about the S-wave velocity and impedance contrasts in the deeper part. However, being constrained by only the *H/V* curve, this part suffers more from trade-off between parameters (*Scherbaum et al.*, 2003), with the deeper part of the model being characterized by a higher uncertainty. This is also confirmed by the larger instability of the S-wave velocity profiles having misfits equal to best-fit +10%.

The estimated S-wave velocity profiles provide a valuable overview of the different velocity structures in the western part of Istanbul (Figures 4.8 and 4.9). The large variability and complexity of the velocity structure, characterized by different impedance contrasts, has been previously confirmed by different authors (e.g., *Ozel et al.*, 2004; *Sørensen et al.*, 2006), and could be responsible for the significant variability in ground motion that lead to the irregular distribution of damage after the 17 August 1999 Kocaeli Earthquake (Figure 4.3b). However, with the exception of the very simple situation where soft sediment deposits overlying a hard bedrock, the identification of possible ground motion amplifications simply from the visual inspection of S-wave velocity profiles is not possible, nor advisable. For this reason, considerations concerning the occurrence and magnitude of site effects at the investigated sites are discussed below, where the theoretical site responses are estimated.

Array A4 provides an estimate of about 2000 m/s for the stiff Paleozoic bedrock. Arrays A1, A5, A6, A7 and A8 show similar high S-wave velocities (around 2000 m/s) at depths greater than 200 m, in agreement with the geology (*Dalgiç*, 2004), but also suggest complicated layering with high impedance contrasts at shallower depths. For example, both the S-wave velocity profile for A7 in the Ataköy district and that of A8 in the Avcilar area are characterized by a considerable impedance contrast at a depth of about 100 m. In particular, at A7, the S-wave velocity increases from about 600 m/s to about 1000 m/s. These shallower impedance contrasts could be responsible for the anomalous ground motion amplification observed (*Cranswick et al.*, 2006) in the frequency range of interest for buildings (i.e. from about 0.5 Hz to 10 Hz).

In the proximity of A6 in the Avcilar district, *Kudo et al.* (2002) estimated the S-wave velocity profiles from circular array observations of microtremors using the SPAC method. It is worth noting in Figure 4.9 the excellent agreement in the S-wave velocity trend between the two estimates. Despite the H/V peak at the lower frequency being closer to the sensibility

limit of our instrument, it allows velocity estimates for the deeper rock formation in good agreement with those obtained by the array A4, A5, A7 and A8, and a depth in agreement with A1.

Another fact that gives us confidence in our results is that the estimated S-wave velocity structure of A7, until a depth of about 120 m, is in good agreement with suspension PS Logging measurements performed at the Atakoy Vertical Array Site (*Ansal et al.*, 2007; Figure 4.9). Finally, arrays A2 and A3 also show a strong impedance contrast at a depth of about 100 m.

Theoretical site response

The final step in the 2D array recording analysis consists of estimating the theoretical site response function, starting from the retrieved S-wave velocity profiles. The procedure followed is discussed in *Parolai et al.* (2007), and is based on computing synthetic seismograms using the improved Thompson-Haskell propagator matrix method (Wang, 1999). Synthetic seismograms are generated for a standard receiver configuration of 15 equally-spaced receivers using a seismic source at 5 km depth, considering both the estimated sedimentary cover structures and a pure halfspace model (i.e. the theoretical reference site). Then, all records were analyzed, and the results averaged. Finally, FFT spectra of recordings were calculated and the Theoretical Horizontal-to-Vertical spectral ratios (*THV*) computed. Although this method provides a simplified wavefield with respect to reality (i.e. it does not take into account wave diffraction and scattering), it allows site-response functions to be obtained that are able to capture the main features of the experimental ones (*Parolai et al.*, 2007).
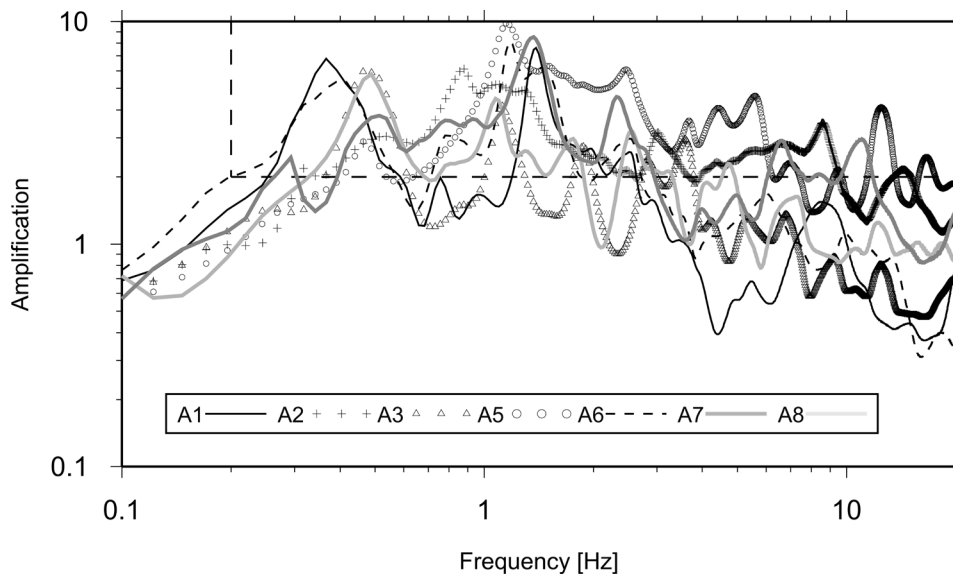

Figure 4.10 *H/V* ratios at the surface station from synthetic seismograms considering the model obtained by the arrays. The dashed line bounds amplification higher than 2.

Figure 4.10 shows the *THV* ratios at the surface station from synthetic seismograms considering the model obtained by the arrays, with the exception of A4, which is located on the Paleozoic bedrock. As expected for the presence of various high impedance contrasts in the S-wave velocity profile, both at large (> 200 m) and medium (about 100 m) depths, high levels of amplification are observed for many models, both at low (around 0.5 Hz) and high (>1 Hz) frequencies. Despite the simplified synthetic wave field, the presence of amplification higher than a factor of 2 over a wide frequency range for the *THV* ratio curves, provides a clear picture of the site-response complexity for the western part of Istanbul (Figure 4.10).

Bakir et al. (2007) identified the districts of Avcilar, Ataköy, Bakirköy, and Fatih as areas of the city where heavier damage in the event of future earthquakes are expected due to resonance effects and quasi-coincidence with the eigenperiods of the typical residential buildings in these areas. It is worth noting that for array A6 in Avcilar, high levels of amplification are estimated at both low (i.e. 0.5 Hz) and high frequencies (i.e. 1-2 Hz), in agreement with the observation of *Bakir et al.* (2007) and *Tezcan et al.*, (2002) and *Ergin et al.*, (2004) of an high site amplification hazard risk. Similar observations also hold for the Ataköy (A7) and Bakirköy (A8) districts, where the theoretical site response (Figure 4.10) indicates, in agreement with theoretical studies (*Sørensen et al.*, 2006) and experimental observations (*Birgören and Özel*, 2006) ground motion amplifications well above a factor of 2 in the frequency range 0.2 – 10 Hz.
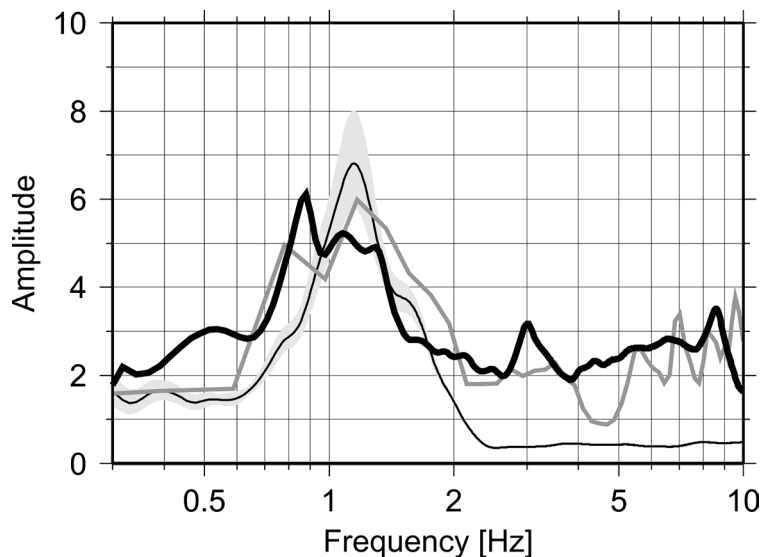
Figure 4.11 IERRS station TOPKP. Average *H/V* spectral ratios from seismic noise (thin black line) +/- 95% confidence interval (grey area), *H/V* spectral ratios of two earthquakes (dark grey line) with M ~ 4 recorded by IERRS stations (Table 4.1), *H/V* ratios (thick black line) at the surface station from synthetic seismograms considering the model obtained by the array A2.

Finally, Figure 4.11 shows the comparison between the *THV* ratio curves for the model of the array A2 located in the Fatih district, and the empirical *EHV* amplification function

evaluated at the nearby (~1 km) IERRS station TOPKP (Figure 11). As shown by *Harmandar et al.* (2006), the spatial variation of ground motion over this distance is very small, and the results can be reasonably compared. We note how the *THV* response is able to capture all of the main characteristics of the empirical *EHV*. In particular, differently from the *H/V* from seismic noise that only fits well the fundamental resonance peak (f_o) at about 1 Hz, the *THV* reproduces both f_o and also the overall shape of the *EHV* in the frequency range from 2 Hz to 10 Hz.

Conclusion

The western part of the megacity Istanbul has been studied by means of an extensive survey of environmental seismic noise measurements. Comparison of *H/V* curves from single station seismic noise measurements with those obtained by earthquake recordings indicates that the former are a good proxy for the fundamental resonance frequency. Therefore, a high number of single station seismic noise measurements has been carried out in western Istanbul allowing the mapping of fundamental resonance frequency. The fundamental frequency map is in remarkable agreement with the geological map, both in identifying the boundaries of the Paleozoic bedrock outcrops in the northern and eastern parts of the investigated area (characterized by H/V curves without amplification or fundamental resonance frequencies over 10 Hz), and the identification of areas with soft sedimentary covers in the south-western part. Other studies [e.g. *Tezcan et al.,* 2002; *Ergin et al.*, 2004; *Sørensen et al.*, 2006; *Birgören and Özel*, 2006, *Kudo et al.*, 2002; *Bakir et al.*, 2007) focused their activities only at sites characterized by the presence of soft sediments. They concluded that such situations are responsible for the anomalous ground motion amplification during earthquakes. Our results confirm this conclusion, having, in addiction, a broader area coverage. In fact, the fundamental frequency map presented in this study provides a general overview of those area in the whole western Istanbul characterized by fundamental resonance frequencies that lie in the same range of those observed for the typical residential buildings in these regions (i.e. from 0.5 to 10 Hz).

Seismic noise measurements using 2-D arrays were carried out in areas with different surficial geology. The joint inversion of Rayleigh wave dispersion and *H/V* curves, using a combination of different methods to manage the severe non-linearity of the problem, allowed the retrieval of the S-wave velocity structure for some hundreds of meters. The estimated S-wave velocity profiles confirm the existence of different mechanical structures in the western part of the metropolitan area, which are in most of the cases (A1, A2, A3, A5, A6, A7 and A8) characterized by strong impedance contrasts. The complex nature of such S-wave

velocity structures determine theoretical site responses characterized, for most of the sites, by amplification factors well above than 2 in the frequency band from 0.2 Hz to 10 Hz.

Comparing the theoretical site response from 2D arrays with the empirical ones from an earthquake recorded at the nearby seismic station TOPKP indicates that, 2D array seismic noise methods allow for the estimation of the most relevant and reliable information about the local S-wave structure for site response. Therefore, further 2D array seismic noise measurements and analysis will be subject of future investigations.

Chapter

5

Site effects assessment in Bishkek (Kyrgyzstan) using earthquake and noise recording data*

5 Site effects assessment in Bishkek (Kyrgyzstan) using earthquake and noise recording data

Abstract

Kyrgyzstan, which is located in the collision zone between the Eurasian and Indo-Australian lithosphere plates, is prone to large earthquakes as shown by its historical seismicity. Hence, an increase in the knowledge and awareness of local authorities and decision makers of the possible consequence of a large earthquake, based on improved seismic hazard assessments and realistic earthquake risk scenarios, is mandatory to mitigate the effects of an earthquake. To this regard, the Central Asia Cross-Border Natural Disaster Prevention (CASCADE) project aims to install a cross-border seismological and strong motion network in Central Asia and at support microzonation activities for the capitals of Kyrgyzstan, Uzbekistan, Kazakhstan, Tajikistan and Turkmenistan. During the first phase of the project, a temporary seismological network of 19 stations was installed in the city of Bishkek, the capital of Kyrgyzstan. Moreover, single station noise recordings were collected at nearly 200 sites. In this study, the site amplifications occurring in Bishkek are assessed by analyzing 56 earthquakes extracted from the data streams acquired continuously by the network, as well as from the single station noise measurements. A broad-band amplification (starting at ~ 0.1 and 0.2 Hz), is shown by the Standard Spectral Ratio (SSR) results of the stations located within the basin. The reliability of the observed low frequency amplification was validated through a time-frequency analysis of de-noised seismograms. Discrepancies between Horizontal-to-Vertical Spectral Ratio (HVSR) and SSR results are due to the large amplification of the vertical component of ground motion, probably due to the effect of converted waves. The single station noise results, once their reliability was assessed by their comparison with the earthquake data, have been used to produce the first fundamental resonance frequency map for Bishkek, whose spatial variation shows a good agreement with the presence of an impedance contrast within the Tertiary sedimentary cover.

Introduction

Kyrgyzstan, which is located in the collision zone between the Eurasian and Indo-Australian lithosphere plates, is prone to large earthquakes as shown by its historical seismicity. In particular, between the end of the 19th and the beginning of the 20th centuries, several destructive earthquakes occurred in Kyrgyzstan, such as the Belovodski earthquake of August 3, 1885 (maximum intensity IX), that struck the city of Kara-Balti just west of Bishkek (Bishkek developed as a city during the 20th century), and the Ms=8.2 Kemin

earthquake of January 3, 1911 (Figure 5.1). This earthquake killed several hundred people and had a strong impact on the environment, triggering several mudflows and landslides (*Abdrakhmatov et al.*, 2003). Recently, on October 5, 2008, a magnitude 7.0 event (Figure 5.1) occurred along the border triangle between Kyrgyzstan, Tajikistan, and China. This earthquake caused the loss of about 350 lives, confirming the urgency of developing international programs for earthquake risk mitigation in Kyrgyzstan.

The occurrence of close and large earthquakes makes Kyrgyzstan the region with one of the highest seismic hazard in the world (*Zhang*, 1999). The probabilistic seismic hazard maps at regional scale computed for Kyrgyzstan (*Abdrakhmatov et al.*, 2003) show a peak ground acceleration of up to 4.5 m/s^2 with a probability to be exceeded of 10% over the next 50 years, confirming the very high hazard of the region.

The high risk level in Kyrgyzstan is not only dictated by the high level of the seismic hazard, but it is also a function of the vulnerability of buildings. The workshop held in Almaty (Kazakhstan) on October 1996 (*Khalturin and Tucker*, 1997) on the "Strategies for urban earthquake risk management for the Central Asian Republics" pointed out that the seismic resistance of Soviet-era buildings was significantly lower than was officially proclaimed. Analysing the devastating effects of the 1988 Armenian and 1995 Sakhalin earthquakes, the authors observed that "*Millions of people in Central Asia live in the same types of buildings as those collapsed in Armenia and Sakhalin. If an earthquake of the same size occurs near one of the Central Asian capitals, the tragedies of Leninakan, Spitak, and Neftigorsk will be repeated on a much bigger scale, unless urgent measures are taken*". The assessment of the urban earthquake risk of two Central Asian cities, i.e. Bishkek (Kyrgyzstan) and Tashkent (Uzbekistan), has been the subject of a NATO Science for Peace Project funded in 2001 (*Erdik et al.*, 2005). The project evaluated the seismic hazard for the two cities accounting to a first-order approximation of the potential site amplification effects, quantifying the building vulnerability and, finally, evaluating the urban earthquake risk. The project provided the indication that the expected number of night-time casualties in Bishkek under exposure to earthquake with a 2% probability of exceedance in 50 years is about 34.000. Moreover, about 90.000 people are expected to suffer injuries that will need to be treated at hospitals.

The effect of a large earthquake close to a major city can actually cause not only a large number of casualties, but also an economic collapse. Hence, an increase in knowledge and awareness of local authorities and decision makers of the possible consequence of a large earthquake is mandatory to mitigate the effects of an earthquake (building collapse, damage to lifelines, activation of landslides that can affect industrial, chemical or nuclear waste storage sites, and other sites of importance for security) and can only be based on improved seismic

hazard assessments and realistic earthquake risk scenarios. To accomplish this task, however, hazard assessment should be performed only after having calibrated the required ground motion empirical equation with data collected in the area and having considered the effect of shallow geological material in modifying earthquake ground motion. To this regard, the Central Asia Cross-Border Natural Disaster Prevention (CASCADE) project, financed by the German Federal Foreign Office, aims to install of a cross-border seismological and strong motion network in Central Asia, and to carry out microzonation studies in the capitals of Kyrgyzstan, Uzbekistan, Kazakhstan, Tajikistan and Turkmenistan. During the first phase of the project, a temporary seismological network of 19 stations was installed in the city of Bishkek, the capital of Kyrgyzstan, located over thick Quaternary and Tertiary deposits (Figure 5.1, top).
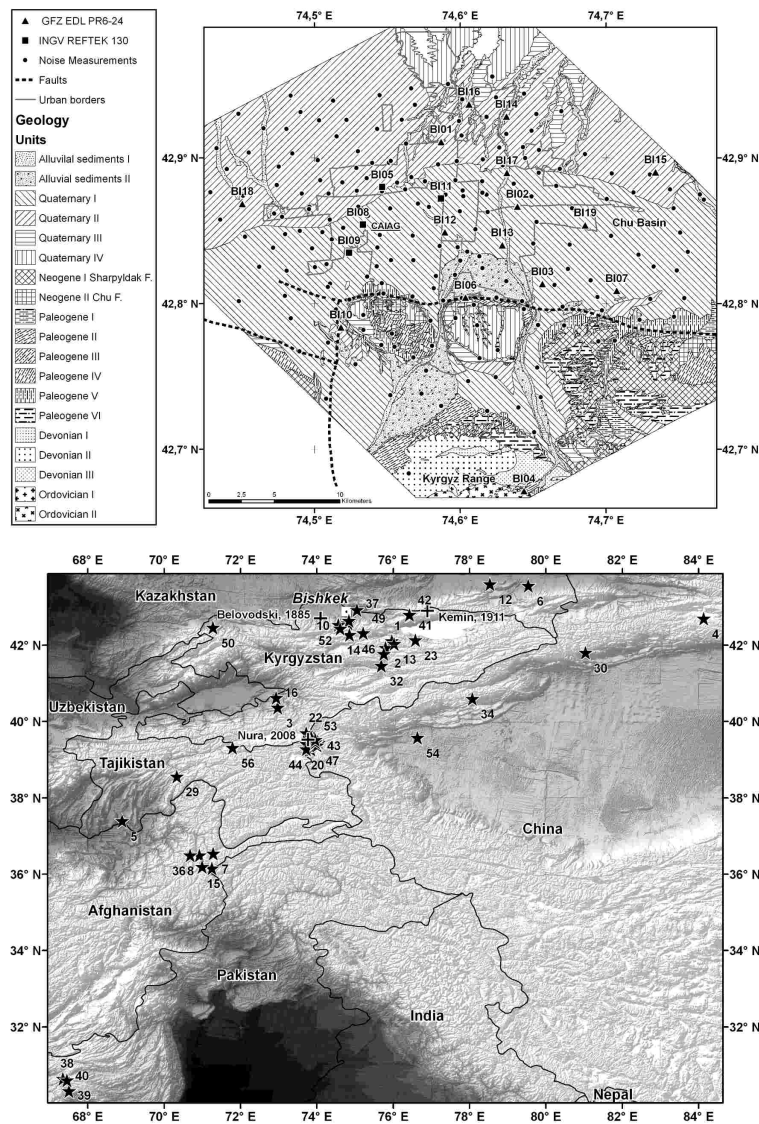
Figure 5.1 Top. Locations of the temporary stations (squares and triangles) installed in Bishkek and of the single station noise measurements (circles). A geological sketch of the area is also shown. Bottom. Epicenters (stars) of the earthquakes used in this study (Table 5.1). Event 55 in Table 5.1, occurred in the Sea of Okhotsk (Russia) is not shown in Figure. Crosses indicate the location of historical earthquakes mentioned in the text.

Moreover, noise recordings were collected by means of nearly 200 single station noise measurements as well as a number of array configurations. Measurements were taken in the actual urban area of the town, as well as in the area to the south where the basin is bordered by the active Issyk-Ata fault. In this study, we analyse the earthquake and noise data for identifying spatial ground motion variability. The reliability of the observed low frequency amplification was validated through a time-frequency analysis of de-noised seismograms. Finally, the single station noise results, once calibrated by comparison with the earthquake data results, have been used to produce the first fundamental resonance frequency map for Bishkek.

Geological and geophysical setting

The town of Bishkek (Figure 5.1) is located in one of the largest depression of the Northern Tien Shan, the Chu basin. This basin is bounded by the Kyrgyz Range to the south and the Chu-Lli mountains in the north. The Kyrgyz Range is mainly made up of Ordovician granite and fine-grained Devonian sedimentary rocks. It is cut by several short, irregular imbricate thrust faults that are laterally truncated by strike slip faults (*Bullen et al.*, 2001). The Paleozoic bedrock is thrust northward over ~4 km of Cenozoic molasse at the margin of the Chu basin. The latter is some 50 km wide and 150 km long. The deformation front is stepped northward into the Chu basin, exposing a thick succession of Neogene strata along the Issyk-Ata fault, located ~10 km north of the basin margin structure. Below the urban area of Bishkek the Paleozoic basement depth is expected to generally decrease from the north (~1 km) to south (~3 km). However, in the south west of the study area, a local deepening of the basement to more than 3 km can be expected. The seven thick Tertiary formations overlying the Paleozoic bedrock are respectively made, from bottom to top, of siltstones and sandstones (Kokturpak and Kokomeren Formations, respectively), claystones (Sera Firma Formation), mudstones (Dzhel'dysu Formation), sandstones and pebbly conglomerate (Saryagach Formation), mudstones and sandstones (Chu Formation), and coarse-pebble conglomerate (Sharpyldak Formation) (*Bullen et al.*, 2001). In particular, the shallowest part of the Sharpyldak formation is made up of poorly sorted, matrix supported, fan conglomerates with granitic boulders as large as 1 m in diameter. Quaternary sediments with a thickness of 200-300 m overlie the Cenozoic deposits. To the south of the studied area, alluvial material made up of rubble and gravel with a thickness of between 15 and 40 m outcrops. The same material can be found within the urban area along the major rivers. In the southern half of the Bishkek territory, alluvial gravels, rubble and sandy material (with a thickness ranging between 25 and 50 m) constitute the shallowest geological layers. The lower Quaternary sediments made up

of rubbly-bench gravel with clay-sand lenses and break stone bench gravel outcrop in the northern part of the town. Occasionally, older Quaternary alluvial proluvial of rubbly-bench gravel with clay-sand lens outcrop in the northern part of the town.

Since information about the S-wave velocity in the shallow sedimentary layers was not available, an array measurement of seismic noise was carried out. We used all the available 19 stations and the array was installed near the position of station BI08 of the temporary seismological network (Figures 5.1, top and 2a).
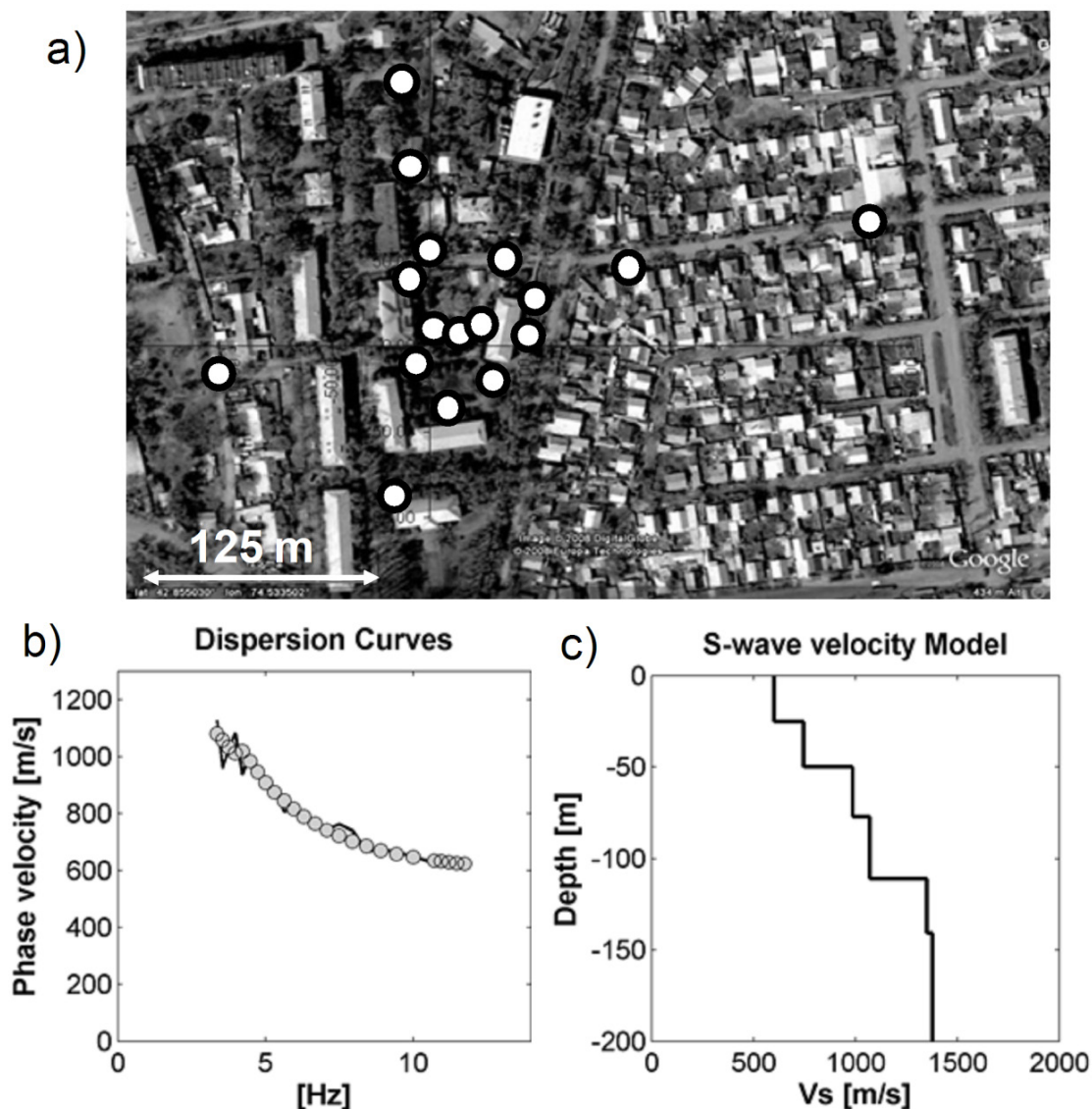
Figure 5.2 Results of the array inversion performed close to station BI08 (Figure 5.1). a) Array geometry (white circles); b) observed dispersion curve (black line) and reconstructed (gray circles); c) S-wave velocity model obtained by inverting the dispersion curve in panel b).

Seismic noise was recorded simultaneously by all stations for a few hours at 500 samples per second sampling rate. Simultaneous recordings of one hour of noise were used and divided in 60 second length windows. Only the vertical component was analyzed. Recordings were corrected for the instrumental response, considering the calibration parameters of each sensor, and the data have been analysed using the Extended Spatial Autocorrelation method (ESAC)

(*Ohori et al.*, 2002; *Okada*, 2003; *Parolai et al.*, 2006 and 2007). The obtained dispersion curve (Figure 5.2b), ranging between 3 to 13 Hz, shows a normal dispersive behaviour. The highest frequencies already show a quite high Rayleigh wave phase velocity (600 m/s) that increases up to 1100 m/s for the lower frequencies. These values are consistent with the existence of stiff Quaternary alluvial material made up of rubble and gravels in the study area. Due to the simplicity of the dispersion curve a simplified linearized inversion (e.g. *Parolai et al.*, 2006 and reference therein) was carried out.

The obtained model (Figure 5.2c) shows a regular increase of velocity with depth, starting from nearly 600 m/s in the shallowest layers (0-25 m depth) and increasing to 1380 m/s at the deepest ones. Note that the investigated depth range lies within the Quaternary sedimentary cover and it is reliable (as estimated by resolution matrix analysis here not reported) down to nearly 200 m depth.

Earthquake data

From August 16 2008 a temporary seismological network was installed in Bishkek (Figure 5.1, top). The network consisted of fifteen EDL 24bit acquisition systems equipped with thirteen short-period Mark-L4-C-3D sensors, one Güralp CMG-ESPC 60 and a IO-3D 4.5 Hz sensor, and four Reftek-130 digitizers connected to Lennartz LE3D-5s. Stations were operated in continuous mode until the middle of November 2008 and were installed in the cellars of public buildings or private houses in order to cover the urban area of Bishkek. One station (BI04) was installed in the Kyrgyz range with the aim of having a reference station for the site effect estimation analysis. However, this station, for logistic problems, could only be installed over a thin layer of detritus (mainly rubble and gravel) deposited on the slope of the hill. Furthermore, due to problems with power supply and the extremely low temperatures, it only worked for one month. All stations recorded at 100 samples per seconds.

From the continuous data streams recorded by the network, the recordings of 56 earthquakes were extracted using a slightly modified version of the procedure proposed by *Galiana-Merino et al.* (2008). The distribution of their epicentres is shown in Figure 5.1, with Table 5.1 listing the main parameters of the earthquake sources. The data set includes 50 crustal earthquakes with magnitude between Ml=1.6 and Mw=6.6, that occurred at distances between about 35 and 1527 km from station BI08. The recordings of 5 deep earthquakes, with magnitude between mb=5.1 and Mw=5.8 that occurred in the Pamir-Hindu Kush seismic zone, are also included in the data set. Finally, a magnitude Mw=7.3 earthquake that occurred at a distance of 5685 km in the Sea of Okhotsk (Russia) at a depth of 492 km (not shown in Figure 5.1), completes the data set.
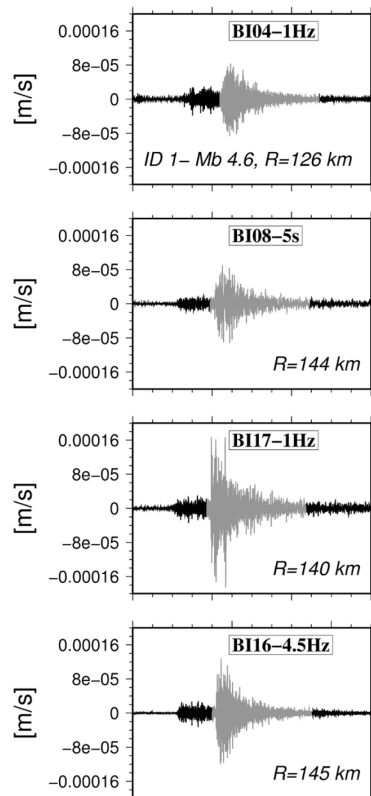
Figure 5.3 Recordings at four different stations of the 21.08.08 (mb = 4.6, ID = 1) earthquake (Table 5.1). The windows selected for the analysis are shown in gray. In each panel, the station ID (Figure 5.1), the epicentral distance R and the high pass corner frequency of the sensor are shown.

The different energy content of the earthquake recordings (due to different hypocentral distances and magnitudes) allows us to widen the frequency range investigated. Figure 5.3 shows the recordings of a mb = 4.6 earthquake that occurred 144 km from station BI08 (event 1 in Table 5.1). Note the different waveforms depending on the position of the station. The following analyses were performed considering frequencies with a signal-to-noise (SNR) ratio larger than 3 (estimated by considering the Fast Fourier Transform (FFT) of a noise window as wide as the signal window). Based on the results of previous studies (e.g. *Strollo et al.*, 2008a,b), that showed that the short period sensors provide reliable seismic noise recordings down to frequencies of ~0.1 Hz, no a priori choice of the investigated frequency band was carried out. We corrected the recordings for the instrumental response and the spectra were smoothed using a triangular window equal-spaced in logarithm scale (10% of the central frequency).

Horizontal-to-Vertical spectral ratio (HVSR)

The HVSR (*Lermo and Chavez-Garcia*, 1993) method belongs to the class of so-called non-reference site methods (*Bard*, 1995). Although there is not a theoretical basis demonstrating that HVSR is an estimate of the site transfer function, and *Parolai and*

- 114 -

Richwalski (2004) showed using numerical simulations that it underestimates the amplification at frequencies larger than the fundamental one, it is generally considered useful for estimating the fundamental resonance frequency of a site (e.g. *Field and Jacob*, 1995).
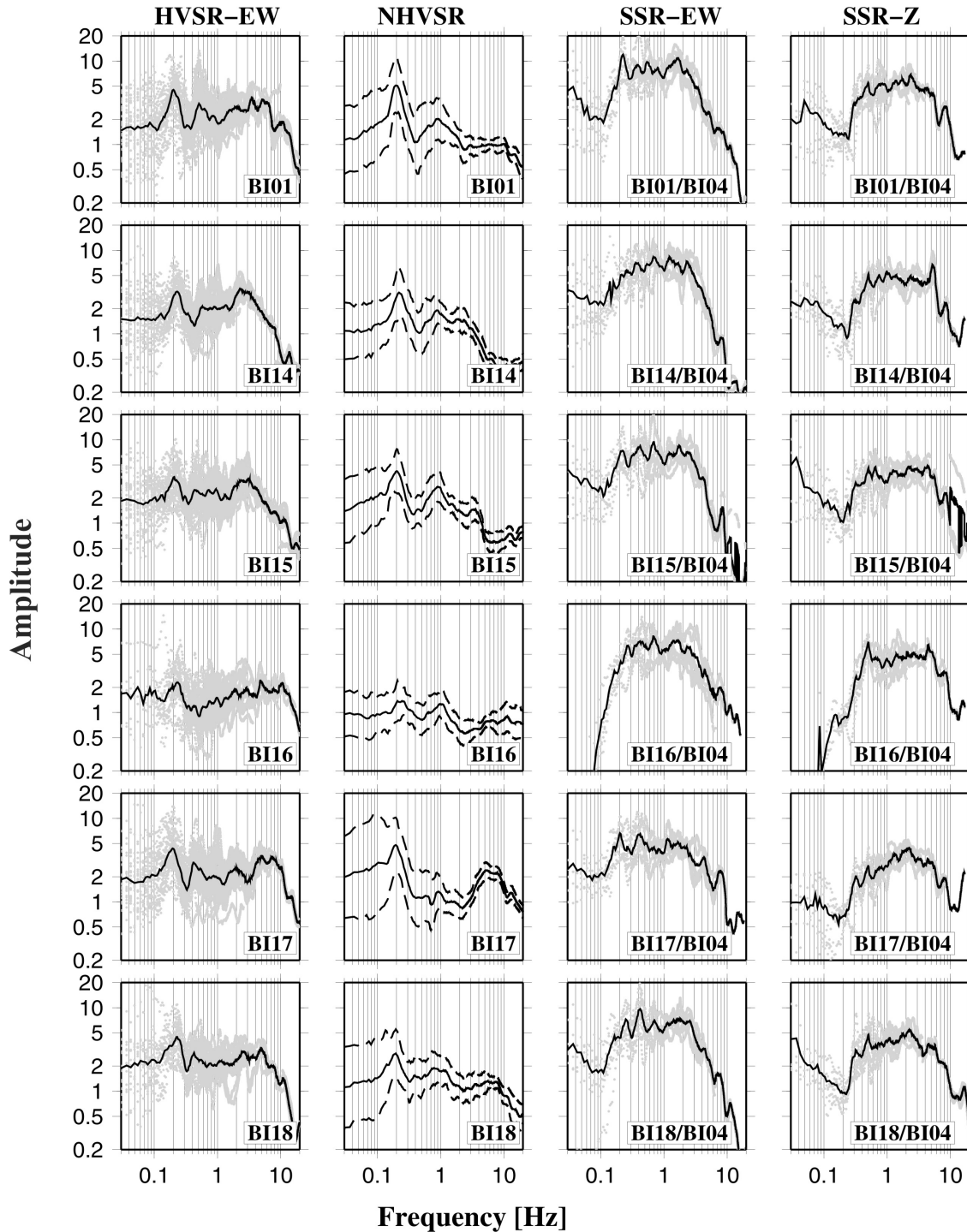
Figure 5.4a Different types of spectral ratios computed for the seismic stations installed in Bishkek. First column: Horizontal-to-Vertical spectral ratio (HVSR) for the S-wave windows selected over the East-West component; second column: Horizontal-to-Vertical spectral ratio of noise recordings (NHVSR); third column: Standard Spectral Ratios (SSRs) between the EW S-wave spectrum computed at each station and the correspondent spectrum at the reference station BI04; fourth column: the same as in the third column but for the vertical component. In the first, third, and fourth columns, the gray dots represent spectral ratios computed at frequencies where the signal to noise ratio is greater than 3, while the black curve is the average ratio. In the second column, the mean ratio ± one standard deviation (dashed lines) is shown.

After having tested several criteria for the signal window selection (including fixed window length and energy criteria), the data analysis was carried out using windows of fixed 50 second length. This was due to the requirement of including enough low-frequency cycles that, due to the thickness of the sedimentary cover in the area, were expected to be of interest for estimating the resonance frequency of the investigate sites. Figure 5.3 shows examples of windows of signal selected for the following analysis.
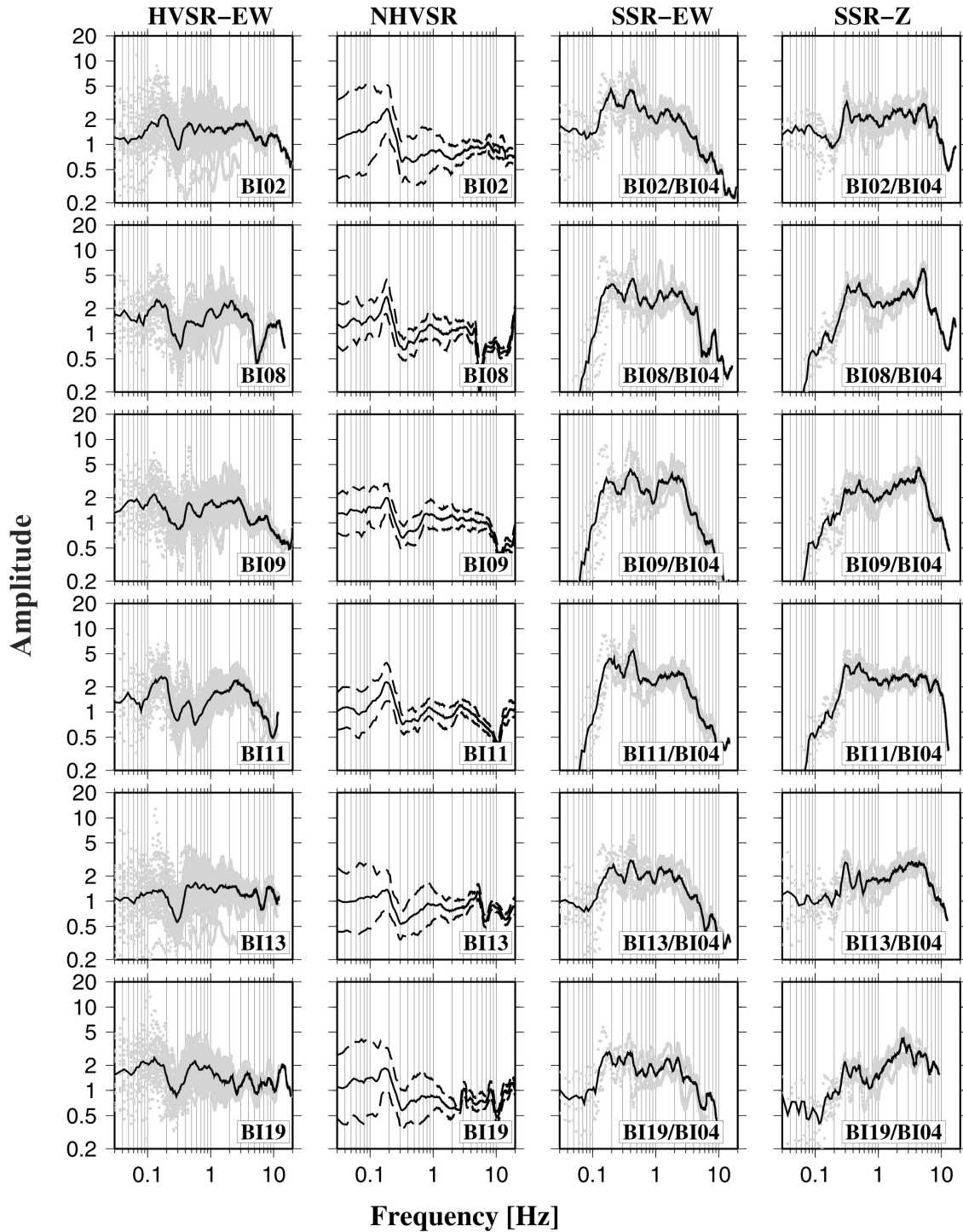
Figure 5.4b continue from 5.4a

The results in Figure 5.4 and 5.5 (first column) show that HVSR for the stations installed in the northern part of the town over the older Quaternary material (Figure 5.1, BI01, BI05, BI14, BI15, BI16, BI17, BI18), clearly show a first resonant peak at ~0.2 Hz. Although the HVSR were computed considering the two horizontal components separately, Figures 5.4 and 5.5 show the results only for the east-west (EW) component, as similar trends are also obtained for the North-South (NS) component (not shown). After a narrow through around 0.3 Hz, the HVSR is almost flat and then shows a bump starting from between 2-3 Hz up to 10 Hz (in the case of station BI17).
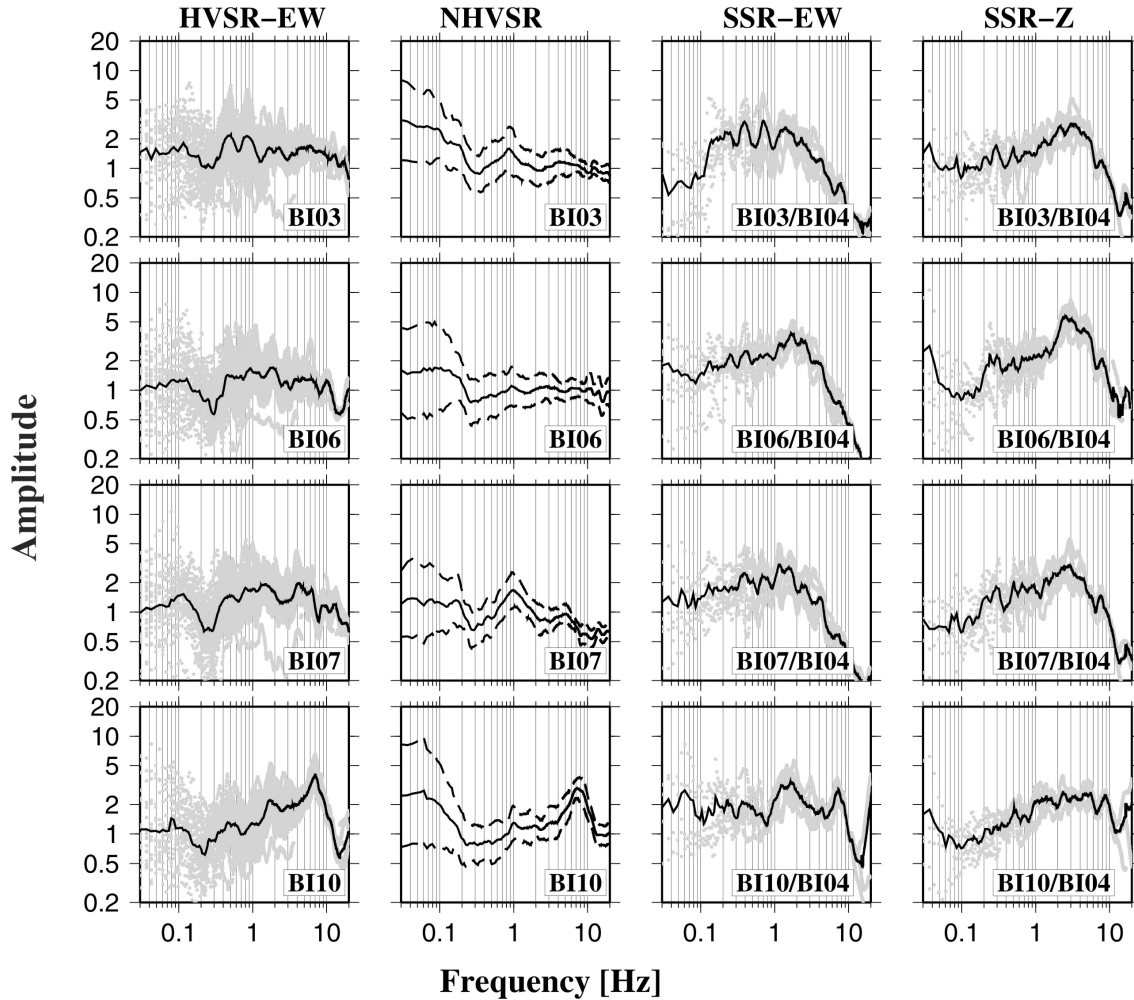
Figure 5.4c continue from 5.4b

The stations located in the central part of the urban area (BI02, BI08, BI09, BI11, BI12, BI13, BI19) show a smaller-amplitude low-frequency peak (between 0.1 and 0.2 Hz) followed by a very large trough and then by a nearly flat HVSR. The stations located at the southern margin of the investigated area, where the Tertiary material makes a tectonic contact with Quaternary sediments (BI03, BI06, BI07 and BI10), show a peculiar behaviour strongly dependent on small scale changes in the surface geology. While the HVSR of BI10 is nearly flat up to 1 Hz and then rapidly increases, showing a large peak at 7 Hz, the HVSR of BI06

resemble those of the station located in the central part of the town (nearly flat with a 0.3 Hz trough). A similar HVSR shape is shown by station BI07 and BI03. Finally, it is worth noting that the HVSR at station BI04 (Figure 5.5), which was supposed to be a possible reference station, can be considered flat only up to nearly 2 Hz. At higher frequencies, large amplifications are shown with a main peak at ~ 5 Hz.
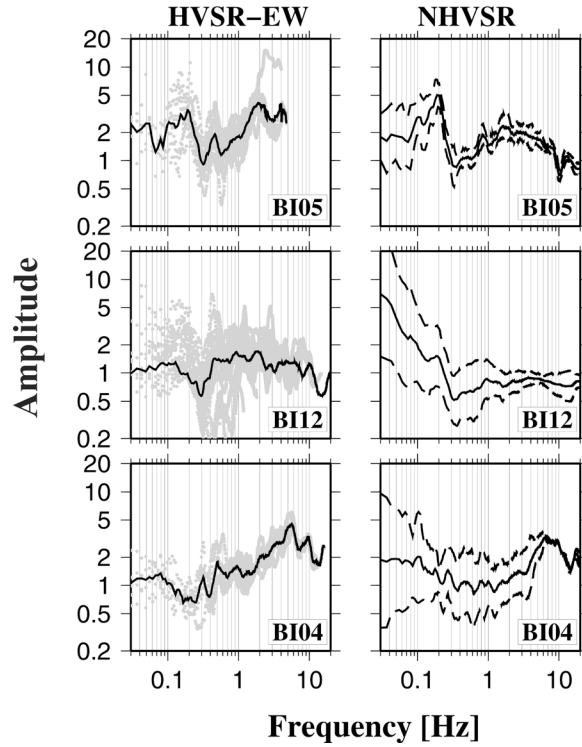
Figure 5.5 Horizontal to vertical spectral ratios for earthquake recordings (left) and noise (right), at 3 different stations of the temporary network (see caption of Figure 5.4 for explanations).

HVSR of de-noised seismograms

The reliability of the low (0.1-0.2 Hz) frequency peak in the HVSR, being calculated for frequencies with high SNR ratio and its relation with the arrival of the larger amplitude phases (S-wave train) was evaluated by de-noising the seismograms using a S-transform based approach (*Parolai*, 2009) and analysing the distribution of energy on the time frequency plane.

The S-transform (*Stockwell et al.*, 1996) is a time-frequency localization spectral method similar to the short-time Fourier transform (*Gabor*, 1946), but with a Gaussian window whose width scales inversely, and whose height scales linearly, with the frequency.

The S-transform of a function $h(t)$ is defined as:

$$S(\tau, f) = \int_{-\infty}^{\infty} h(t) \frac{|f|}{\sqrt{2\pi}} e^{-\frac{(\tau-t)^2 f^2}{2}} e^{-i2\pi ft} dt \qquad (1)$$

Where t is the time, f the frequency and τ is a parameter that controls the position of the

- 118 -

Gaussian window along the t-axis. Recently, *Parolai* (2009) applied to the S-transform coefficients the continuous thresholding function proposed by *Yoon and Vaidyanathan* (2004) that was shown to outperform the traditional soft and hard-thresholding schemes and can be adapted to the characteristic of the input signal for de-noising seismograms corrupted by noise. The resulting method was found to be very effective, in particular when compared with standard filtering approaches, and hence, in this study, the seismic recordings have been de-noised following the *Parolai* (2009) procedure. The Fourier spectra of the de-noised signal have been in turn used to calculate the HVSR. This approach offers two main advantages:

1) The HVSR is calculated only on signal, avoiding the subjective choice about the frequency band to be used on the basis of an average SNR ratio.

2) The Fourier spectrum of the filtered signal might be estimated by integrating the $S(\tau, f)$ of the filtered signal along the time axes, also using frequency dependent time window of integration. This would allow a comparison, if required, for an equal number of cycles of the frequency content.

In this study, the Fourier transform of the spectrum was obtained by integrating for the whole duration of the seismogram. Finally, the HVSR was calculated between the integrated raw Fourier spectra.

Figure 5.6 shows, as an example, the EW and Z recordings and their correspondent S-transforms of event 1 in Table 5.1.

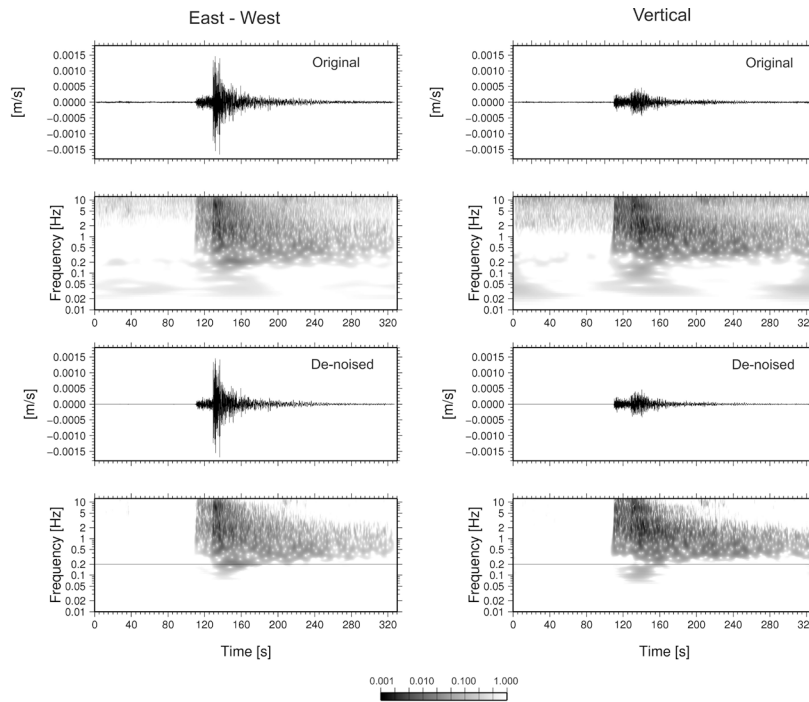**Figure 5.6** De-noising procedure applied in the time-frequency analysis, considering the east-west (left) and vertical (right) components. From top to bottom are shown the original recording of event 1 (Table 5.1) recorded at station BI17, the S-transform of the original recording, the de-noised recording and its S-transform. The color bar is for the S-transform results. See text for details about the procedure.

The filtered seismograms and their S-transforms are also shown. We note that just after the S-waves, an arrival with high energy occurs with a frequency around 0.2 Hz that was identified as the resonance frequency of the site, on the EW component of the ground motion, but not observable on the vertical one. The Fourier spectrum of the de-noised EW component signal (Figure 5.7) clearly shows a large amplification peak at around 0.2 Hz. Interestingly, after applying the de-noising procedure, signal content down to 0.06 Hz can be observed. The HVSR for this station, determined by combining spectral ratios from four earthquakes (events 1, 6, 15, and 36 in Table 5.1), with different magnitudes and occurring at different hypocentral distances are shown in Figure 5.8. Although affected by a large scatter due to the calculation of the spectral ratios from raw spectra, the trend of the HVSR shows, in agreement with the results shown for this station in Figure 5.4, a clear peak at around 0.2 Hz. These results indicate that the low frequency peak in HVSR is due to the amplification of the horizontal component of ground motion occurring just after the S-wave arrival. They also confirm the reliability of the HVSR results obtained for these low frequencies, independent of the SNR ratio threshold chosen and the length of the window used for the analysis.
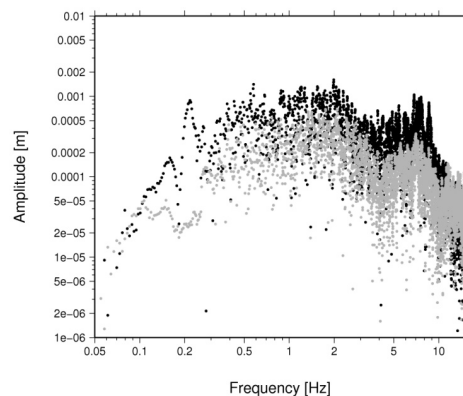
Figure 5.7 Fourier amplitude spectra of the de-noised seismograms shown in Figure 5.6. For each frequency, the black and gray dots represent the amplitude for the east-west (EW) and vertical (Z) components, respectively.
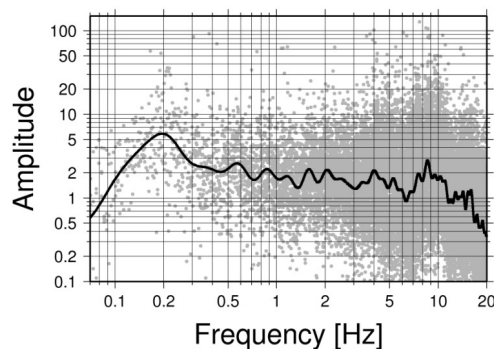
Figure 5.8 Horizontal (east-west) to vertical spectral ratios (gray circles at station BI17) obtained by considering de-noised seismograms from 4 different events (ID 1, 6, 15, and 36 in Table 5.1). The black line represents the trend observed in the data by performing a polynomial fit (Wessel and Smith, 1991).

Standard Spectral Ratio

The Standard Spectral Ratio technique (SSR) (e.g. *Borcherdt*, 1970; *Parolai* et al., 2000) consists of comparing records at nearby sites, using one as the reference. It is assumed that records from the reference site (in general, a station installed on outcropping hard bedrock) contain the same source and propagation effects as records from the other sites. Therefore, the spectral ratio directly provides the site response.

Although station BI04 was not found to be an ideal reference site, it might still be used as a reference station for the frequency range lower than 2 Hz. In fact, over this frequency range, the HVSR results show values of nearly one. Furthermore, the distance between this station and the other stations of the network is short enough to assume that only minor propagation effects are affecting the SSR results over this frequency range. Due to the instrumental problems of station BI04, only 7 events (see Table 5.1) could be used for estimating the SSR. Since stations BI05 and BI12 have not recorded the events available for BI04, the SSR analysis cannot be carried out for these two stations. Results obtained for the East-West (EW) and vertical (Z) components of ground motion are shown in Figure 5.4 (third and fourth column, respectively). Differently from the HVSR, results of all the stations in the basin show very similar behaviour for the horizontal component SSR. In particular, a broad amplification is observed with clear distinct peaks between 0.1 and 0.2 Hz (increasing from South to North), 0.4 Hz and between 1 and 2 Hz. Occasionally, some stations (e.g. BI03, BI15) also show distinct amplification peaks at 0.6-0.7 Hz. Above 2 Hz, the large de-amplification effect is due to the amplification occurring at the reference site. Stations BI10, BI07 and BI06, located at the southern margin of the basin, show different behaviours. BI10 is nearly flat with a small amplification at around 1.5 Hz. BI07 and BI06 show only moderate amplification, increasing nearly linearly from the lower frequencies up to 1-2Hz. The following decaying trend is not reliable due to the amplification affecting the reference station over that frequency range.

The differences between the HVSR and SSR results can be easily explained by considering the SSR results obtained by analysing the vertical component of ground motion. In fact, the vertical component SSR of the stations within the basin (Figure 5.4, fourth column) are showing large amplifications with peaks at frequencies (~0.3-0.5 Hz) systematically larger than those observed on the horizontal component results. These peaks are particularly large, even occasionally becoming predominant, for the stations BI13, BI08, BI09, BI11 located on the younger Quaternary sediments outcropping in the southern part of the urban area. The positions of these peaks coincide with the spectral troughs in the HVSR. Considering that

- the HVSR of the reference station is not affected by the narrow spectral troughs at 0.3-0.5 Hz (indicating that no amplification of the vertical component in that frequency range take place outside of the basin), and

- the role of surface waves might be ruled out, since the amplitude peaks in the low frequency range are occurring at different frequencies on the vertical and horizontal components,

the results might be interpreted considering the effect of converted waves on the recorded ground motion. In fact, previous studies (e.g. *Takahashi et al.*, 1992; *Parolai and Richwalski*, 2004) showed that at the boundaries between shallow geological layers, significant P-to-S conversion and S-to-P conversion can take place and, therefore, affect the HVSR results.

Figure 5.9 (left) shows the vertical, radial and transverse component seismograms at station BI13 (strongly affected by amplification on the vertical component) of event 1 (Table 5.1). It is remarkable how from just a few tenths of seconds before the S-wave arrival the vertical component shows significant ground motion lasting for several seconds. By contrast, Figure 5.9 (right) shows the vertical, radial and transverse component seismograms at the same station of an mb = 5.2 earthquake that occurred at ~800 km hypocentral distance (ID 15 in Table 5.1), that is much farther than the first example. Only the first tens of seconds before the S-wave arrival are shown. In this case, it is clear how the first trough and the second peak in the vertical component are also observed, although shifted, on the radial one. The large amount of energy in the radial component recordings in the P-wave window for a nearly vertical incidence event suggests that wave conversion takes place. The shift between peaks and troughs observed for different components might account for the different wave velocity propagation.
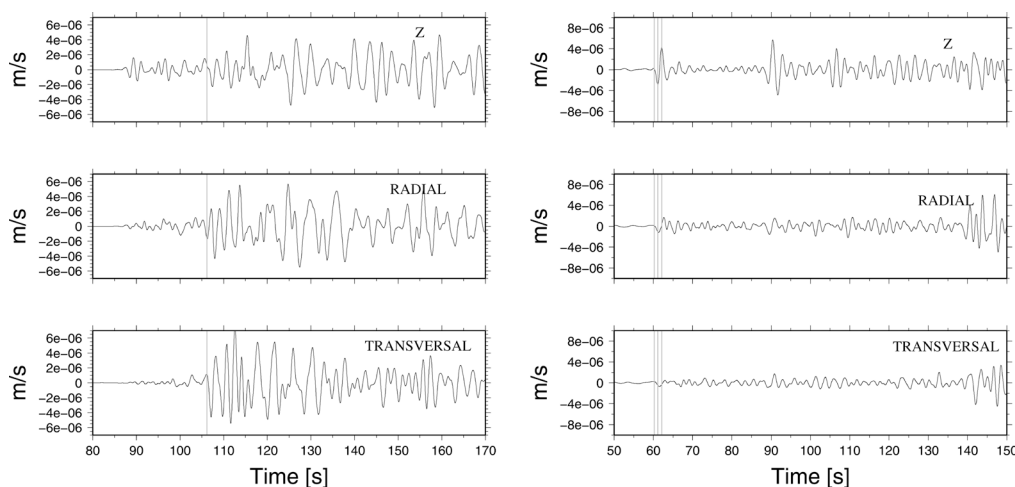
Figure 5.9 Vertical (top), radial (middle) and transversal (bottom) seismograms of events 1 (left) and 15 (right) of Table 5.1, recorded at station BI13. For event 15, only the first tens of seconds before the S-wave arrivals are shown. The time values on x-axis are referred to a generic reference time. Vertical gray lines indicate approximately the S-wave arrivals (left panels) and the arrival time of the first three peaks on the vertical component (right panels).

Noise data

Seismic noise was collected at 196 sites in the urban area of Bishkek and in the southern surroundings where Quaternary layers overlap the folded Tertiary material (Figure 5.1). One EDL 24 bit acquisition system, equipped with a short-period Mark-L4-C-3D sensor, was used for the measurements. Noise recorded in continuous mode by the temporary seismological network was also included in the analysis. Depending on the station, ten to thirty 60 second noise windows have been considered for each measurement points. Time series have been tapered at both ends with a 5% cosine taper and their Fast Fourier Transform (FFT) calculated. The FFT have been smoothed using a Konno-Ohmachi window (*Konno and Ohmachi*, 1998) fixing the parameter b that determines the degree of smoothing to 40. For each 100 second window the horizontal-to-vertical spectral ratio (NHVSR) was computed (*Nogoshi and Igarashi*, 1970; *Nakamura*, 1989) and the logarithmic average of the NHVSR estimated. Figure 5.4 (second column) shows the NHVSR computed for sites where the temporary seismic network was installed, considering the pre-event noise windows. A generally good agreement between the fundamental frequency of resonance obtained from the HVSR (first column) and the NHVSR (second column) is observed.
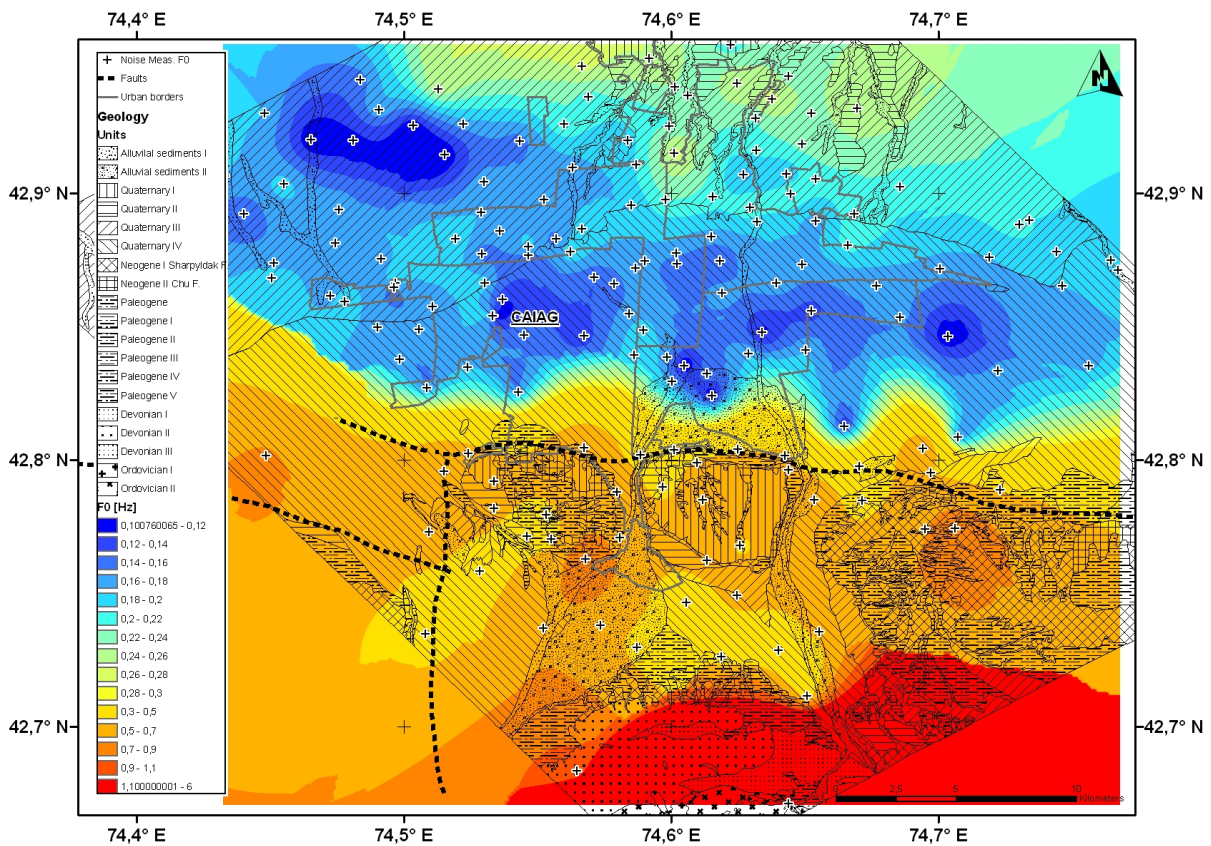

Figure 5.10 Map of the fundamental frequency of resonance estimated from noise measurements for the area around Bishkek (Kyrgyzstan).

The results presented in Figure 5.10 show that in the urban area of Bishkek, north of

the outcropping Tertiary material, the fundamental resonance frequency of soil spans, consistent with the SSR results, from nearly 0.3 Hz to the North to ~0.1 Hz in the South. The general decrease of the fundamental resonance frequency from North to South is consistent with the geological structure of the basin, which shows an increase in the thickness of the Quaternary and Tertiary sedimentary cover towards the south (*Bullen et al.*, 2001, their Figures 4 and 5). Considering the high value of the S-wave velocity characterising the shallow Quaternary layers (Figure 5.2), the low value of the resonance frequency might be indicative of a deep impedance contrast, likely to exist between the Sharpyldak and Chu formations. The lower-resonance frequencies observed in the south-western part of the area are consistent with a thickening of the sedimentary cover as proposed by *Bullen et al.* (2001) and in the references therein.

The occasionally observed very low frequency peak (lower than 0.1 Hz) in the southernmost part of the investigated area could be related (similarly to the fundamental resonance frequency in the urban area) to the contact between the Sharpyldak and Chu formation. Note that in this area, due to the geological structure forming a sincline in the Tertiary material, the thickness of the Sharpyldak formation can reach values even larger than those below the urban area (*Bullen et al.*, 2001, their Figure 5). However, due to the technical limitation of the used geophone, we cannot consider fully reliable results obtained below 0.1 Hz (*Strollo et al.*, 2008,a,b) and we therefore refrain from analysing them too deeply to avoid misinterpretation. Finally, the increase of the fundamental frequency of resonance in the southernmost part of the investigated area, toward the Kyrgyz Range, is in agreement with the expected lateral variations due to an outcropping of the Chu and Sharpyldak formations, which generates a small basin made up of Quaternary material (*Bullen et al.*, 2001, their Figure 5).

In conclusion, we remark that although the NHVSR shape, especially at intermediate frequencies, might be different from the SSR one at the corresponding stations, their variability is consistent with that of the SSR. That is, differently from what we observed by comparing the HVSR results with the SSR ones, stations showing similar SSR also show similar NHVSR

Discussion and Conclusions

In this study we analysed earthquake and seismic noise recordings collected in the area of Bishkek (Kyrgyzstan). Results showed that significant amplification (~5) affect the ground motion in the case of earthquakes. Of particular relevance is the wideness of the frequency band that can be amplified, ranging from nearly 0.1 Hz to more than 2 Hz. Several peaks can

be distinguished in the calculated site responses that may be a result of the complex geological setting (with several overlapping units) of the area. Considering both the high velocities estimated by means of array measurements in the shallow sedimentary cover and its thickness, it is likely that the wideness of the amplified frequency band might indicate a small damping of ground motion, which may be due to the stiffness of the material through which the waves propagate.

Recently, the slope of topography was suggested (*Wald and Allen*, 2007) as proxy parameter for estimating Vs30 and therefore for soil classification in terms of site effects. On one hand, we found that the slope of the topography in the studied area (ranging between 0.0015 in the northern part of the basin and 0.3 in the Kyrgyz range), computed using the GTOPO30 topographic model (see Data and Resources), is a reliable proxy for estimating the shear-wave velocity in the shallowest 30 meters (Vs30) of the Quaternary layer covering the central and southern part of Bishkek, since it indicates velocities between ~400 m/s and 760 m/s (NEHRP class C), compatible with the S-wave velocity profile obtained by our array measurements. On the other hand, the velocity for the northern part seems to be underestimated, since the velocities estimated from the slope correspond to class D, while neither the site response nor the local geology shows any significant variations. Moreover, note that station BI04, installed in the Kyrgyz range, that would be classified as NEHRP class B (rock site) was found to show significant amplification above 2 Hz. Finally, a site classification only based on Vs30 is not adequate to account for the broad-band site amplification, since it completely fails to describe the site amplifications occurring at frequencies smaller than 1 Hz.

We verified by a careful time-frequency analysis that the lowest frequency peak in the SSR and HVSR was to be ascribed to resonance occurring just after the S-wave arrival. However, we found significant differences between the SSR and the HVSR results at frequencies higher than the resonant one. As a possible mechanism responsible for this disagreement, after a careful and thorough analysis of several recordings, we propose the role of converted phases. Previous papers (e.g. *Takahashi et al.*, 1992; *Parolai and Richwalski*, 2004) showed in fact that similar behaviour can be due to wave conversions when a large impedance contrast exists.

The single noise station measurements, once calibrated through a comparison with the earthquake data results, allowed us to enlarge the area of investigation improving also the spatial resolution. We found that, differently from the HVSR results, the spatial consistency of the NHVSR curves was equivalent to that of the SSR one. In particular, the fundamental resonance frequency was better evaluated using NHVSR than HVSR. This can be explained

considering the different composition of the seismic noise (mainly dominated by surface waves) and the earthquake wavefields, where converted phases can affect the vertical component of the ground motion at frequencies close to the fundamental resonance frequency of the site. Innovatively for the area, a first map of the fundamental resonance frequency of soil was calculated, showing that a large impedance contrast within the Tertiary sedimentary cover might be responsible for the first amplification peak of ground motion. However, considering the broad band amplification shown by the SSR results, the fundamental resonance frequency map can be considered as providing the lower bound of frequency from which amplification starts.

Since our results are based only on weak motion data, future projects should be devoted to investigating soil behaviour for the case of strong ground motion, both considering the geotechnical characteristic of the shallow geological material and the water table depth, and including the recordings of strong motion data. To this regards, future projects, as a continuation of the CASCADE one, will aim at the installation of a strong motion network in Bishkek. Finally, the obtained results will be considered, while re-assessing the seismic hazard and risk for Bishkek, in the framework of the Global Earthquake Model (*Global Earthquake Model, n.d.*) program, contributing to a harmonised risk assessment in Central Asia.

Table 5.1 List of earthquake parameters for the 56 events extracted from the continuous data streams and used in the analysis (Figure 5.1, bottom). The location and magnitude parameters are from the ISC catalogue (*ISC, n.d.*). The epicentral distances and back-azimuths to station BI08 are also reported. The symbol * indicates events used for the SSR method.

ID	Date	OT	Lat.	Lon.	h(km)	Mag(type)	Dist.(km)	BAZ(BI08)
1*	2008/08/21	17:19:54.40	42.1030	75.9650	10.0f	4.6(mb)	144.11	124.94
2*	2008/08/21	19:34:06.94	41.9300	75.8040	33.0	4.3(mb)	146.47	134.13
3*	2008/08/24	10:04:37.50	40.3610	72.9740	6.7	4.1(mb)	306.04	205.58
4*	2008/08/30	12:46:45.58	42.6966	84.1352	2.0	5.5(mb)	783.49	88.01
5	2008/09/01	04:24:31.02	37.3900	68.9000	2.0	5.4(mb)	773.29	220.10
6*	2008/09/02	20:49:40.28	43.5544	79.5439	230.4	4.9(mb)	413.45	77.44
7*	2008/09/05	04:57:52.58	36.5360	71.2910	188.0	5.3(mb)	755.18	202.60
8*	2008/09/06	05:47:39.9	36.4900	70.9300	18.1	5.8(Mw)	771.75	204.72
9	2008/09/10	07:55:01.24	42.5741	74.8174	18.8	2.0(Ml)	38.86	143.21
10	2008/09/13	13:40:28.34	42.5330	74.5599	17.8	2.7(Ml)	35.79	176.49
11	2008/09/13	18:18:41.02	42.5314	74.5694	18.0	2.8(Ml)	36.03	175.27
12	2008/09/17	19:37:34.70	43.5990	78.5400	14.6	4.0(mb)	335.00	74.32
13	2008/09/20	02:41:18.30	42.0316	76.0275	19.9	1.9(Ml)	152.98	126.22
14	2008/09/20	04:15:51.86	42.2699	74.8597	100.0f	2.9(Ml)	70.27	157.52
15	2008/09/24	17:59:33.55	36.1530	71.2530	33.0	5.2(mb)	796.35	201.75
16	2008/09/26	22:23:22.50	40.6210	72.9360	37.0	4.2(mb)	281.47	208.62
17	2008/10/05	15:52:51.00	39.5330	73.8240	35.0f	6.6(Mw)	374.04	189.36
18	2008/10/05	16:11:10.42	39.5080	73.8880	33.0	5.6(mb)	375.99	188.47

19	2008/10/05	16:36:18.20	39.4920	73.8900	35.0f	5.1(mb)	377.72	188.41
20	2008/10/05	17:00:26.75	39.2640	73.8430	33.0	4.3(mb)	403.39	188.48
21	2008/10/05	18:27:39.40	39.4080	73.7320	35.8	5.1(mb)	389.04	190.20
22	2008/10/05	21:46:06.73	39.6940	73.7240	42.0	4.6(mb)	357.85	191.16
23	2008/10/07	16:43:29.80	42.1280	76.5860	27.0	4.0(mb)	186.68	114.94
24	2008/10/09	03:13:42.00	39.3770	73.9780	29.0	4.7(mb)	389.44	187.04
25	2008/10/09	14:43:19.40	39.4470	73.9340	122.7	4.9(mb)	382.18	187.74
26	2008/10/13	08:07:44.31	36.1870	71.0010	35.0f	5.1(mb)	800.69	203.37
27	2008/10/13	09:23:35.08	39.5800	73.8580	35.0f	5.0(mb)	368.44	189.04
28	2008/10/13	16:05:25.04	39.5000	73.8140	10.0f	5.0(Mw)	377.80	189.41
29	2008/10/13	17:16:09.99	38.5590	70.3380	11.0	5.3(mb)	594.10	217.90
30	2008/10/18	20:53:55.90	41.8000	81.0400	7.9	4.0(mb)	547.46	100.16
31	2008/10/18	21:15:24.75	42.6396	74.8415	4.1	1.6(Ml)	34.70	133.37
32	2008/10/19	01:27:15.50	41.4611	75.6909	14.2	3.1(Ml)	181.95	147.98
33	2008/10/20	19:58:01.73	41.7706	75.7582	35.0f	2.5(Ml)	157.06	139.69
34	2008/10/22	16:46:09.68	40.5960	78.0750	17.8	4.3(mb)	386.53	129.32
35	2008/10/23	05:50:45.60	39.4200	73.9340	210.0	4.8(mb)	385.16	187.68
36	2008/10/26	01:28:56.06	36.4900	70.6830	19.9	5.5(mb)	780.41	206.22
37	2008/10/28	01:05:23.05	42.9220	75.0563	15.0f	1.6(Ml)	43.28	79.81
38	2008/10/28	23:10:00.70	30.6390	67.3510	2.0	6.4(Mw)	1500.03	207.46
39	2008/10/28	23:17:23.89	30.3174	67.5086	14.0f	4.3(mb)	1527.21	206.40
40	2008/10/29	11:32:43.13	30.5980	67.4550	19.0	6.4(Mw)	1500.34	207.04
41	2008/11/01	05:48:01.33	42.7841	76.4509	26.3	3.7(mb)	156.61	92.21
42	2008/11/02	17:58:29.69	42.7940	76.4250	20.0	3.7(mb)	154.43	91.85
43	2008/11/04	14:22:23.92	39.4440	74.0550	35.0f	4.8(mb)	381.31	186.19
44	2008/11/04	15:46:52.91	39.2730	73.7260	35.0f	4.1(mb)	403.93	189.91
45	2008/11/06	14:23:51.80	39.4780	74.0170	16.8	4.8(mb)	377.90	186.74
46	2008/11/06	21:14:16.40	42.2980	75.2359	35.0f	2.2(Ml)	84.48	136.83
47	2008/11/07	09:21:17.26	39.3730	74.0110	26.9	4.6(mb)	389.56	186.62
48	2008/11/08	01:30:44.19	39.4790	73.9490	2.0	4.6(mb)	378.49	187.62
49	2008/11/09	02:48:04.54	42.3160	75.2200	2.0	2.1(Ml)	82.13	136.56
50	2008/11/09	03:31:29.76	42.4597	71.2813	35.0f	3.9(mb)	269.50	261.73
51	2008/11/09	19:22:49.43	39.4540	73.9650	18.3	4.5(mb)	381.07	187.36
52	2008/11/10	23:24:37.41	42.4345	74.6160	35.0f	1.8(Ml)	47.17	171.71
53	2008/11/13	20:52:08.87	39.5150	73.9600	35.0f	4.7(mb)	374.40	187.55
54	2008/11/18	00:15:12.28	39.5720	76.6380	492.0	3.5(mb)	405.19	153.55
55	2008/11/24	09:02:58.00	54.1800	154.3100	56.6	7.3(Mw)	5684.71	47.72
56	2008/11/26	16:41:23.36	39.3100	71.7970	10.0f	4.2(mb)	455.91	211.10

Table 5.1 continuation of the table from the previous page.

Bibliography

Abdrakhmatov K., Havenith H-B., Delvaux D., Jongmans D. and Trefois P. (2003) Probabilistic PGA and Arias Intensity maps of Kyrgyzstan (Central Asia), *Journal of Seismology*, 7, 203-220.

Aki K. (1957) Space and time spectra of stationary stochastic waves, with special reference to microtremors, *Bulletin Earthquake Research Institute*, 35, 415-456.

Ambraseys N.N., Finkel C.F. (1991) Long-term seismicity of Istanbul and of the Marmara Sea region, T*erra Nova*, 3, 527-539.

Andrews D. J. (1986) Objective determination of source parameters and similarity of earthquakes of different size, 37, 259-267.

Ansal A., Laue J., Buchheister J., Erdik M., Springman S.M., Studer J., Koksal D. (2004) Site characterization and site amplification for a seismic microzonation study in Turkey. Proceedings of the 11P[thP] Intl. Conf. On Soil Dyn. and Earthquake Engng, (11P[thP] ICSDEE) and the 3rd Intl, *Conference On Earthquake Geotechnical Engineering (3P[rdP] ICEGE)*,January 7-9, Berkeley, CA, 53-60.

Ansal A.M., Kurtulus A. (2007) Suspension PS Velocity Logging Measurements at Atakoy Vertical Array Site, Istanbul, *Data Report.*

Arai H. and K. Tokimatsu (2000). Effects of Rayleigh and Love waves on microtremor H/V spectra, paper presented at *12th World Conference on Earthquake Engineering*, N. Z. Soc. for Earthquake Eng., Auckland, N. Z.

Arai H., Tokimatsu K. (2004) S-wave velocity profiling by inversion of microtremor H/V spectrum, *Bulletin of the Seismological Society of America*, 94, 1, 53-63.

Bard P.Y. (1995) Effects of surface geology on ground motion: recent results and remaining issues, in *10th European Conference on Earthquake Engineering*, 305-323, Duma, Balkema, Rotterdam.

Beyen K, Erdik M. (2004) Two-dimensional nonlinear site response analysis of Adapazari plain and predictions inferred from aftershocks of the Kocaeli earthquake of 17 August 1999, *Soil dynamics and Earthquake Engineering*, 24, 261-279.

Bindi D., Parolai S., Cara F., Di Giulio G., Ferretti G., Luzi L., Monachesi G., Pacor F. and Rovelli A. (2009) Site Amplifications Observed in the Gubbio Basin, Central Italy: Hints for Lateral Propagation Effects, *Bulletin of the Seismological Society of America*, 99(2A), 741-760, doi:10.1785/0120080238.

Bindi D., Parolai S., Grosser H., C. Milkereit, and S. Zunbul (2006) Cumulative Attenuation along Source-to-Receiver Paths in Northwestern Turkey, *Bulletin of the Seismological Society of America*, 96(1), 188-199, doi:10.1785/0120050037.

Birgören G, Özel O. (2006) Determination of site effects and ground motion lengthening in Istanbul area derived from small earthquake recordings. Proceedings of the 8P[thP] U.S., *National Conference on Earthquake Engineering*, April 18-22, San Francisco, California, USA, Paper No. 1908.

Bonilla L.F., Steidl J. H., Lindley G.T., Tumarkin A. G. and R. J. Archuleta (1997) Site amplification in the San Fernando Valley, California: variability of site-effect estimation using the S-wave, coda, and H/V methods, *Bulletin of the Seismological Society of America*, *87*(3), 710.

Borcherdt R. D. (1970) Effects of local geology on ground motion near San Francisco Bay, *Bulletin of the Seismological Society of America*, 60(1), 29-61.

Bragato P. L., Laurenzano G. and Barnaba C. (2007) Automatic Zonation of Urban Areas Based on the Similarity of H/V Spectral Ratios, *Bulletin of the Seismological Society of America* , 97(5), 1404-1412, doi:10.1785/0120060245.

Bromirski P.D., Duennebier F.K. and Stephen R.A. (2005) Mid-ocean microseisms, *Geochemist, Geophysics, Geosystems*, 6, Q04009, doi:10.1029/2004GC000768.

Bullen M. E., Burbank D. W., Garver J.J. and Abdrakhmatov K. Ye. (2001) Late Cenozoic tectonic evolution of the northwestern Tien Shan: New Age Estimates for the initiation of mountain building, *Geological Society of America Bulletin*, 113, 1544-1559.

Campillo M. (2006) Phase and correlation in 'Random' seismic fields and the reconstruction of the Green Function, *Pure Applied Geophysics*, 163, 475-502.

Caniani D., Pascale S., Sdao F. and Sole A. (2007) Neural networks and landslide susceptibility: a case study of the urban area of Potenza, *Nat Hazards*, 45(1), 55-72.

Capon J. (1969) High-resolution frequency-wavenumber spectrum analysis Proceedings of the IEEE 57 (8), 1408-1418.

Cara F., Di Giulio G., Milana G., Bordoni P., Haines J. and Rovelli A. (2010) On the Stability and Reproducibility of the Horizontal-to-Vertical Spectral Ratios on Ambient Noise: Case Study of Cavola, Northern Italy, 100(3), 1263-1275, doi:10.1785/0120090086.

Castro R.R., Anderson J.G. and Singh S.K. (1990) Site response, attenuation and source spectra of S waves along the Guerrero, Mexico, subduction zone, *Bulletin of the Seismological Society of America*, 80(6A), 1481.

Castro R.R., Gallipoli M. R. and Mucciarelli M. (2004) An attenuation study in Southern Italy using local and regional earthquakes recorded by seismic network of Basilicata, online Available from: http://www.earth-prints.org/handle/2122/854 (Accessed 16 September 2010).

Chatelain J., Guillier B., Cara F., Duval A., Atakan K., Bard P. and The WP02 SESAME team (2008), Evaluation of the influence of experimental conditions on H/V results from ambient noise recordings, *Bullettin of Earthquake Engineering*, 6(1), 33-74, doi:10.1007/s10518-007-9040-7.

Chávez-García F.J. and M. Rodríguez (2007) The correlation of microtremors: empirical limits and relations between results in frequency and time domains, *Geophysical Journal International*, 171(2), 657-664.

Chavez-Garcia, F. J., and Tejeda-Jacome J. (2010) Site response in Tecoman, Colima, Mexico-I: Comparison of results from different instruments and analysis techniques, *Soil Dynamics and Earthquake Engineering*, 30(8), 711-716, doi: 10.1016/j.soildyn.2010.03.001.

Chiauzzi, L., Masi A., Mucciarelli M., Vona M., Pacor F., Cultrera G., Gallovic F. and Emolo A. (2010) Building damage scenarios based on exploitation of Housner Intensity derived from finite faults ground motion simulations submitted *to Natural Hazards*.

Cooley J. W. and Tukey J. W. (1965) An algorithm for machine calculation of complex Fourier series Math. *Comput.* 19, 297-301.

Cranswick E., Ozel O., Meremonte M., Erdik M., Safak E., Mueller C., Overturf D., Frankel A.(2000) Earthquake Damage, Site Response, and Building Response in Avcilar, West of Istanbul, Turkey, *International Journal for Housing Science and Its Applications*, ISSN 0146-6518, Special Issue: Kocaeli Earthquake 1999, Oktay Ural, Editor-In-Chief, Vol. 24, No 1, 85-96.

D'AmicoV., Picozzi M., Albarello D., Naso G., Tropenscovino S. (2004) Quick estimate of soft sediments thickness from ambient noise horizontal-to-vertical spectral ratios: a case study in southern Italy, *Journal Earthquack Engineering*, 8(6), 895-908.

Dalgiç S. (2004) Factor affecting the greater damage in the Avcilar area of Istanbul during the 17 August 1999 Izmit earthquake, *Bulletin of Engineering Geology and the Environment*, 63, 221-232.

Davis J. C. (1986) Statistics and Data Analysis in Geology, 2nd ed., John Wiley and Sons (WIE).

Delgado J., Lopez Casado C., Giner J., Estevez A., Cuenca A. and Molina S. (2000) Microtremors as a geophysical exploration tool: applications and limitations, *Pure and Applied Geophysics*, 157, 1445-1462.

Di Nocera S., Anagnostopoulos S., Pescatore T., Russo B., Senatore M. R. and Tramutoli M. (1988) Note illustrative della carta geologica dell'alta valle del Basento (Appennino Lucano-Italia), in *Atti del Convegno: Ambiente fisico, uso e tutela del territorio di Potenza*, Potenza, Italy.

Dolce M., Masi A., Marino M. and M. Vona (2003) Earthquake damage scenarios of the building stock of Potenza (Southern Italy) including site effects, *Bulletin of Earthquake Engineering* , 1(1), 115-140.

Endrun B. (2010), Love wave contribution to the ambient vibration H/V amplitude peak observed with array measurements, *Journal of Seismology*, doi:10.1007/s10950-010-9191-x.

Erdik M., Aydinoglu N., Fahjan Y., Sesetyan K., Demircioglu M., Siyahi B., Durukal E., Ozbey C., Biro Y., Akman H., Yuzugullu O. (2003) Earthquake Risk Assessment for Istanbul Metropolitan Area, *Earthquake Engineering and Engineering Vibration*, 2, 1.

Erdik M., Rashidov T., Safak E., Turdukulov A. (2005) Assessment of seismic risk in Tashkent, Uzbekistan and Bishkek, Kyrgyz Republic, *Soil Dynamics and Earthquake Engineering*, 25, 473-486.

Ergin M., Özalaybey S., Aktar M., Yalçin M.N. (2004) Site amplification at Avcilar, Istanbul, *Tectonophysics*, 391: 335-346.
Essen H.H., Krüger F., Dahm T. and Grevemeyer I. (2003) On the generation of secondary microseisms observed in northern and central Europe, *Journal of geophysical Research*, 108,

NO. B10, 2506, doi:10.1029/2002JB002338.

Fäh D., Kind F., Giardini D. (2001) A theoretical investigation of average H/V ratios, *Geophysical Journal International*, 145, 535-549.

Field E.H. and Jacob K. H. (1995) A comparison and test of various site response estimation techniques, including three that are non reference-site dependent, *Bulletin of the Seismological Society of America*, 86, 991-1005.

Forbriger T. (2006) Low Frequency limit for H/V studies due to tilt, *AG-Seismology session* Oct. 04-06th 2006, Haidhof.

Friedrich A., Krüger F. and Klinge K. (1998) Ocean generated microseismic noise located with the Gräfenberg array, *Journal of Seismology*, 47-64.

Gabor D. (1946) Theory of communications, *Journal of Institution of Electrical Engineering*, 93, 429-457.

Galiana-Merino J. J., Rosa-Herranz J. L. and Parolai S. (2008) Seismic P Phase Picking Using a Kurtosis-Based Criterion in the Stationary Wavelet Domain *IEEE Transactions on geoscience and remote sensing*, 46(11), 3815-3826, doi: 10.1109/TGRS.2008.2002647.

Gavarini C. and Gruppo di lavoro (1999) Proposta di riclassificazione sismica del territorio nazionale, *Ingegneria Sismica*, 1, 5-14.

Global Earthquake Model (n.d.), GEM at a glance www.globalquakemodel.org, online Available from: http://www.globalquakemodel.org/ (Accessed 26 September 2010).

Gruenthal G. European Macroseismic Scale (1998) *Cahiers du Centre Européen de Géodynamique et de Séismologie* 15-99.

Guillier B., Atakan K., Chatelain,J-L., Havskov J., Ohrnberger M., Cara F., Duval A-M., Zacharopoulos S., Teves-Cosat P., The SESAME Team (2008) Influence of instruments on the H/V spectral ratios of ambient vibrations, *Bullettin Earthquake Engineering*, DOI 10.1007/s10518-007-9039-0.

Gutenberg, B. (1921) *Handbuch der Geophysik*, 4, 264:298.

Haghshenas E., Bard P., Theodulidis N. and SESAME WP04 Team (2008) Empirical evaluation of microtremor H/V spectral ratio, *Bullettin Earthquake Engineering*, 6(1), 75-108, doi:10.1007/s10518-007-9058-x.

Harmandar E., Durukal E., Erdik M., Ozel O. (2006) Spatial Variation of Ground Motion in Istanbul, *Poster presentation ID 1633* Potential for Very Large Earthquake Disasters in the European Mediterranean Region, European Geophysical Union, Vienna 2006.

Herrmann R.B., Ammon C.J., Julia J., Mokhtar T. (1999) Joint inversion of receiver functions and surface-wave dispersion for crustal structure, *Proc. 21st Seismic Research Symposium Technologies for monitoring the comprehensive Nuclear test Ban treaty* September 21-24, 1999, Las Vegas, Nevada, USA, published by Los Alamos National Laboratory, LA-UR-99-4700.

Herrmann RB. (2002) Computer Programs in Seismology, Version 3.2, Saint Louis University 2002.

Holcomb L.G. (1989) A direct method for calculating instrument noise levels in side-by-side seismometer evaluations , *U.S. Geological Survey Open-File Rept*, 89-214.

Horike, M. (1985) Inversion of phase velocity of long period microtremors to the S-wave velocity structure down to the basement in urbanized areas *Journal Physics of the Earth*, 33, 59-96.

Housner G. W. (1952) Spectrum intensities of strong motion earthquakes, in the Proceedings of the Symposium of Earthquake and Blast Effects on Structures, *Earthquake Engineering Research Institute*, Los Angeles, California.

Ibs-von Seht M. and Wohlenberg J. (1999) Microtremor measurements used to map thickness of soft sediments, *Bulletin of the Seismological Society of America*, 89, 250-259.

INGV DPC-S3 (n.d.), DPC_INGV S3, online Available from: http://esse3.mi.ingv.it/ (Accessed 16 September 2010).

INGV earthquake catalogue (n.d.), Italian Earthquake Catalogue, online Available from: http://storing.ingv.it/cfti4med/ (Accessed 16 September 2010).

INGV Italian Hazard map (n.d.), Italian Hazard maps, online Available from: http://esse1.mi.ingv.it/ (Accessed 16 September 2010).

INGV-MEDnet (n.d.), MedNet - RCMT, online Available from: http://mednet.rm.ingv.it/rcmt.php (Accessed 21 September 2010).

ISC (n.d.), International Seismological Centre, online Available from: http://www.isc.ac.uk/index.html (Accessed 25 September 2010)

ISTAT demographic data (n.d.), ISTAT demographic data, online Available from: http://demo.istat.it/pop2009/index1.html (Accessed 17 September 2010).

Itaca (n.d.) Itaca, online Available from: http://itaca.mi.ingv.it/ItacaNet/ (Accessed 21 September 2010).

Jung K. (1934) Ueber mikrosesmische Unruhe und Brandung, *Zeitschrift für Geophysik*,10, 325-329.

Khalturin V. and B. Tucker (1997) Lessons from Armenia and Sakhalin for Central Asia, Report of the October 1996 Workshop in Almaty (Kazakhstan) on "Strategies for Urban Earthquake Risk Management for the Central Asian Republics", *IRIS Newsletter*.

Konno K. and Ohmachi T. (1998) Ground-motion characteristics estimated from spectral ratio between horizontal and vertical components of microtremor, *Bulletin of the Seismological Society of America* , 88, 228-241.

Kudo K., Kanno T., Okada H., Ozel O., Erdik M., Sasatani T., Higashi S., Takahashi M., Yoshida K. (2002) Site-Specific Issues for Strong Ground Motions during the Kocaeli, Turkey, Earthquake of 17 August 1999, as Inferred from Array Observations of Microtremors and Aftershocks, *Bulletin of the Seismological Society of America* , 92(1), 448-465.

Lachet C. and P.-Y. Bard (1994) Numerical and theoretical investigations on the possibilities and limitations of Nakamura's technique, *Journal of Physics of the Earth*, 42**,** 377-397.

Lachet C., Hatzfeld D., Bard P., Theodulidis N., Papaioannou C. and Savvaidis A. (1996) Site effects and microzonation in the city of Thessaloniki (Greece) comparison of different approaches, *Bulletin of the Seismological Society of America*, 86(6), 1692-1703.

Lahr J.S. (n.d.) HYPOELLIPSE Title and Contents Pages, online Available from: http://pubs.usgs.gov/of/1999/ofr-99-0023/ (Accessed 14 September 2010).

Langston C.A. (1979) Structure Under Mount Rainier, Washington, Inferred From Teleseismic Body Waves, *Journal of Geophysical Research*, *84*(B9), PP. 4749-4762, doi:197910.1029/JB084iB09p04749.

Lermo J. and Chavez-Garcia F. J. (1993) Site effect evaluation using spectral ratios with only one station, *Bullettin of the Seismological Society of America*, 83(5), 1574-1594.

Longuet-Higgins M.S. (1950) A theory of the origin of microseisms, *Philos. Trans. R. Soc. London*, Ser. A, 243, 2-36.

Lucente F. P., Piana Agostinetti N., Moro M., Selvaggi G. and Di Bona M. (2005) Possible fault plane in a seismic gap area of the southern Apennines (Italy) revealed by receiver function analysis, *Journal of Geophysical Research*, 110(B4), B04307.

Luzi L., Bindi D., Franceschina G., Pacor F., and Castro R. R. (2005) Geotechnical Site Characterisation in the Umbria-Marche Area and Evaluation of Earthquake Site-Response, *Pure and Applied Geophysics*, 162(11), 2133-2161.

Marcellini A. and Pagani M. (2004) Recent advances in earthquake geotechnical engineering and microzonation, *Springer.*

Marzorati S. and D. Bindi (2006) Ambient noise levels in north central Italy, *Geochem. Geophys. Geosyst.*, 7, Q09010, doi:10.1029/2006GC001256.

Masi A., Vona M. and Mucciarelli M. (2010) Selection of Natural and Synthetic Accelerograms for Seismic Vulnerability Studies on RC Frames, *Journal of Structural Engineering* 1(1), 136, doi:10.1061/(ASCE)ST.1943-541X.0000209.

McNamara D.E., Buland R.P. (2004) Ambient noise levels in the continental United States, *Bulletin of the Seismological Society of America*, 94*,* 1517-1527.

Moro M., Amicucci L., Cinti F. R., Doumaz F., Montone P., Pierdominici S., Saroli M., Stramondo S. and B. Di Fiore (2007) Surface evidence of active tectonics along the Pergola-Melandro fault: A critical issue for the seismogenic potential of the southern Apennines, Italy, *Journal of Geodynamics*, 44(1-2), 19-32, doi: 10.1016/j.jog.2006.12.003.

Mucciarelli M. (1998) Reliability and applicability of Nakamura's techniqueusing microtremors: an experimental approach, *Journal Earthquake Engineering* 2, 625-638.

Mucciarelli M., Gallipoli MR. (2006) Comparison between Vs30 and other estimates of site amplification in Italy *First European Conference on Earthquake Engineering and Seismology*

(a joint event of the 13th ECEE and 30th General Assembly of the ESC) Geneva, Switzerland, 3-8 September 2006 Paper Number: 270.

Nakamura Y. (1989) A method for dynamic characteristics estimations of subsurface using microtremors on the ground surface *Q. Rept. Railway Technical Research Institute Japan 30*, 25-33.

Nogoshi, M., and T. Igarashi (1970) On the amplitude characteristics of microtremor (part 2), *Journal Seismological Society of Japan*, *24*, 26-40.

Ohori M, Nobata A, Wakamatsu K. (2002) A comparison of ESAC and FK methods of estimating phase velocity using arbitrarily shaped microtremor analysis *Bulletin of the Seismological Society of America*, 92, 2323-2332.

Okada H. (2003) The microtremor survey method, Geophysical monograph series 12, American Geophysical Union, Washington.

Oth A., Bindi D., Parolai S. and Wenzel F. (2008) S-Wave Attenuation Characteristics beneath the Vrancea Region in Romania: New Insights from the Inversion of Ground-Motion Spectra, *Bulletin of the Seismological Society of America*, 98(5), 2482-2497, doi:10.1785/0120080106.

Ozel O., Sasatani T, Kudo K, Okada H, Kanno T, Tsuno S, Yoshikawa M, Noguchi S, Miyahara M, Goto H. (2004) Estimation of S-Wave Velocity Structures in Avcilar-Istanbul from Array Microtremor Measurements, *Geophysics*, 12, 2.

Ozmen B. (2004) Isoseismal Map of Izmit Earthquake, in 'Izmit Körfezi Depreminin Hasar Durumu (Rakamsal Verilerle)', Damage in the İzmit Bay Earthquake (with quantitative data), published by Turkiye Deprem Vakli, Istanbul.

Parolai S. (2009) Denoising of Seismograms Using the S Transform, *Bulletin of the Seismological Society of America*, 99, 226 -234.

Parolai S., Bindi D. and Augliera P. (2000) Application of the generalized inversion technique (GIT) to a microzonation study: numerical simulations and comparison with different site-estimation techniques, *Bulletin of the Seismological Society of America*, 90(2), 286.

Parolai S., Bormann P., Milkereit C. (2001) Assessment of the natural frequency of the sedimentary cover in the Cologne area (Germany) using noise measurements. J*ournal Earthquake Engineering*, 5 (4), 541-564.

Parolai S., Bindi D. and Trojani L. (2001a), Site Response for the RSM Seismic Network and Source Parameters in the Central Apennines (Italy), *Pure and Applied Geophysics.*, *158*(4), 695-715, doi:10.1007/PL00001200.

Parolai, S., Bormann, P., Milkereit C. (2002) New relationships between Vs, thickness of the sediments and resonance frequency calculated by means of H/V ratio of seismic noise for the Cologne area (Germany), *Bulletin of the Seismological Society of America*, 92 (6), 2521-2527.

Parolai S., Mucciarelli M., Gallipoli M.R., Richwalski S.M., Strollo A. (2007) Comparison of empirical and numerical site responses at the Tito test site (Southern Italy), *Bulletin of the*

Seismological Society of America, 97(5), 1413-1431.

Parolai S., Picozzi M., Richwalski S.M., Milkereit C. (2005) Joint inversion of phase velocity dispersion and H/V ratio curves from seismic noise recordings using a genetic algorithm, considering higher modes, *Geophysical Research Letters*, 32, L01303, doi: 10.1029/2004GL021115.

Parolai S., Richwalski S.M., Milkereit C. and D. Faëh C. (2006) S-wave velocity profiles for earthquake engineering purposes for the Cologne area (Germany) *Bullettin Earthquake Engineering*, 4, 65-94.

Parolai S. and S. M. Richwalski (2004) The importance of converted waves in comparing H/V and RSM site response estimates, *Bulletin of the Seismological Society of America*, 94(1), 304.

Parolai S., Bindi D., Baumbach M., Grosser H., Milkereit C., Karakisa S. and Zunbul S. (2004) Comparison of different site response estimation techniques using aftershocks of the 1999 Izmit earthquake, *Bulletin of the Seismological Society of America*, 94(3), 1096.

Parolai, S., Richwalski, S.M., Milkereit, C. and Bormann, P. (2004) Assessment of the stability of H/V spectral ratios and comparison with earthquake data in the Cologne area (Germany), *Tectonophysics*, 390, 57-73.

Pedersen H.A, Krüger F. and Svekalapko S.T.W.G. (2007) Influence of the seismic noise characteristics on noise correlations in the Baltic shield, *Geophysical Journal International*, 168, 197-210.

Pergalani F., L. Luzi V. Petrini A. Pugliese R. Romeo and T. Sanò (1999) Criteria for a Seismic Microzoning of a large Area in Central Italy, *Soil Dynamics and Earthquake Engineering,* Vol, *18*, 279-296.

Pergalani F., Compagnoni M. and Petrini V. (2008) Evaluation of site effects using numerical analyses in Celano (Italy) finalized to seismic risk assessment, *Soil Dynamics and Earthquake Engineering*, 28(12), 964-977, doi:10.1016/j.soildyn.2008.05.004.

Peterson J. (1993) Observations and modeling of seismic background noise, *U.S. Geol. Surv. Open-File Rept,* 93-322-95.

Picozzi M, Albarello D. (2007) Combining genetic and linearized algorithms for a two-step joint inversion of Rayleigh wave dispersion and H/V spectral ratio curves, *Geophysical Journal International*, 169: 189: doi: T10.1111/j.1365-246X.2006.03282.x.

Picozzi M., Parolai S., Albarello D. (2005) Statistical Analysis of Noise Horizontal to Vertical Spectral Ratios (HVSR), *Bulletin of the Seismological Society of America*, 95, doi: 10.1785/0120040152.

Plesinger A. and Wielandt E. (1974) Seismic noise at 2 Hz in Europe *Journal Geophysics*, 40, 131-136.

Rey J., Faccioli E. and Bommer J.J. (2002) Derivation of design soil coefficients (S) and response spectral shapes for Eurocode 8 using the European Strong-Motion Database, *Journal of Seismology*, 6(4), 547-555.

Richwalski S.M, Picozzi M., Parolai S., Milkereit C., Baliva F., Albarello D., Roy-Chowdhury K., Van Der Meer H, Zschau J. (2007) Rayleigh wave dispersion curves from seismological and engineering-geotechnical methods: A comparison at the Bornheim test site (Germany), *Bulletin of Earthquake Engineering*, 4, 349-361.

Riedesel M.A., Moore R. and Orcutt J.A. (1990) Limits of sensitivity of inertial seismometers with velocity transducers and electronic amplifiers, *Bulletin of the Seismological Society of America*, 80(6), 1725-1752.

Riepl J., Bard P., Hatzfeld D., Papaioannou C., and Nechtschein S. (1998) Detailed evaluation of site-response estimation methods across and along the sedimentary valley of volvi (EURO-SEISTEST), *Bulletin of the Seismological Society of America*, *88*(2), 488-502.

Rodgers P.W. (1992) Frequency limits for seismometers as determined from signal-to-noise ratios. Part 1. The electromagnetic seismometer, *Bulletin of the Seismological Society of America*, 82(2), 1071-1098.

Rodgers P.W. (1994) Self-noise spectra for 34 common electromagnetic seismometer/preamplifier pairs, *Bulletin of the Seismological Society of America*, 84(1), 228-228.

Rodriguez V.H. and Midorikawa S. (2002) Applicability of the H/V spectral ratio of microtremors in assessing site effects on seismic motion, *Earthquake Engineering and Structural Dynamics*, 31(2), 261-279.

Scherbaum F., Hinzen K.G., Ohrnberger M. (2003) Determination of shallow shear wave velocity profiles in Cologne, Germany area using ambient vibrations, *Geophysical Journal International*, 152, 597-612.

Sleeman R., Van Wettun A., Trampert J. (2006) Three-channel correlation analysis: a new technique to measure instrumental noise of digitizers and seismic sensors, *Bulletin of the Seismological Society of America*, 96, 258-271.

Sørensen M., Oprsal I., Bonnefoy-Claudet S., Atakan K., Martin Mai P., Pulido N., Yalciner C. (2006) Local site effects in Ataköy, Istanbul, Turkey, due to a future large earthquake in the Marmara Sea, *Geophysical Journal International* , 167, 1413-1424.

Steidl J. H., Tumarkin A.G. and R. J. Archuleta (1996) What is a reference site?, *Bulletin of the Seismological Society of America*, 86(6), 1733-1748.

Stephen R.A., Spiess F.N., Collins J.A. , Hildebrand J.A., Orcutt J.A., Peal K.R., Vernon F.L. and Wooding F.B. (2003) Ocean Seismic Network Pilot Experiment *Geochem. Geophys. Geosyst.*, 4(10) , 1092, doi:10.1029/2002GC000485.

Stockwell R.G., Mansinha L. and Lowe R.P. (1996) Localization of the Complex Spectrum: The S Transform, *IEEE Trans. Signal. Process.*, 44, 998-1001.

Strollo A, Parolai S., Jäkel K.H., Marzorati S. and Bindi D. (2008a) Suitability of short-period sensors for retrieving reliable H/V peaks for frequencies less than 1 Hz, *Bulletin of the Seismological Society of America*, 98, 671-681, doi:10.1785/0120070055.

Strollo A., Bindi D., Parolai S. and Jaekel K.-H. (2008b) On the suitability of 1 s geophone for ambient noise measurements in the 0.1–1 Hz frequency range: experimental outcomes *Bulletin of Earthquake Engineering*, 6, 141-147, doi 10.1007/s10518-008-9061-x.

Takahashi K., Ohno S., Takemura M. , Ohta T., Sugawara Y., Hatori T. and Omote S. (1992) Observation of earthquake strong motion with deep borehole: generation of vertical motion propagating in surface layers after S-arrival, *Proc. Of the 10Pth P World Conf. on Earthquake Engineering*, 3, 1245-1250.

Tezcan S.S., Kaya E., Bal L.E., Özdemir Z. (2002) Seismic amplification at Avcilar, Istanbul, *Engineering Structures*, 24, 661-667.

Tokimatsu K., Tamura S., Kojima H. (1992) Effects of multiple modes on Rayleigh wave dispersion characteristics, *Journal* of *Geotechnical Engineerin*g, 118, 1529-1543.

Triantafyllidis P., Hatzidimitriou P.M. and Suhadolc P. (2001) 1-D Theoretical Modeling for Site Effect Estimations in Thessaloniki: Comparison with Observations, *Pure and Applied Geophysics*, *158*(12), 2333-2347.

Tryon, R. C. (1939) Cluster analysis, *McGraw-Hill,* New York.

Ueong Y. S. (2009) A study on feasibility of SI for identification of earthquake damages in Taiwan, *Soil Dynamics and Earthquake Engineering*, 29(1), 185-193.

University of Jena (n.d.), Geodynamisches Observatorium Moxa, online Available from: Valley.

Wald LA., Mori J. (2000) Evaluation of Methods for Estimating Linear Site-Response Amplifications in the Los Angeles Region*, Bulletin of the Seismological Society of America*, 90, S32-S42.

Wald D. J. and T. I. Allen (2007) Topographic Slope as a Proxy for Seismic Site Conditions and Amplification, *Bulletin of the Seismological Society of America*, 97, 1379-1395; DOI: 10.1785/012006026.

Wang RA. (1999) Simple Orthonormalization Method for Stable and Efficient Computation of Green's Functions, *Bulletin of the Seismological Society of America*, 89, 733-741.

Wathelet M. (2005) Array recordings of ambient vibrations: surface-wave inversion. *PhD thesis*, Université de Liège, Faculté des Sciences Appliquées.

Webb, S.C. (1998), Broadband seismology and noise under the ocean *Reviews of Geophysics*, 36, 105-142.

Wessel P. and Smith W.H.F. (1991) Free software helps map and display data *Eos Trans., AGU* 72, 441-461.

Wesson V. (2004) ESandS Seismology Research Centre, online Available from: http://www.seis.com.au/TechNotes/TN200410A_SNR.html (Accessed 5 September 2010).

Wetterzentrale (n.d.), Wetter : Wetterzentrale : Top Karten : Archiv Reanalysis - Europa, online Available from: http://www.wetterzentrale.de/topkarten/fsreaeur.html (Accessed 5 September 2010).

Wielandt E. (2002) Chapter 5: Seismic sensors and their calibration. In: Bormann, P. (Ed.) (2002). IASPEI New Manual of Seismological Observatory Practice, GeoForschungsZentrum Potsdam, Vol. 1, 46 pp.

Yamanaka H, Ishida H. (1996) Application of Generic algorithms to an inversion of surface-wave dispersion data *Bulletin of the Seismological Society of America*, 86, 436-444.

Yoon B.J. and Vaidyanathan P.P.n(2004) Wavelet-based denoising by customized thresholding, *IEEE Int. Conf. On Acoustic Speech and signal processing (ICASSP)* Montreal, May 2004.

Zhang P., Yang. Z., Gupta H.K, Bhatia S.C. and Shedlock KM. (1999) Global seismic hazard assessment program (GSHAP) in continental Asia, *Annali di Geofisica*, 42, 1167-90.

Appendix A

Further combination mentioned but not showed in Chapter 2: *REFTEK 72A* and *PDAS* digital acquisition systems coupled with *1, 2* and *4,5* Hz sensors.
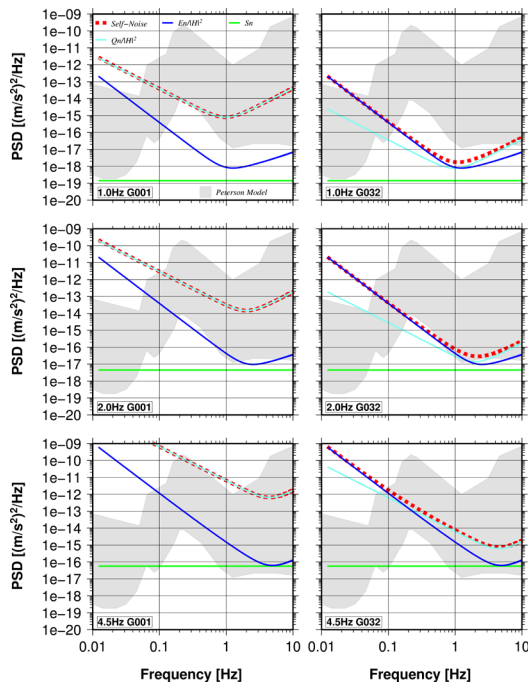
Figure A1a: Comparison of different components of self-noise for the REFTEK 72A: Electronic Noise (E_n blue), Quantization Noise (Q_n light blue), Suspension Noise (S_n green) and total self-noise (thick dashed red); the grey shading indicates the area delimited by the NLNM and NHNM of Peterson (1993). Left: Results obtained for a gain equal to 1 and different SPESs. Right: Results obtained for a gain equal to 32 and different SPESs.
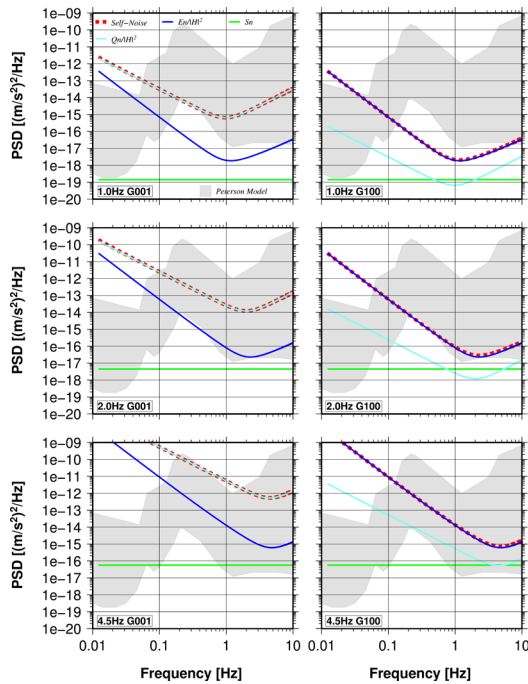
Figure A1b: Comparison of different components of self-noise for the PDAS: Electronic Noise (E_n blue), Quantization Noise (Q_n light blue), Suspension Noise (S_n green) and total self-noise (thick dashed red); the grey shading indicates the area delimited by the NLNM and NHNM of Peterson (1993). Left: Results obtained for a gain equal to 1 and different SPESs. Right: Results obtained for a gain equal to 100 and different SPESs.
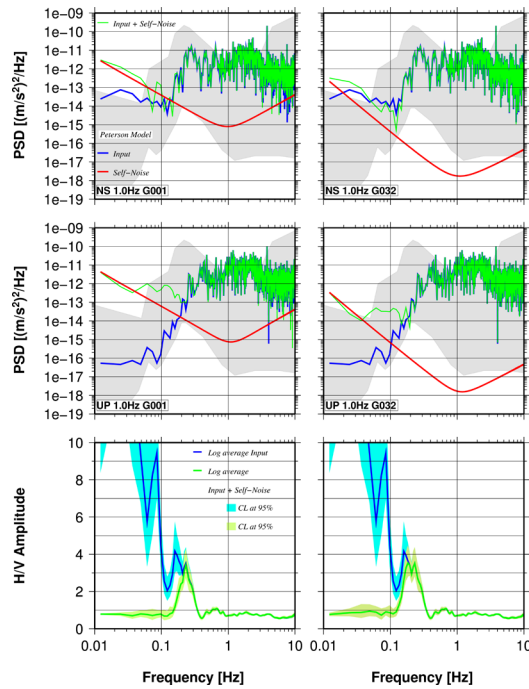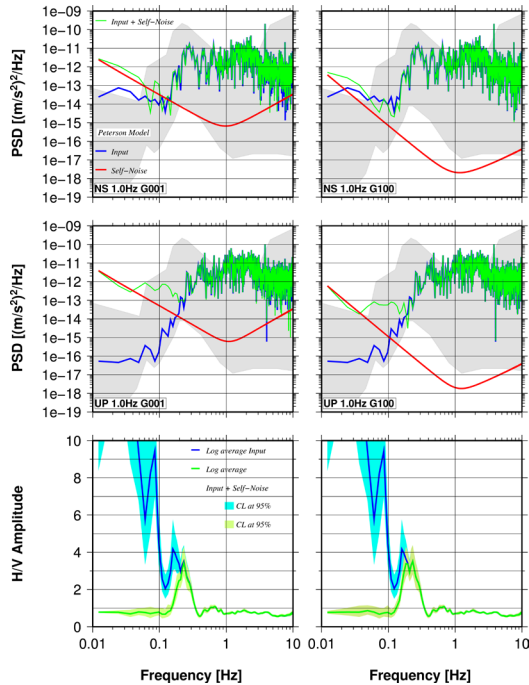
Figure A2a: Self-noise (red), ambient seismic noise (input) from broad-band recordings (blue) and input plus self-noise PSD (thin green) for the REFTEK 72A DAS with gain=1 (left side) and gain=32 (right side) coupled with a 1 Hz SPESs; the grey shading indicates the area delimited by the NLNM and NHNM of Peterson (1993). NS components are shown in the top panels while the UP components are in the center. The bottom panels show the corresponding average H/V spectral ratios of input from the broad-band recordings (blue) and average H/V spectral ratios of input plus self-noise (green); for both the shaded area indicates the 95 % confidence intervals (CL).
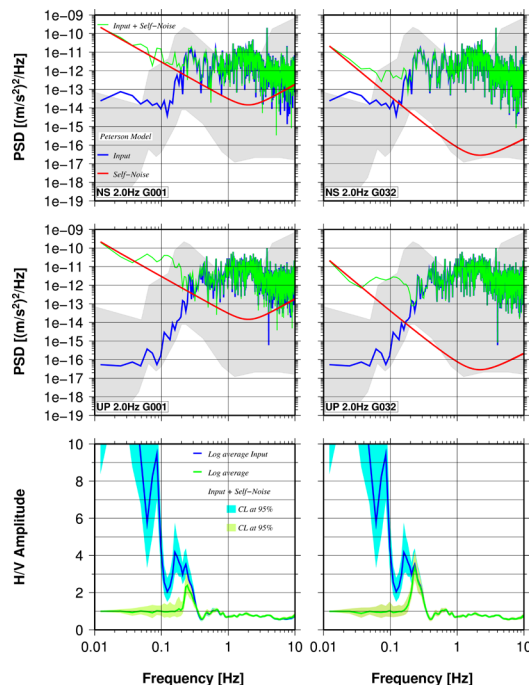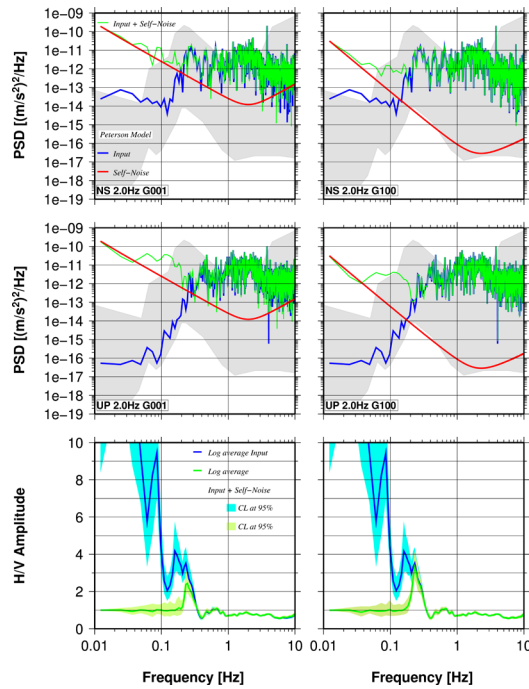

Figure A2b: Self-noise (red), ambient seismic noise (input) from broad-band recordings (blue) and input plus self-noise PSD (thin green) for the REFTEK 72A DAS with gain=1 (left side) and gain=32 (right side) coupled with a 2 Hz SPESs; the grey shading indicates the area delimited by the NLNM and NHNM of Peterson (1993). NS components are shown in the top panels while the UP components are in the center. The bottom panels show the corresponding average H/V spectral ratios of input from the broad-band recordings (blue) and average H/V spectral ratios of input plus self-noise (green); for both the shaded area indicates the 95 % confidence intervals (CL).
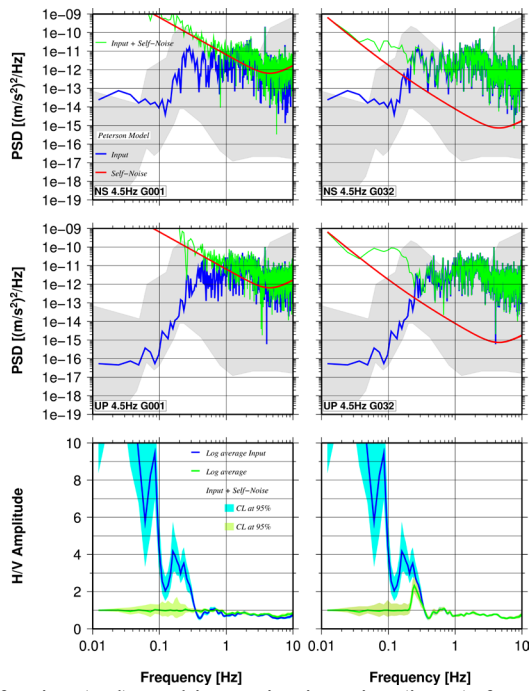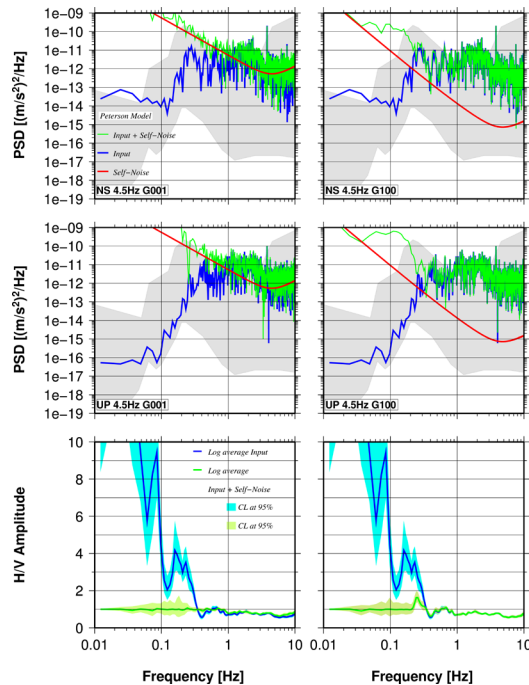
Figure A2c: Self-noise (red), ambient seismic noise (input) from broad-band recordings (blue) and input plus self-noise PSD (thin green) for the REFTEK 72A DAS with gain=1 (left side) and gain=32 (right side) coupled with a 4.5 Hz SPESs; the grey shading indicates the area delimited by the NLNM and NHNM of Peterson (1993). NS components are shown in the top panels while the UP components are in the center. The bottom panels show the corresponding average H/V spectral ratios of input from the broad-band recordings (blue) and average H/V spectral ratios of input plus self-noise (green); for both the shaded area indicates the 95 % confidence intervals (CL).

Figure A3a: Self-noise (red), ambient seismic noise (input) from broad-band recordings (blue) and input plus self-noise PSD (thin green) for PDAS DAS with the gain=1 (left side) and the gain 100 (right side) coupled with a 1 Hz SPES; the grey shading indicates the area delimited by the NLNM and NHNM of Peterson (1993). NS components are shown in the top panels while the UP components are in the centre. The bottom panels are the corresponding average H/V spectral ratios of input from broad-band recordings (blue) and average H/V spectral ratios of input plus self-noise (green); for both the shaded area indicates the 95 % confidence intervals (CL).

Figure A3b: Self-noise (red), ambient seismic noise (input) from broad-band recordings (blue) and input plus self-noise PSD (thin green) for PDAS DAS with the gain=1 (left side) and the gain 100 (right side) coupled with a 2 Hz SPES; the grey shading indicates the area delimited by the NLNM and NHNM of Peterson (1993). NS components are shown in the top panels while the UP components are in the centre. The bottom panels are the corresponding average H/V spectral ratios of input from broad-band recordings (blue) and average H/V spectral ratios of input plus self-noise (green); for both the shaded area indicates the 95 % confidence intervals (CL).

Figure A3c: Self-noise (red), ambient seismic noise (input) from broad-band recordings (blue) and input plus self-noise PSD (thin green) for PDAS DAS with the gain=1 (left side) and the gain 100 (right side) coupled with a 4.5 Hz SPES; the grey shading indicates the area delimited by the NLNM and NHNM of Peterson (1993). NS components are shown in the top panels while the UP components are in the centre. The bottom panels are the corresponding average H/V spectral ratios of input from broad-band recordings (blue) and average H/V spectral ratios of input plus self-noise (green); for both the shaded area indicates the 95 % confidence intervals (CL).

Appendix B

Spectral ratios and signal to noise ratio for all the stations used in Chapter 3
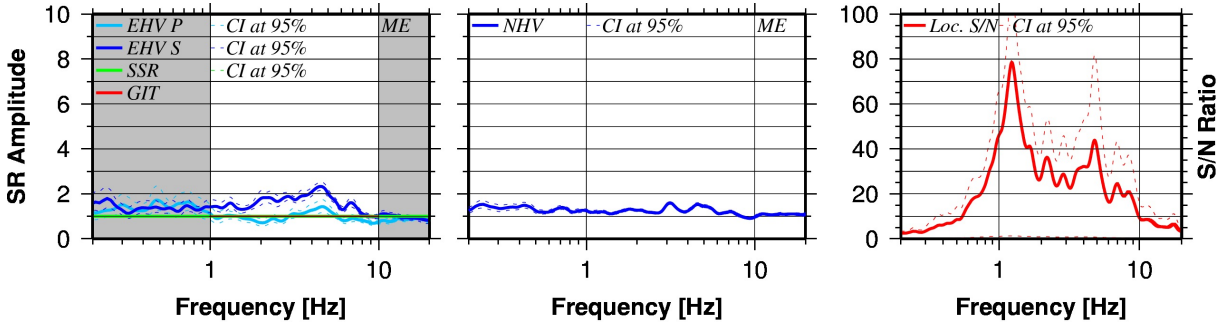
Figure B1 Standard spectral ratio for RS site. Left panel, EHV calculated for both P and S phases respectively showed in light blue and blue; SSR and GIT are represented respectively in green and red The gray shadow indicate the frequency band with signal to noise ratio smaller than 3. NHV is showed in the central panel. Right panel, average signal to noise ratio of the events used.
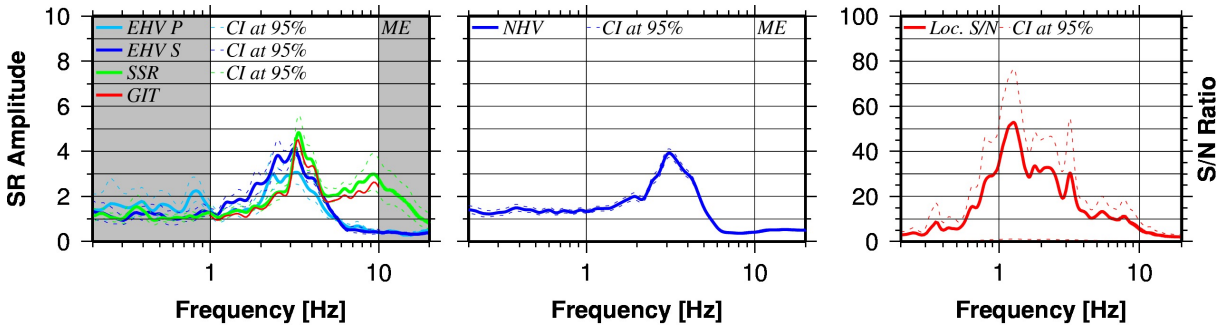
Figure B2 same as figure B1 but for site CD.
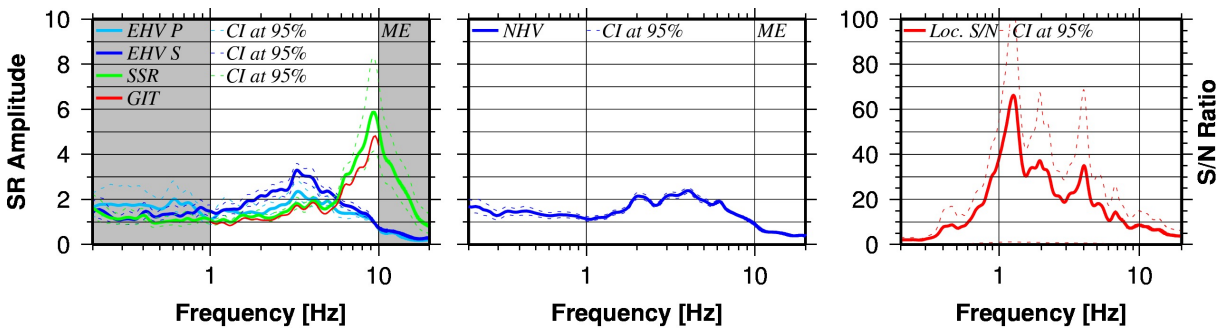
Figure B3 same as figure B1 but for site FA.
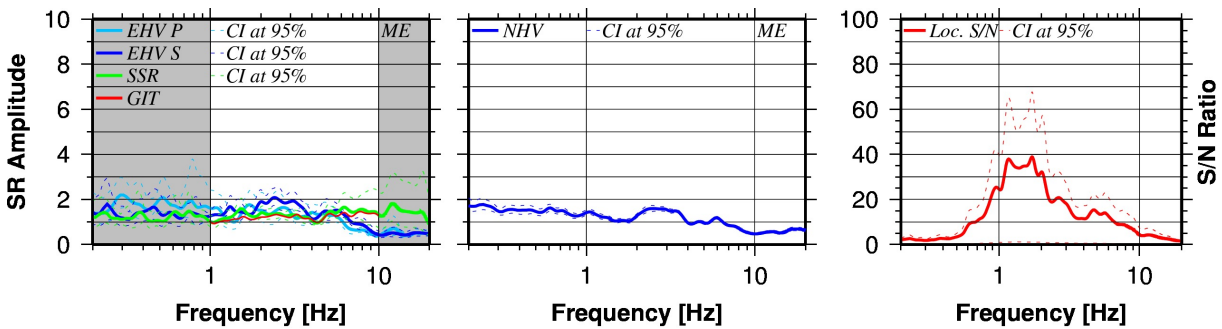
Figure B4 same as figure B1 but for site GL.
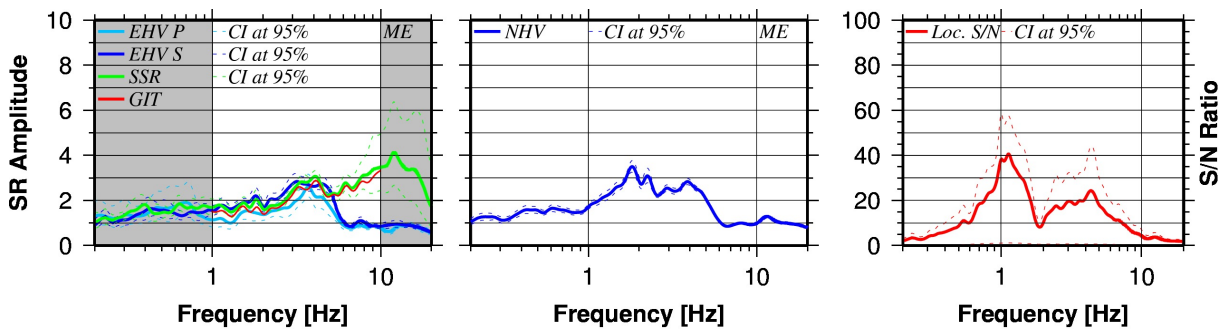
Figure B5 same as figure B1 but for site GM.
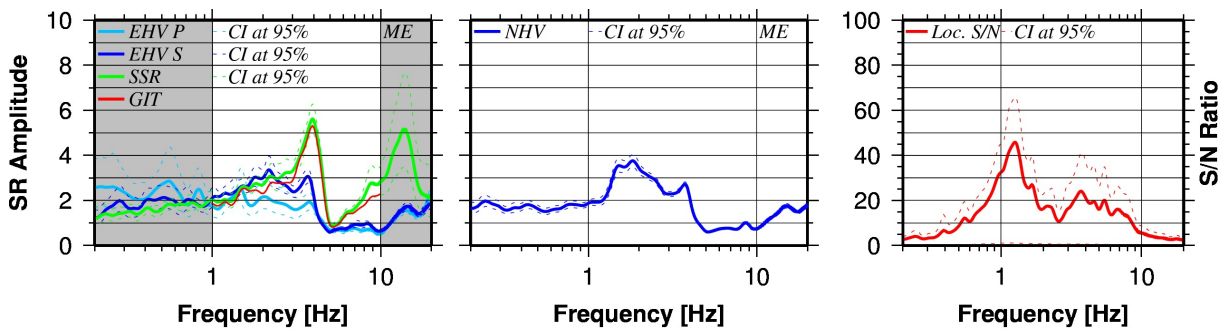
.**Figure B6** same as figure B1 but for site GT.
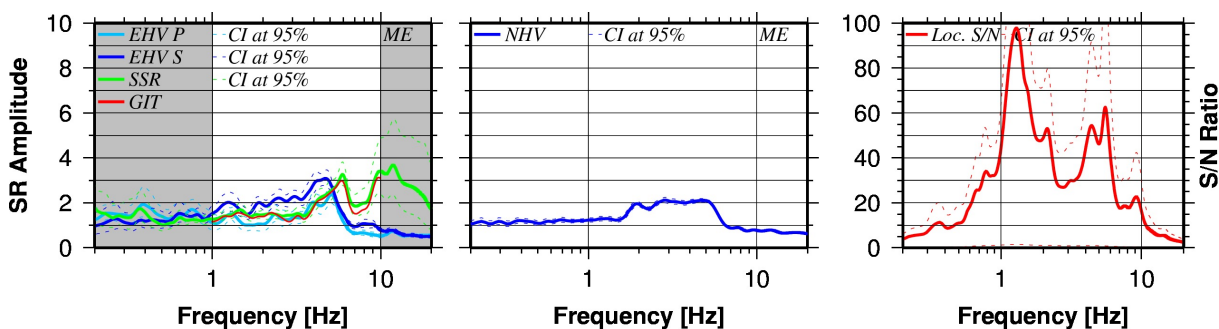
Figure B7 same as figure B1 but for site MU
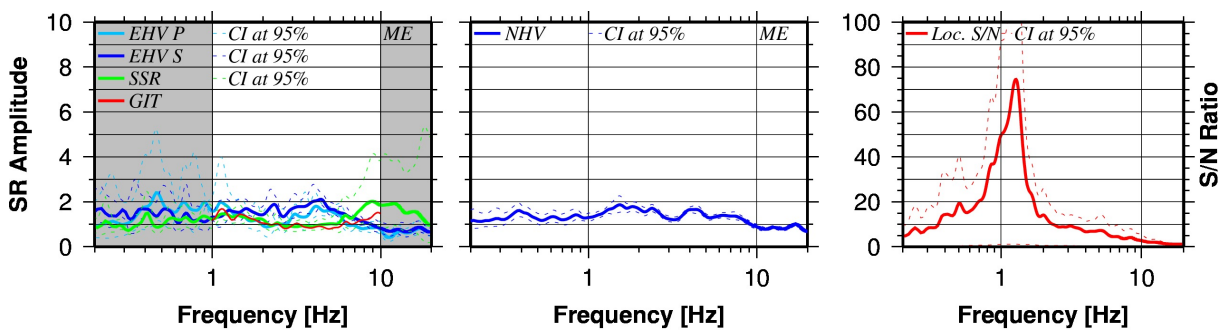
Figure B8 same as figure B1 but for site OC
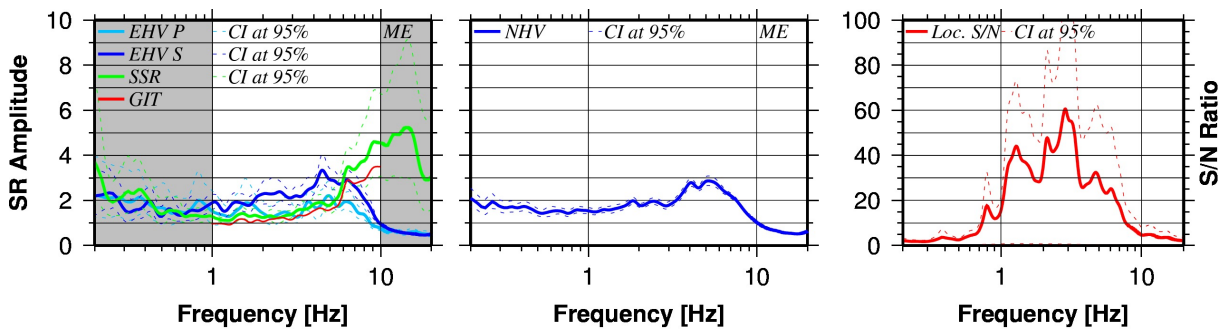
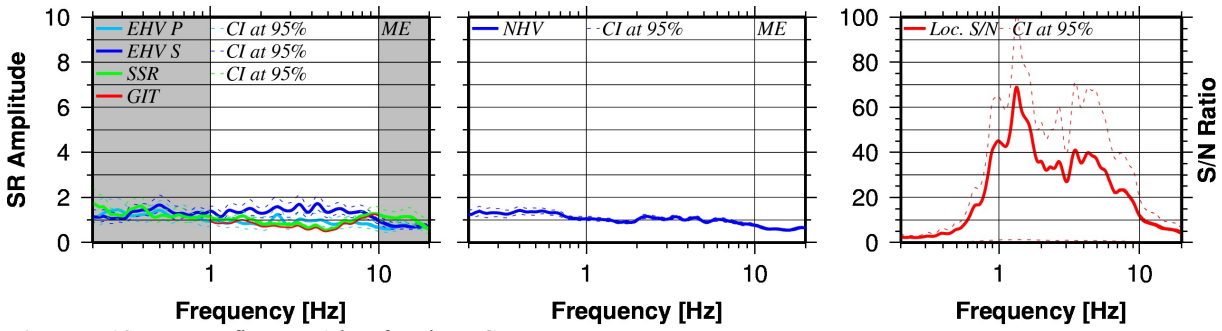**Figure B9** same as figure B1 but for site PA

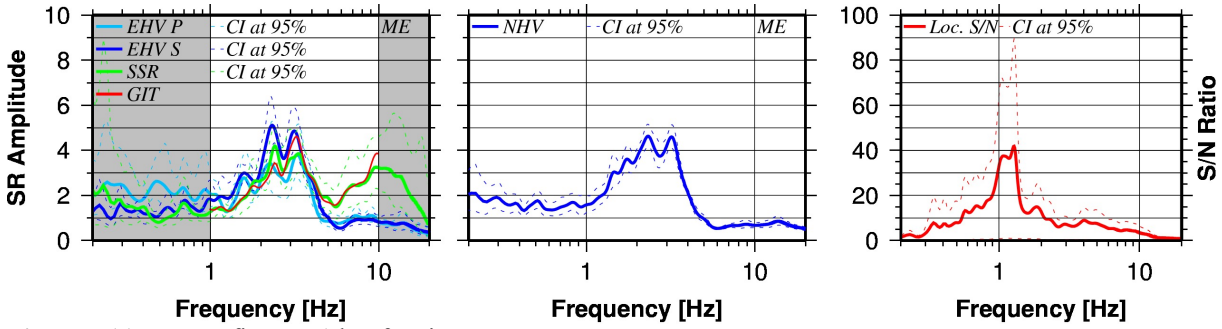**Figure B10** same as figure B1 but for site RG
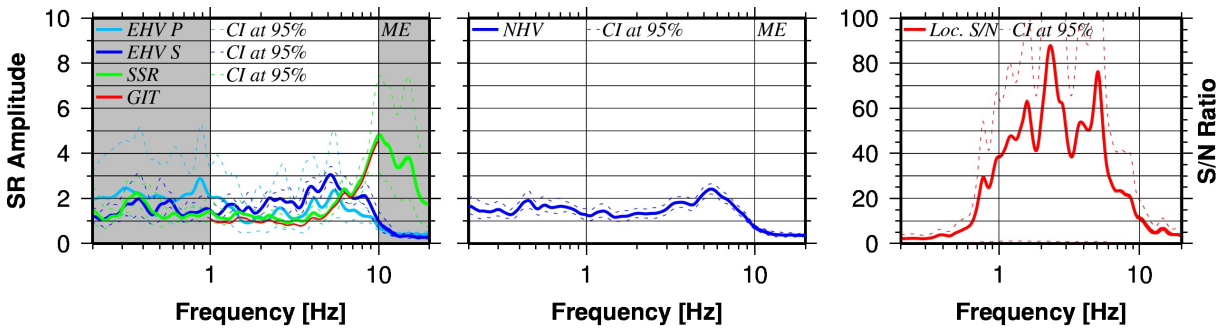

Figure B11 same as figure B1 but for site RT.
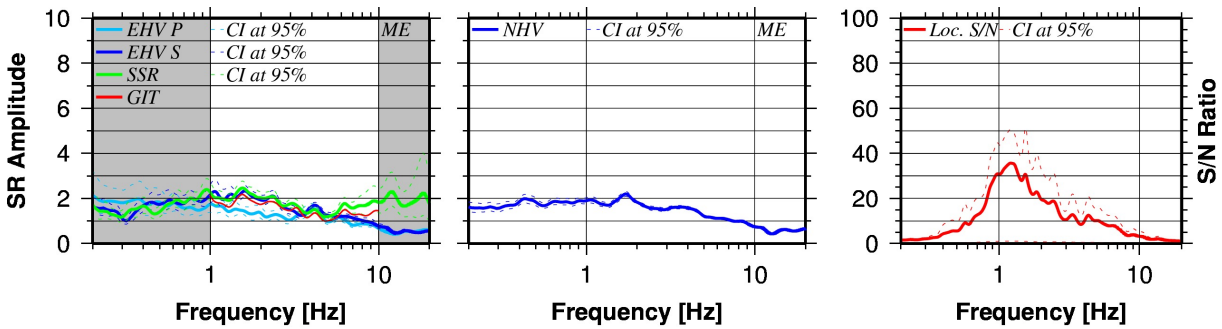

Figure B12 same as figure B1 but for site SC
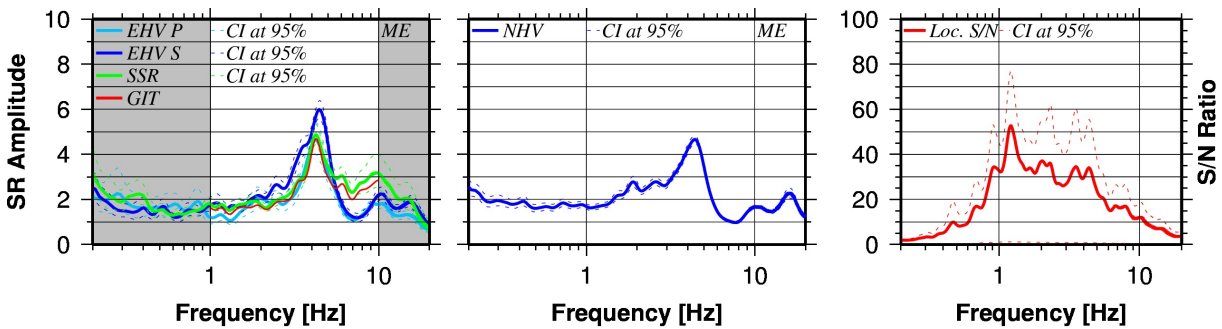

Figure B13 same as figure B1 but for site SP.

Figure B14 same as figure B1 but for site TF.